Implementation of Infrared Nondestructive Evaluation in Fiber-Reinforced Polymer Double-Web I-beams

By

Nicholas John Mehl

Thesis submitted to the Faculty of the Virginia Polytechnic Institute and State University in partial fulfillment of the requirements for the degree of

Master of Science
In
Engineering Mechanics

John C. Duke, Jr., Chair
Edmund G. Henneke
Surot Thangjitham

February 13, 2006
Blacksburg, Virginia

(Keywords: Nondestructive evaluation, Infrared thermal imaging, double-web I-beam, Fiber reinforced polymer composites)

Implementation of Infrared Nondestructive Evaluation in Fiber-Reinforced Polymer Double-Web I-beams

Nicholas John Mehl

(ABSTRACT)

When taking steps away from tried and true designs, there is always a degree of uncertainty that arises. With the introduction of fiber-reinforced polymers (FRP) in double-web I-beams (DWIB) to replace steel beams in bridge applications, there are many benefits along with the disadvantages. A bridge has been built with this new type of beam after only short-term proof testing for validation. Nondestructive evaluation (NDE) is a way to implement health monitoring of the bridge beams and needs to be assessed.

The principal underlying infrared thermal imaging (IR) nondestructive evaluation (NDE) is to induce a thermal gradient in the beam through heating and monitor how it changes. Delaminations determined by others to be the critical form of deterioration, would be expected to affect the heat conduction in these beams. This project used a halogen lamp to heat the surface of the beam followed by an observation with an IR camera. Calculations of an ANSYS finite element analysis (FEA) model were compared with a series of laboratory tests. The experimental results allowed for validation of the model and development of an IR inspection procedure. This work suggests that for high quality beams of the type considered that an IR procedure could be developed to detect delaminations as small as one inch in length; however, the size would be underestimated.

Acknowledgements:

Dr. Duke: My advisor and instigator of this project. While our imaginations may have been just different enough to cause us to be on different playing fields most of the time, maturity and patience allowed us to end up in that same spot and that's all that really matters.

Mike Horne: For always being in the lab and willing to help when you should've been spending more time finishing your own work; I really didn't mean to be such a pain in the neck.

Dr. Henneke: For the patience it took to serve on my committee and sticking through until the end.

Dr. Thangjitham: For coming to the project in the later stages and providing the needed support.

Dr. Lesko: Hopefully knowing that I am mot upset in my early failure; I'm much more satisfied with the way things turned out. I just wished for a second chance.

Michael Hayes, John Bausano and all the characters in and associated with the MRG: For providing insight to parts of the beam and its analysis that I didn't understand and couldn't repay.

Delphi Automotive: Even though my dream job came and went, I learned a lot and applied even more to my thesis work that would have made this even more difficult.

Jim: For being a friend and making sure the world could always be viewed just a little bit more interestingly.

Ed: For all the help with supplying a cheap, quiet, furnished place to live when I had to come back and finish things up.

VT Cycling Team and Outdoor Club: For letting me be a normal person once in a while by not being an engineer. Whether I was pouring my heart and soul into making the pedals turn or trudging along a trail carrying way too much in my pack, it was what I needed to keep a firm grip on reality.

My parents: For the endless support even they didn't fully understand why I needed to do this. And for letting me fall back on them when things didn't pan out exactly as planned.

Sue: For everything that being the love of my life may entail…

Table of Contents:

Table of Figures:

Chapter One: What and Why (Background and Objective)

In order to best start this journey through the process and discussion of infrared (IR) thermal imaging of the Dickey Creek fiber reinforced polymer (FRP) double-web I-beam (DWIB) bridge, knowing each of these parts along with how and why they interact will be helpful.

1.1: The Strongwell 36” Double-web I-beam

In the summer of 2001, a bridge in Southwestern Virginia was built with a dark-colored 36” I-beam. To the general observer, nothing would appear different other than the color of the beams that were then covered by a wood deck and a layer of asphalt (see Figure 1.1). However, the structural members of this bridge would be different than any other built in Virginia [Lesko].

Figure 1.1 Bridge Picture

That is, other than the Tom’s Creek Bridge in Blacksburg, Virginia, which was created out of a similar, scaled down prototype 8” DWIB. Other than in size,

the two beams, the 8” and the 36,” were similar in that both were double I-beams with two support webs as shown in Figure 1.2, and both were constructed using a pultrusion technique. Similar to the metal extrusion process, liquid polymer and reinforcing fibers are pulled through a set of dies, heated, and cured into the shape of the double-web I-beam. This creates a continuous external cross-section over any desired length.

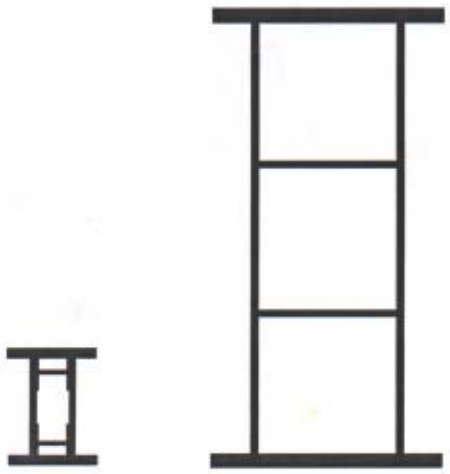

Figure 1.2: Beams

One more common tie between the two beams is their origin. Both were developed and pultruded by Strongwell Corporation and funded by an Advanced Technology Program through the National Institute of Standards and Technology or NIST. NIST was pushing for further material development and how to apply some of the relatively newer technologies like composite materials into applications that typically would have been manufactured out of more common materials like steel.

Material characteristics of the composite beam offer advantages over

conventional steel beams. Individual materials of the composite beam can be positioned or oriented with respect to where they would be most useful over a constant cross section. The pultrusion process allows for continuous fiber architecture and for strategic location of reinforcing materials. In these two instances, the beams are composed of a hybrid carbon and glass fiber arrangement with a vinyl ester matrix. In order to optimize the configuration, the carbon fibers are placed near the outside surfaces of the top and bottom flanges. This architecture takes the more expensive, but lighter and stronger, carbon material and places it where it would be most effective in the smallest quantities while the remainder of the beam is made of fiberglass.

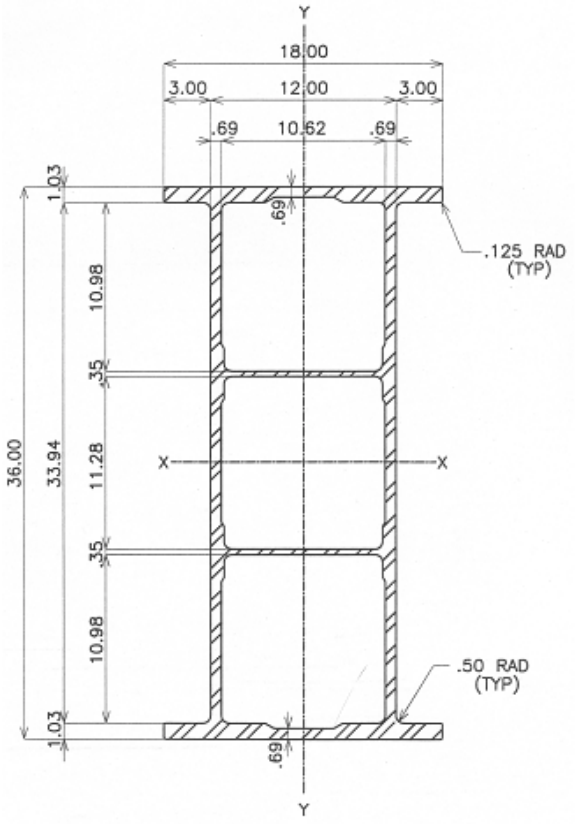

Figure 1.3: Beam with Dimensions

In our situation, once the initial constraints like cost of beam manufacturing are overcome, a composite beam could be engineered to better suit the intended application and could ultimately create a higher quality bridge structure. In a bridge environment, composite materials offer both higher strength and are more corrosion resistant than steels. Also, this composite beam lends itself to being much lighter than a comparable steel beam aiding in the assembly of the bridge.

Taking design into reality, the Dickey Creek Bridge in Marion, VA was created. After it was finished, a new set of challenges arose. Since composite material usage in civil infrastructures is still early in development, a bridge of this nature does not have a standard schedule for testing and maintenance. This is why the Virginia Department of Transportation was interested in having data developed for ultimate strength, fatigue and field inspection. The later of these is the basis for the research to be laid out in the following chapters.

1.2: “Crack” – The Critical Defect

At the same time this project was starting, another group at Virginia Tech was mechanically proof-testing the beams to different load levels as well as also loading several beams to failure [Schniepp, 2002]. A direct result of this study was an indication of where beam failures would initiate. In a standard four-point bending test, these areas are the material transition areas of the flange on the compression side of the beam in bending [Armstrong, 1998] (Figures 1.4 and 1.5).

Figure 1.4: Full Length of a Failed Beam

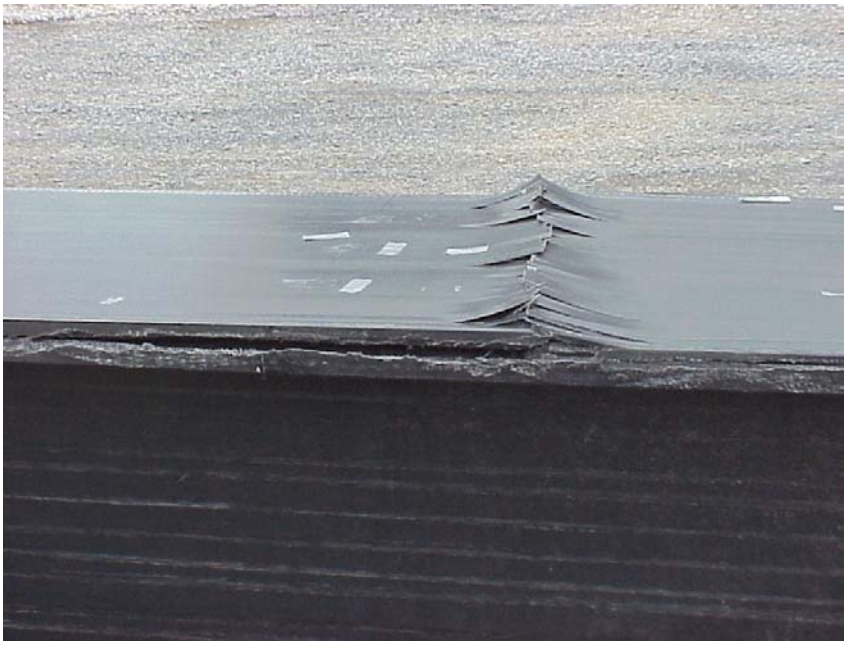

Figure 1.5: Close-up of a Failed Section

The boundary between the regions reinforced by carbon or glass fibers has the highest likelihood of developing defects in that, where the two materials come together, creates resin rich areas of lesser properties due to the way the two different sized fibers interact during the pultrusion process. Since much of the flange is made of a carbon fiber layup, it will be much stronger and stiffer than the remaining glass fiber layers creating a shear plane at the boundary between the two. This, coupled with the manufacturing variances, creates an area that may be full of anomalies.

1.3: Area of Interest

Further defining the sections of the 36" DWIB, an area of interest on the flange with respect to the whole beam is shown in Figure 1.6. This area of the flange holds the boundary region where the failed beams were cracking. This region, the flange, and web are both labeled in Figure 1.7.

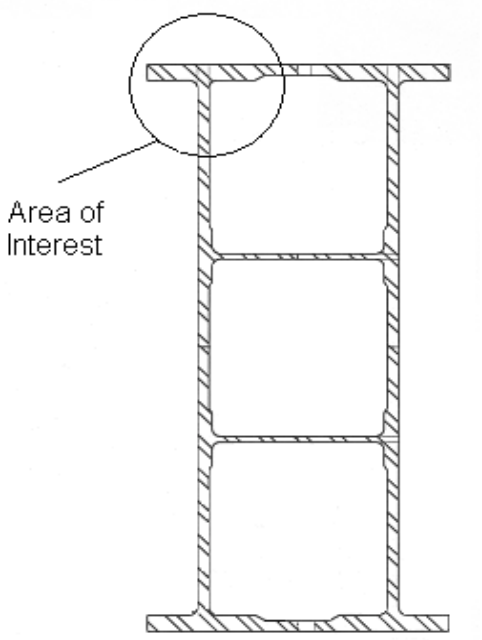

Figure 1.6: Area of Interest on the Beam

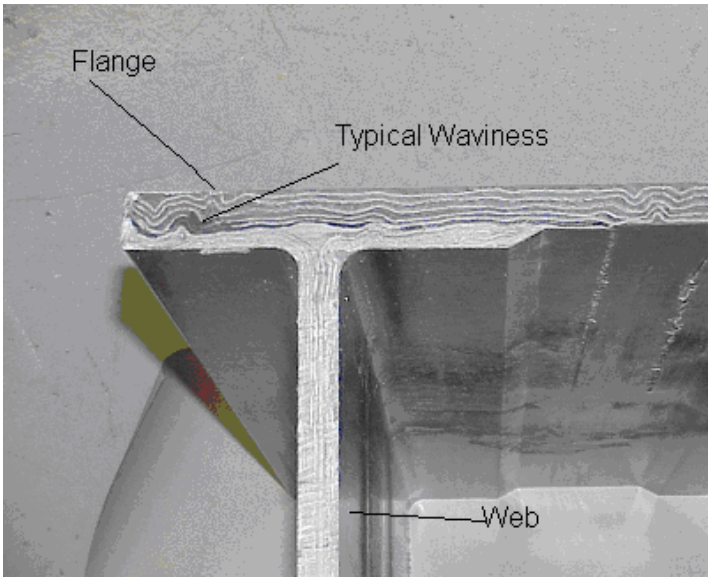

Figure 1.7: Typical Beam Cross-Section

In Figure 1.7, the two basic materials can be distinguished. The lighter regions that make up the web and bottom section of the flange are fiberglass while the darker colored areas are carbon fiber. To denote the material regions, the lower will be called the glass region and the upper will be the carbon region. This upper region consists of carbon fibers layered with glass mat, but, for the most part, is carbon and will be called the carbon region. As for the boundary between the two material regions, the pultrusion process cannot control exactly where the individual materials will end up and the waviness depicted is present throughout the boundary and along the beam length.

Within this area of interest, possible locations for delaminations to originate are depicted in Figure 1.8. Both locations, “A” and “B,” happen along the interface boundary between the carbon and glass regions and on free surfaces. The other research group at VT had determined that the outside region, “A,” was the one of more interest. Furthermore, bridge constraints hindered the

accessibility of region “B,” raising concern that this part of the beam may be difficult for inspection while in the field. Figure 1.9 shows this area as it would be seen along the edge of the flange.

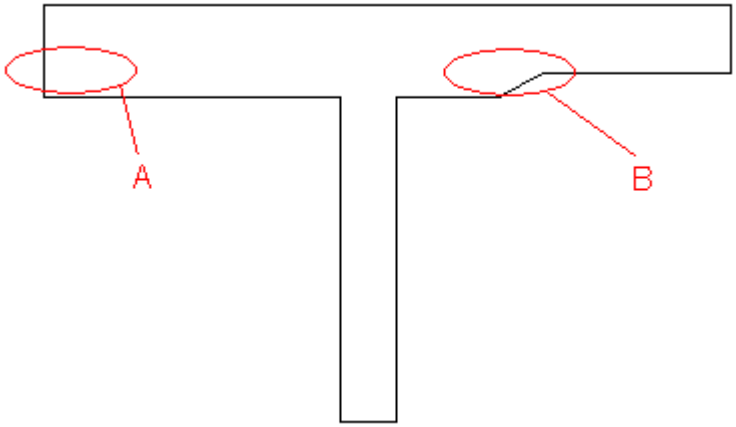

Figure 1.8: Locations of Potential Delaminations in the Area of Interest

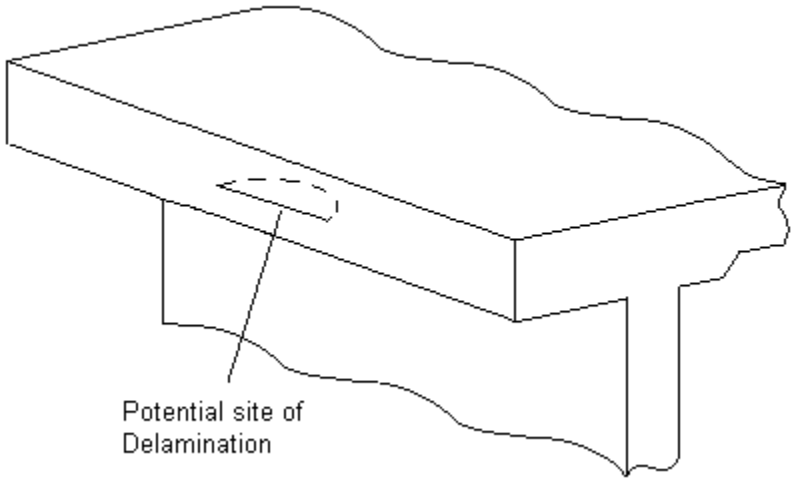

Figure 1.9: Defect Diagram

Taking a cross-section of the outside edge of the flange and, once again, denoting the carbon and glass regions, Figure 1.10 shows a close-up of location "A."

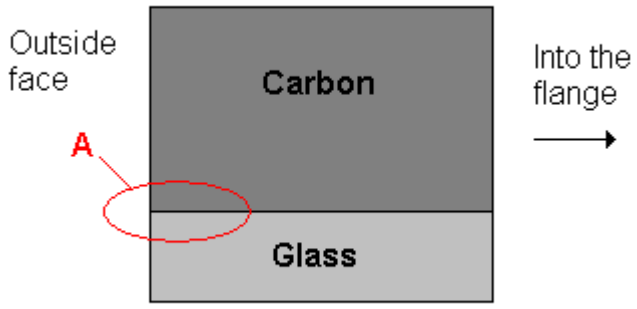

Figure 1.10: Flange Regions with Site "A"

1.4: The NDE Selection Process

A formal definition of NDE would state that the nondestructive nature of the assessment should not alter the material in a way that would affect the serviceability of the component. This definition can be further broken down into subsets that differentiate between the "engineer's" and "physicist's" definitions. The engineering definition would allow material alterations such as drilling holes to aid the inspection as long as the component strength and life would not be reduced. An example would be of a coring procedure used to assess concrete bridge decks where a core is removed and tested. The void is later filled with fresh concrete. The physicist's definition is more restrictive and would be noninvasive; none of the physical characteristics can be changed. Any changes to the material or component under this definition would not be allowed.

A simple procedure of method selection groups criteria into three categories [Duke, 1993]:

Attribute characteristics. Knowing the physical description of an imperfection has its advantages by both being able to find it and eliminating

different techniques that would not be applicable in the search. In other words, how the imperfection affects the material properties will guide the elimination of inappropriate techniques.

To develop the idea of an “imperfection” further, the differences between imperfection, non-conformity and defect, need to be clarified. While these are similar in that they all represent a material that is less than absolute perfection, there is a major difference. That is, all materials include imperfections at the atomic scale. An imperfection can exist in a material without reducing the serviceability of the structure. A defect, on the other hand, is an imperfection that causes the structure to fail, consequently reducing the serviceability. The non-conformity is the line that is drawn to limit the acceptable size of an imperfection that is not yet a defect, but needs to be identified with respect to the safety factor assigned to the material characteristics [Callister, 1997] [Bray, 1997].

Assessment procedure requirements. Once it is known what to look for and where, knowing how to interpret the data obtained from a test is important. Basically, this is the “E” of NDE and, at this point, the imperfection/non-conformity relationship needs to be applied so the results can be understood. In this study, the area of the imperfection is used as the basis for assessing its severity.

Application constraints. Feasibility, the application of multiple procedures, time availability, and ultimately, cost will drive this third area. While a certain type of imperfection can be found and classified in a particular material, having the time, resources, and accessibility to perform the series of tests is another matter. For example, directly related to the beam project, it is not known exactly what is the smallest size of imperfection that will become a non-conformity. Thus in an effort to be certain that imperfections that will become defects in service are detected the objective is to detect the smallest possible imperfection. The reasoning is to be able to give the earliest warning regarding the formation of a

potential defect.

1.5: NDE Selection

After going through the selection steps and weighing the advantages, limitations, as well as equipment and resource availability (see [Bray, 1997] for a comprehensive listing of techniques and processes); the methods selected for further consideration were ultrasound (UT) and infrared thermal imaging.

Initially and conceptually, the ultrasonic method appeared to have the most potential. Using a “composite” material of two bulk materials layered on top of each other directing a UT beam into the piece of “composite” submerged in water as shown in Figure 1.11, there would be a reflection peak in the returned signal for the top surface and back surface. For this example, and the beam application, this is true. There will also be a smaller reflection peak for the boundary between the two materials and an even larger peak at that point if there was a delamination along the boundary. If these boundaries were both smooth and oriented perpendicular to the UT beam, they should produce a detectable reflection. However, this was not the case when using samples of the beam flange. Taking separated sections of the carbon and glass regions and the known speed of sound in water, thicknesses of the sections, and the relative speeds of sound in the carbon and glass regions could be determined by a through-thickness pitch-catch UT procedure as depicted in Figure 1.12. This, then applied to the pulse-echo method, could be used to determine the approximate times that the reflections should appear in the echo pattern and generate data similar to Figure 1.13 [Bray, 1997]. The typical results that were acquired in testing are shown in Figure 1.14. Figures 1.13 and 1.14 are both of the same scale pattern with voltage on the y-axis and time on the x-axis. If Figure 1.13 was superimposed on top of Figure 1.14, the initial spikes would match up but the actual laboratory data did not exhibit either the boundary or back surface reflections.

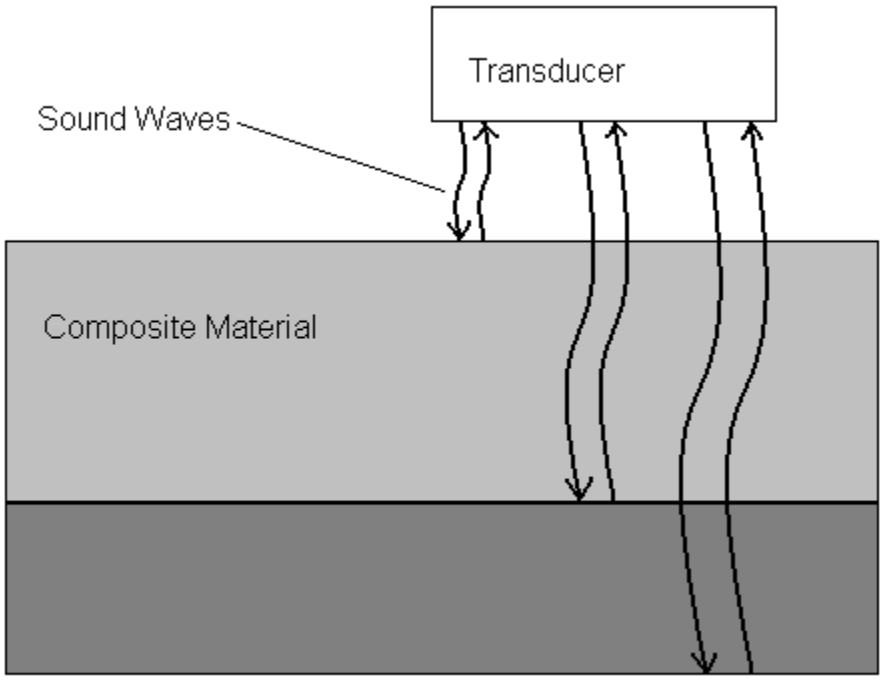

Figure 1.11: Sample Pulse-Echo UT Setup for Analyzing a Composite Material

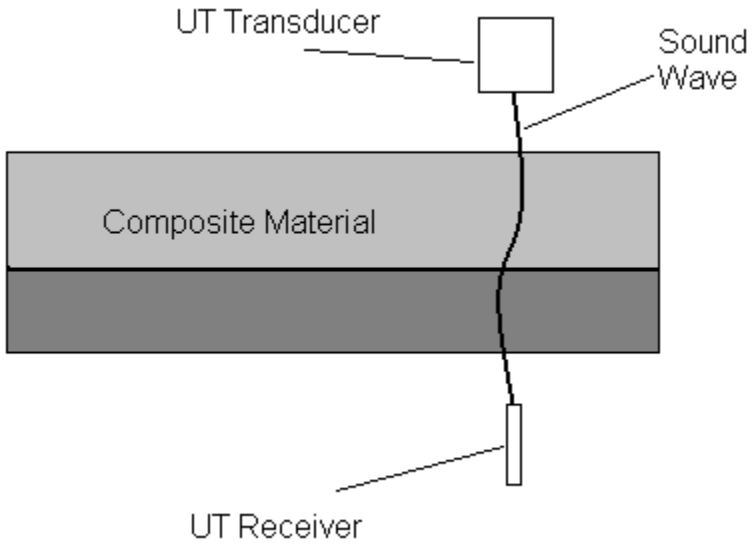

Figure 1.12: Pitch-catch UT Setup

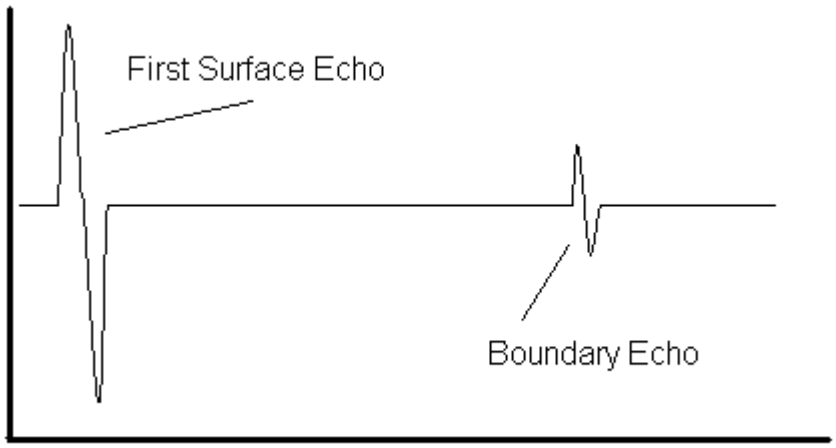

Figure 1.13: Example of a "Perfect" UT Response

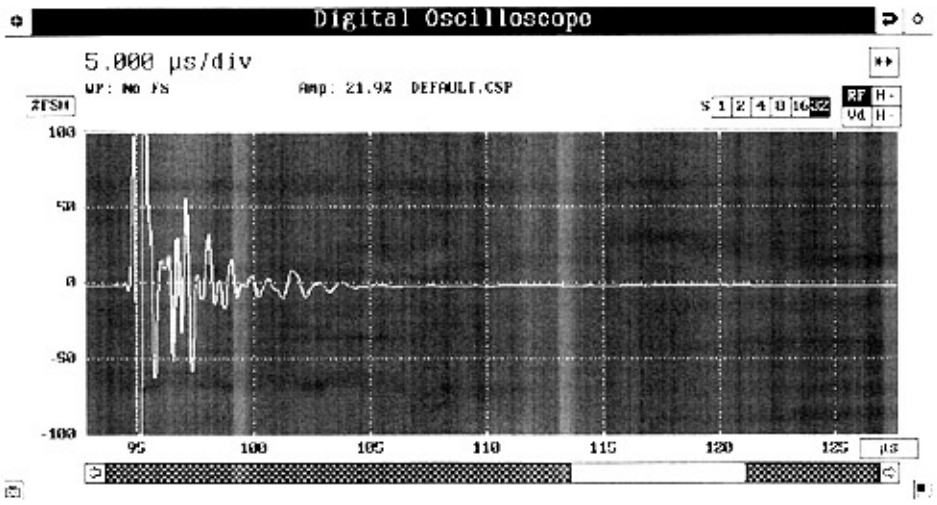

Figure 1.14: Typical UT Response from the Beam

An explanation for the theoretical and experimental discrepancies had to be determined. The nature of the boundary between the carbon and glass regions could be the cause. If it were perfectly flat, this may not have been an issue. But, through the pultrusion process, the materials have the tendency to fluctuate and end up "wavy" as shown in Figure 1.7. Such a boundary produces

irregular interfaces to reflect the ultrasonic wave, and the UT is only detectable if the sound is reflected back to the transducer. Also, in the way the individual fibers will tend to scatter the signal, there will be much attenuation in both the transmitted and reflected signals, further complicating the details of the received signals.

Although non-contact laser based robotic scanning systems have been developed, these systems are at present limited to use only in laboratory or shop floor settings. Field systems more typically involve planar scanners that must be frequently relocated in order to examine large areas. In addition, because of the quality of pultruded composites used for infrastructure applications, numerous imperfections with regard to ultrasound propagation are detected. Consequently, interpreting the scanning data for structures such as the large beams considered here, presents a data processing challenge, as well as being very time consuming if conventional ultrasonic scanning resolution is used. Finally, the need for the UT procedure to be implemented under water adds another testing constraint that is difficult to carry into the field-testing.

Furthermore, and for the reasons that this thesis will later develop, infrared thermal imaging was chosen. The primary reason for selecting the infrared approach was the ability to examine large areas of structures rapidly.

1.6: Heat Transfer

Considering just the basics of IR thermal imaging, the following material will be expanded in the second chapter. However, on the general level of heat energy (q) transfer in solids, this energy will want to move from hotter to cooler areas. This thermal difference is what causes the energy to flow. If there is no difference, there will be no heat transfer. From the standpoint of what is to be discussed later, the thermal conductivity (k) will be a major factor in describing how the heat energy behaves. The conductivity is a material characteristic and is

also directionally dependent if the material is anisotropic. With composite materials in general, the direction of the fibers and layer orientation will dictate its thermal characteristics.

1.7: Infrared Thermal Imaging

Electromagnetic radiation is emitted by all materials above absolute zero and can be viewed using an IR camera as a conventional camera would capture visible light. Different frequencies of light are carried by photons of a corresponding wavelength and when reflected or absorbed by a surface, they will appear as a visible color. In the same way, but in a spectrum below visible light, infrared photon emissions correspond to the temperature of the surface [Beiser, 2003]. With respect to the IR camera, internally, it has a photon detector that measures this emitted energy and displays the surface temperature as a visible color corresponding to a temperature scale in the camera [Thermovision]. By thermally exciting the specimen with some external source, the IR camera registers the emitted energy as electrons shift to a lower energy states and give off photons. As for heating the specimen, the elevated temperatures will cause more powerful radiation from the surface to increase, allowing the observation of the temperature gradients on the surface as a result of the subsurface heat transfer around abnormalities. The IR camera is only able to register wavelengths within the IR range, no matter how many others are emitted.

The raw data from the camera will come in the form of an image with the colors representing different surface temperatures. From the image, the pixel value can be used to plot thermal lines or contours of a particular temperature called isotherms or to graph the temperature distribution across the surface.

1.8: Previous Work with IR Thermal Imaging and Composite Materials

Now that NDE, IR thermal imaging, the imperfection of concern, and the

materials of the beam have been touched upon, reviewing the previous work of others is appropriate. In the larger picture of IR thermal imaging and composites in general, there has been much work done on composite infrastructure applications such as bridge decks in a way that internal through-thickness heating would expose subsurface delaminations in the deck and/or wear surface. This technique will allow for variations in the condition of the structure to be detectable on the surface as thermal irregularities on the surface. Typically the abnormalities in the heat conduction are due to delamination or disbonds, although, in some cases, material anomalies such as lack of resin have been detected [Miceli, 2000] [Alqennah, 2000].

In the same sense, but a bit of a slightly different approach and more directly related to the beam and some similar constraints, efforts have been considered where imperfections are parallel to the observation plane. For a simplistic development, consider a solid, metallic material with a partial hole of some type drilled out from the backside and make the observation plane the same surface area where heat energy is applied. The result will be a thermal difference profile somewhat related to the shape of the hole depending on the depth of the irregularity [Almond, 1994]. How this shape will appear is entirely dependent on the subsurface condition and irregularities appear two to three times larger than the material volume over them [Puttick, 1987].

NASA scientists explored another approach utilizing a different process for simulating imperfections. Instead of leaving an empty hole in the laminate, a hole is drilled and then partially filled, leaving a little air void between the original and the filler material. The observed data with this process will be much more realistic and true to the size of the imperfection [Winfree, 2003].

Thermal Wave, Corp., developed another procedure that should be mentioned. The procedure involves taking multiple, successive images as a function of time of the same surface and then subtracting one image from the

other. By noting inconsistencies in thermal conductivity between data taken from “good” sections of material and “bad” sections, the development of a subsurface material imperfection can be observed [Shepard, 2001].

1.9: Objective

The objective of this project was to develop an NDE procedure that could be used to assess outer flange of the FRP beam in order to detect the initiation of delaminations between the regions reinforced by glass fibers and the portions reinforced by carbon fibers identified as the critical failure mechanism. As a guide to developing this technique, an ANSYS finite element analysis (FEA) model was created to guide the data analysis and method development. The inspection approach selected was to use thermal imaging to measure radiated energy from the surface of the beam in an effort to detect subsurface imperfections.

Chapter Two: Behind the Scenes (Heat Transfer)

As mentioned in the previous chapter, this section will expand upon the subject of heat transfer and its relationship with an anisotropic composite material. Conduction equations will be discussed as well as material and boundary characteristics for the beam flange as a lead-in for the FEA model development in the following chapter.

2.1: Energy Balance of a System

Introducing the heat energy balance equation:

$$\frac{dQ}{dt} = \int_{\partial\beta} q_i \cdot n_i \, dA$$

The overall change in heat energy, Q, within a volume, β, will be equal to the amount of heat flowing into or out of all the parts of the surface of the volume. Treating heat flux as a vector, it is convenient to divide it into two components: parallel and normal to the surface. The resultant of the dot product of the q_i and n_i vectors will yield the magnitude of the component of the flux normal to the surface. The integral sums the heat flow over the surface of the volume. Since heat energy will be flowing both in and out of the volume, the integrated sum will determine whether the overall temperature of volume is raised or lowered [Suryanarayana, 1995].

2.2: Modes of Heat Transfer

The previous section simply required heat flow into or out of a body. However, heat transfer can be broken down into three modes that would allow heat energy to be transferred to or from the surrounding environment: Convection, conduction and radiation. Convection involves heat energy transfer

through the mixing of particles in motion. Conduction is the transfer of energy through direct contact. Radiation is the energy emitted as electromagnetic waves. A key to heat transfer, and common to all three modes, is that the only way for net heat energy to be transferred is through the means of a thermal difference between the two substances [Suryanarayana, 1995] [Chapman, 1984]. An example in which all three are present would be when a stirring a glass of iced lemonade sitting out in the sun. Radiant energy from the sun is warming the drink. The cold ice is then in direct contact with the fluid which it will conductively cool as the ice cubes are warmed. As the drink is stirred, the cooled fluid next to the ice cubes is distributed within the glass and replaced by warmer fluid from the glass surface through convection.

Although all three modes of heat transfer are always present, limiting which ones are considered will have practical advantages. Documented results from NASA scientists has shown when dealing with thermal imaging, all three modes of heat transfer are, in fact, taking place, but if the surface emissivity remains constant, the heat loss due to convection and radiation on the surface are negligible when compared to the heat transferred away from the surface by internal conduction [Zalmalda, 1991]. In addition, since the principle objective is to note what is happening below the surface of a solid beam, convection cannot take place due to no particle movement, leaving conduction as the only mode of heat transfer within a solid.

2.3: Conduction

Conduction is distinguished by its occurrence within or across boundaries in a body [Chapman, 1984]. In this case, heat energy radiated from the external surface will indirectly provide insight to the thermal response of conduction on the material and internal boundaries. The general form of the conduction equation is as follows:

$$q_i = k_{ij} \cdot \partial T/\partial x_j$$

Or, in matrix notation:

$$\begin{pmatrix} q_x \\ q_y \\ q_z \end{pmatrix} = \begin{pmatrix} k_{xx} & k_{xy} & k_{xz} \\ k_{yx} & k_{yy} & k_{yz} \\ k_{zx} & k_{zy} & k_{zz} \end{pmatrix} \cdot \begin{pmatrix} \frac{\partial}{\partial x} T \\ \frac{\partial}{\partial y} T \\ \frac{\partial}{\partial z} T \end{pmatrix}$$

For a material that is isotropic, the conduction will be the same in all directions. This means that $k_{xx} = k_{yy} = k_{zz} = k$ and all other k's are equal to zero, no matter what orientation is represented. The conduction equation for an isotropic material is shown in its matrix form by:

$$\begin{pmatrix} q_x \\ q_y \\ q_z \end{pmatrix} = \begin{pmatrix} k & 0 & 0 \\ 0 & k & 0 \\ 0 & 0 & k \end{pmatrix} \cdot \begin{pmatrix} \frac{\partial}{\partial x} T \\ \frac{\partial}{\partial y} T \\ \frac{\partial}{\partial z} T \end{pmatrix}$$

This matrix equation will yield three scalar equations describing the conduction in the x, y, and z directions at any point within the volume. The heat flux will depend on the thermal gradient defined by the partial derivatives of the temperature with respect to the orthogonal direction denoted. Even in an isotropic material, these values may vary by location because of both the conductivity and the thermal gradient dependency in the results.

2.4 Conduction in a Composite Material

For a fiber reinforced composite material, the isotropic assumption will no

longer be applicable. However, using the coordinate system shown in Figure 2.1, the conduction coefficient values in the x and y directions, transverse to the fibers, will remain equal as k, but will differ from the direction parallel to the fiber axis, k_z. This will yield a bulk material with transversely isotropic properties in which any direction perpendicular to the fiber axis will have the same k value [Zalmalda, 1991]. A composite material, in the form of unidirectional fibers in a solid matrix resin, will exhibit thermal conductivity characteristics that are typically greater in the fiber direction than transversely.

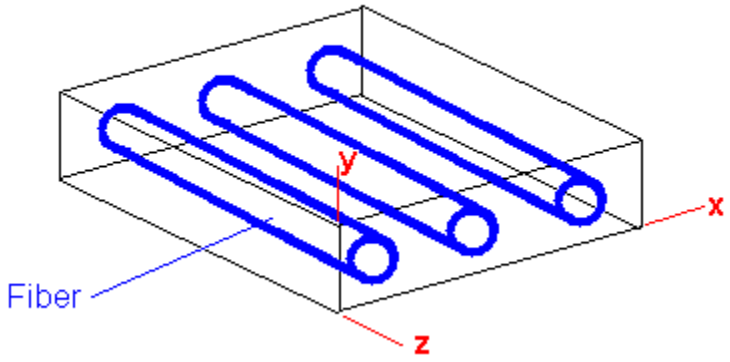

Figure 2.1: Composite Coordinate System

The new conduction equation in matrix form, with the coordinate orientation of Figure 2.1, for a transversely isotropic material can be written as follows:

$$\begin{pmatrix} q_x \\ q_y \\ q_z \end{pmatrix} = \begin{pmatrix} k & 0 & 0 \\ 0 & k & 0 \\ 0 & 0 & k_z \end{pmatrix} \cdot \begin{pmatrix} \frac{\partial}{\partial x} T \\ \frac{\partial}{\partial y} T \\ \frac{\partial}{\partial z} T \end{pmatrix}$$

For use in multilayered, multi-oriented composite system such as the beam flange (reference Figure 1.7 for a cross-section of the layers), composite laminar theory (CLT) needs to be employed in order to determine how all of the individual layers will interact and the final averaged bulk material values over the thickness. When involving multiple layers and orientations, all three k values will most likely differ.

2.5: Boundaries

For the purpose of this study, a boundary may be considered as the division plane between two entities of different conductivity values. And for what is needed here, that definition will suffice since the boundary of interest will be the interface between the carbon and glass regions. More importantly, this will also be the region of concern since delaminations along this boundary will influence the way this boundary will behave.

Conductivity across a delamination will depend on the nature of contact between the two opposing surfaces of the delamination. If the two material regions have separated and are not in full contact, as in Figure 2.2, the resistance to heat transfer across the boundary will be higher and restrict the heat energy flow in that direction [Suryanarayana, 1995]. In all actuality, the two surfaces may be in contact with each other but not perfectly with the areas of non-contact acting as the resistance [Winfree, 2003]. How well the two surfaces are in contact cannot always be determined and in the qualitative approach to uncovering imperfections along the boundary that will be used in this study, any type of abnormality with what will be determined “good” data will be considered imperfect.

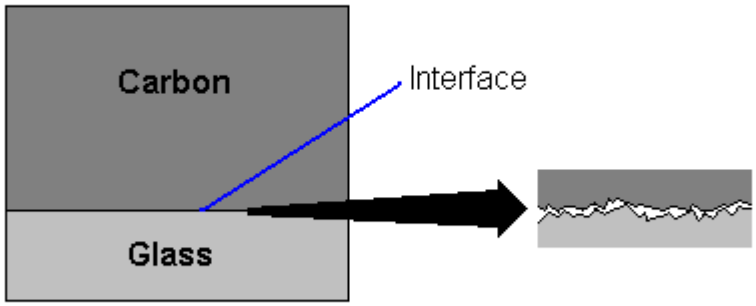

Figure 2.2: Material Interface with Imperfection

The effect of a delamination at the boundary between material regions will change the way heat energy will travel through the boundary. As a general rule, the heat energy will still move in all directions, but conduction, being a gradient driven process as well as dependant on the conductivity of the material, may have the higher gradient across the boundary but also the lower conduction. If the resultant of the gradient and the conductivity along the boundary is greater than across, the heat energy will be more likely to flow along the boundary instead of crossing it. Either way, the observed results should be different than those of a material with a mechanically connected boundary and be detectable with thermal imaging.

Another type of boundary that should be mentioned here but only indirectly affects the area of interest at the material interface is the outer edge of the flange. As the conductive thermal energy reaches the outside surface it is either radiated or convectively cooled by the surrounding air. For the most part, the consequence of this is that the edges of the flange will appear to be just slightly cooler than the majority of the material. As the primary region of interest is located near the center of the flange, this effect will be “negligible” when compared to the effects of conductivity at the boundary region. For the sake of

discussion, the top and bottom surfaces of the flange will be considered insulated and no heat transfer modes other than conductivity will be considered [Zalmalda, 1991].

2.6: The Beam Flange-Applying the Heat

Referencing the beam flange so the heat transfer concepts can be developed consistently with the intended application, the area of the flange of interest is depicted in Figure 2.3. In the figure, the orientation of the materials as well as how the heat energy will be applied can be seen. In general, the carbon layers will be more conductive than the glass layers [Callister, 1997].

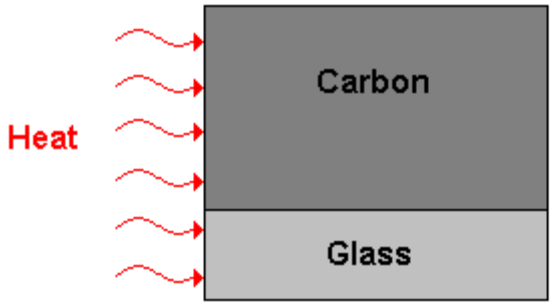

Figure 2.3: Heat Energy Application and Orientation of Materials in Beam Flange

For the experimental measurements, a heat lamp will use radiant energy to elevate the surface temperature. In order for the surface to be "uniformly" heated, the absorptivity of both the carbon and glass regions must be equal. Assuming a "gray" surface, Kirchhoff's Law states the absorptivity and emissivity are equal to each other [Suryanarayana, 1995]. Throughout the analysis and laboratory testing, the emissivity of the flange surface was assumed uniform and a visual inspection would show that the surface does not appear different over the two regions.

Figure 2.3 shows the heat being applied on the face of the flange when viewed from the outside. This location was chosen in that early experimental testing showed that large amounts of energy would have to be applied in order to heat the flange through its entire thickness from the top or bottom surfaces and be able to view the reaction of the boundary between the regions. For reasons and testing constraints to be discussed in Chapter Seven, this was not acceptable and left only the outside face for heating. Since this was also the area to be viewed with the camera, it made the heating and observation surfaces common. As a benefit and since equal amounts of energy per surface area were to be applied to both the carbon and glass regions, any anomalies below the surface would be visible due to disruptions in the thermal gradients created by the different conductivities of the regions [Coakley, 2004].

Chapter Three: Building the Model (Analytical Process)

Now that all of the pieces of this undertaking are in place, putting them together in a coherent matter and producing results is necessary. By using computer models simulating the beam flange, two with delaminations and a third without, the analytical results can be compared and contrasted to the experimental results, validating the procedure and analytical method in general.

3.1: Overview of ANSYS and the Models

For starters, ANSYS is a solid modeling program with finite element analysis (FEA) capabilities. It is produced by ANSYS, Inc. and the version used was ANSYS 7.1. In a transient thermal analysis mode, it has the ability to apply a thermal load along with boundary conditions to produce results of heat energy transferred throughout a volume with respect to defined material properties and orientations.

Within a volume, ANSYS has the ability to define individual layers of a composite material and associate ply orientations with material characteristics for each layer making it exceptionally useful for analysis in laminates. However, due to constraints of the IR camera to be discussed in chapter four, and mesh limitations outlined in section 3.4, using a model of that detail would not be useful due to the lack of resolution of the laboratory results. Therefore, the carbon and glass regions were modeled as bulk materials with derived average material values for each region.

By using different models, one intact and the other with a simulated delamination, the results of the analysis can be compared and contrasted with each other and then with the experimental results. The “intact” model allows for conduction between the two material volumes to be unrestricted while the “delaminated” models will introduce a thin, third material along the interface with

reduced material values to restrict the conduction between the material regions.

The methodology of constructing the models consisted of determining material values as well as several iterations of geometries for the volumes, volume divisions, meshes, and loading characteristics.

3.2: Volumes

Modeling of the entire flange of the DWIB would necessitate a large model and since the applied thermal loading was localized, a smaller representative section of the flange could be used and allow for a much smaller model. Creating a model, mesh, and developing similar loading conditions to the laboratory experimentation showed that the heat energy was not penetrating further than a half inch into the flange in the z-direction. The resulting flange geometry for the simplified model was selected as 1 x 8 x 1 inch (depth into the flange by distance along the length of the beam by thickness of the flange). The ensuing collection of volumes consisted of six volumes, three of each material, and is shown in Figure 3.1 with the carbon region being gray and the glass, blue. The reasoning behind the divisions along the z-axis was to create a surface on the y-z face to apply the initial conditions. This was a requirement to create a smaller face on the entire surface that would allow only part of the entire face to be heated. Without doing this, the initial loading would have had to cover the entire face and not allowed for conduction in the z-direction at the edges of the heated region into the unheated regions.

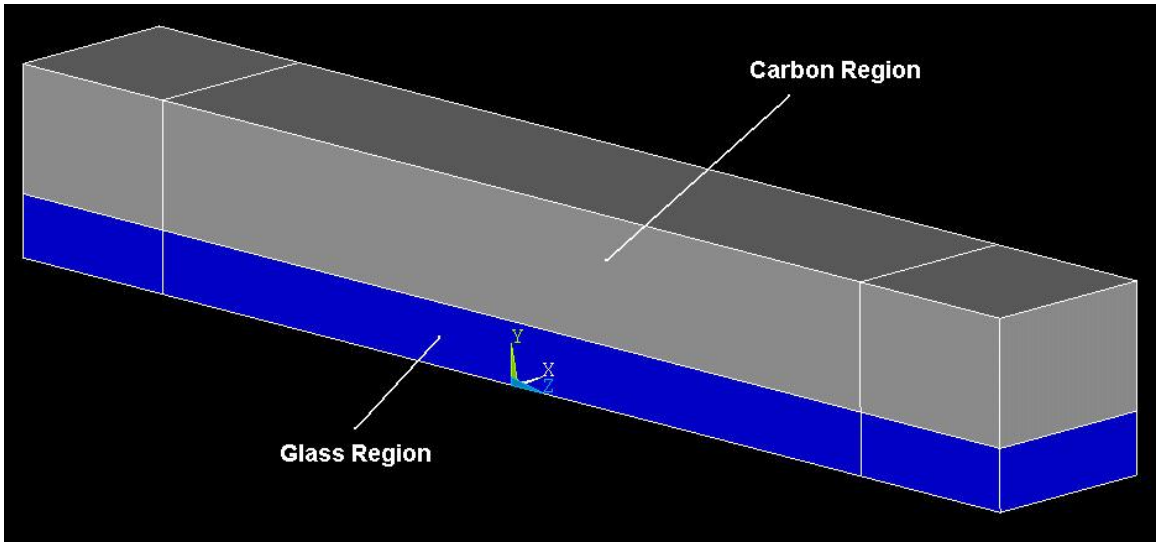

Figure 3.1: ANSYS Model of Beam Flange Volumes – "Intact" Model – Isometric View

The second of the models included the "delamination." Since ANSYS would not allow a gap of "nothing" to be a delamination, a thin slab of a third material was introduced between the carbon and glass regions. The development of this material will be discussed in section 3.5 while the model volumes are depicted in Figure 3.2. The red section between the grey and blue carbon and glass regions is the delamination material.

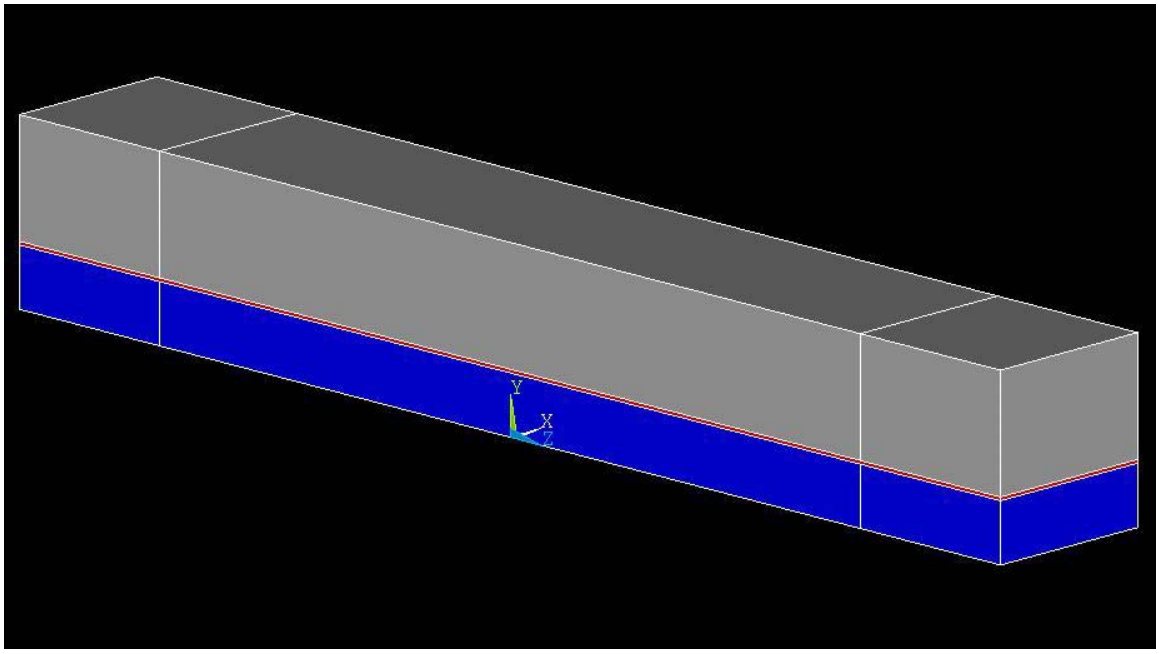

Figure 3.2: "Delaminated" Model – Isometric View

The third model was derived from the full-length delamination model. However, instead of a single volume for the delamination region, it was divided into three. This allowed for a one inch center section to be designated as delaminated and the others to be normal carbon regions. A close-up of the face is seen in Figure 3.3.

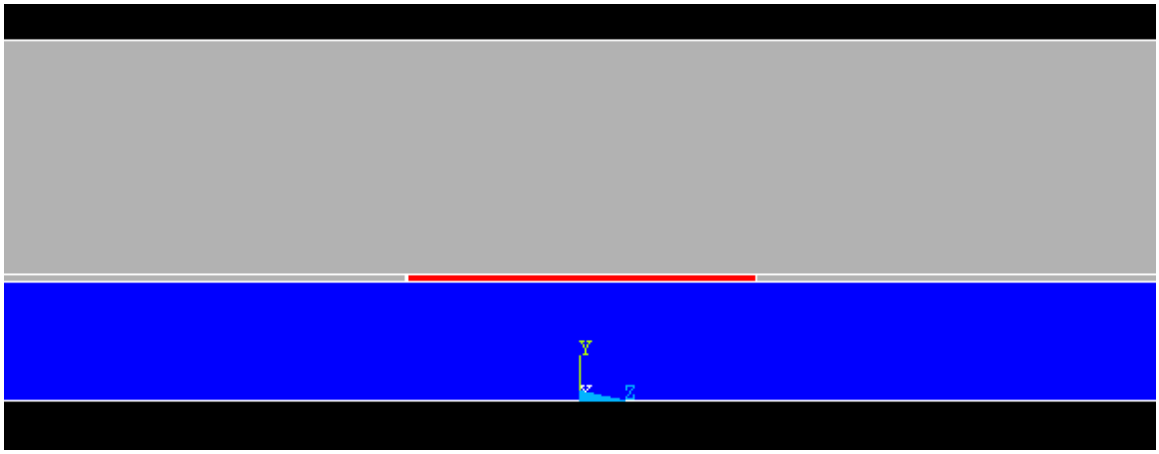

Figure 3.3: Delamination model with 1 inch Center Section

3.3: Material Values

A primary factor in producing accurate FEA results is having data values that are appropriate. While material values for both the carbon and glass regions of the beam flange were not available, another study at Virginia Tech had determined the ply orientation, thicknesses and volume fractions of the layers in the flange [Hayes, 2003]. Using a CLT program called CompositePro (version 2.1 by Peak Innovations), this layup was modeled and the material values in Tables 3.1 and 3.2 were calculated using as much of the actual beam data as was available. Also, in Section 2.4, it was mentioned that transverse isotropy was assumed for a unidirectional composite layer. However, the results of the CLT program did not show transverse isotropy due to the layering effect on having unidirectional layers as well as fiberglass mat and other layers such as +/- 45 degrees in between the unidirectional layers.

Table 3.1: Material Values of the Glass Region

Density	1797 kg/m^3
Specific Heat, C_p	1087 J/kg K
Fiber-direction Conductivity, k_z	.4501 W/m K
Transverse Conductivity, k_x	.4001 W/m K
Transverse Conductivity, k_y	.2493 W/m K

Table 3.2: Material Values of the Carbon Region

Density	1627 kg/m^3
Specific Heat, C_p	1057 J/kg K
Fiber-direction Conductivity, k_z	44.69 W/m K
Transverse Conductivity, k_x	.4050 W/m K
Transverse Conductivity, k_y	.3107 W/m K

Material values for the type of fiberglass, E-glass, and vinyl ester are generally in agreement between sources since there is little variation between manufacturers. However, this doe not hold true for carbon fiber. The carbon material varies widely with manufacturing process and grade [Hyer, 1998, Gibson, 1994, Donnet, 1990, Matweb]. Several varieties of carbon fiber were used in generating material values for the carbon region and were tested against the laboratory results. The high modulus carbon from the CompositePro material database fit the best to the beam materials and was used to achieve the values in table 3.2.

3.4: Developing the Mesh

With respect to meshing in ANSYS 7.1, there are two different mesh types

that were appropriate for a thermal analysis and a 3-D solid, SOLID 70 and SOLID 90. These two elements were similar except that the SOLID 90 also included a mid-point node along the edges of the element. Of the two, the SOLID 70 was more appropriate for the situation and was used as a brick element. When meshing the volumes, the material values and orientation could be designated, ensuring the material properties were oriented correctly. Also, since FEA uses the mesh elements to implement boundary conditions as well as material properties, the discussion of Section 1.8 stated that conductivity will drive the thermal analysis. With respect to the boundary conditions, convection and radiation surface conditions can be applied to the elements.

Directly relating to meshed layered composite materials, one may ask why a layered mesh that ANSYS has developed specifically for composites was not used. Simply, the version used, ANSYS 7.1, does not yet handle thermal analysis. While if it did, it would be a great attribute for generating even more accurate results associated with the theoretical layup of the flange.

With respect to determining the appropriate size of the mesh of the bulk regions, the best way to handle this was to compare the results of progressively smaller meshes. A 5 mm mesh allowed for two divisions in the glass region and four in the carbon region and was the starting point. It is shown in Figure 3.4. Two other meshes were also created, a 2.5 mm and a 1.25 mm, which doubled and quadrupled the divisions, respectively. Under the same loading conditions, vertical line profiles at the center of the flange section were extracted from ANSYS for the three meshes and are shown in Figure 3.5. The results were sampled at the 1st second time interval and will be the same for all results shown in this chapter. The temperature difference at the boundary node between the carbon and glass regions node was less than of a hundredth of a degree C between the 5 mm and 1.25 mm meshes. Since the degree of precision to a hundredth of a degree was not necessary in this study, the only benefit of using

the smaller mesh would be to have smaller divisions along the surface to generate the temperature profile. But, with respect to the reduced computational time and the use of “bulk” materials, the larger mesh was determined to be sufficient in modeling the appropriate trends and will be used for the remainder of this discussion.

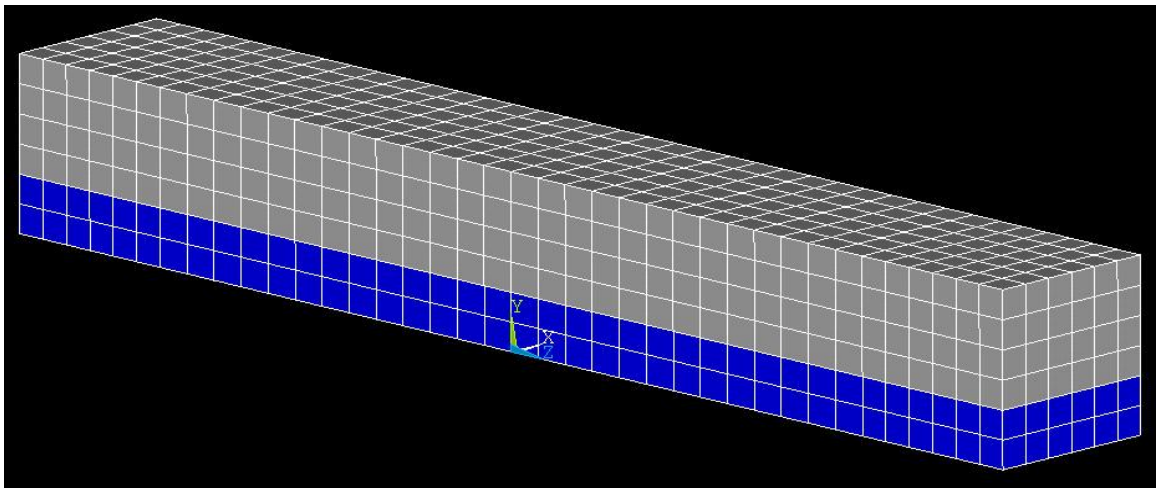

Figure 3.4: Meshed “Intact” Model – Isometric View

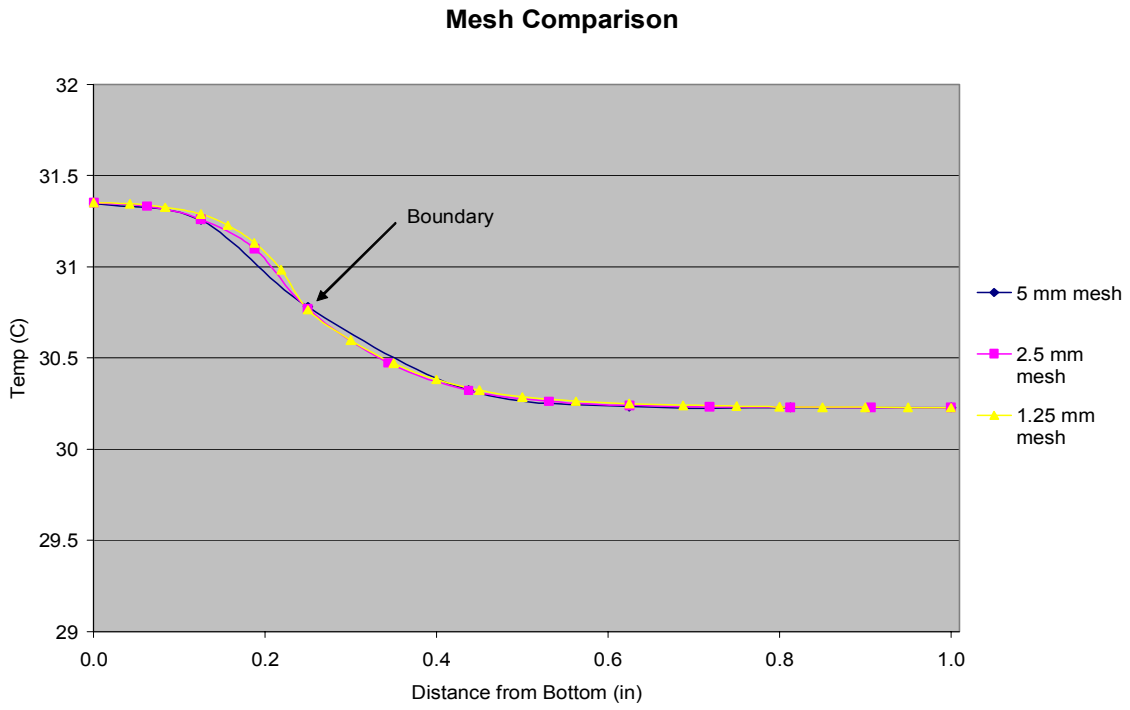

Figure 3.5: Nodal Solution Temperature Profile for the Different Meshes

Figure 3.6 shows the "delaminated" model with its mesh. In order to determine if the mesh size would affect the material values in the delamination region, the values for the carbon region were entered into the delamination material. The desired result would be similar output from the models with and without a delamination. Running the two models under the same conditions, the results showed that the difference in the mesh size did not affect the results significantly and are displayed in Figure 3.7.

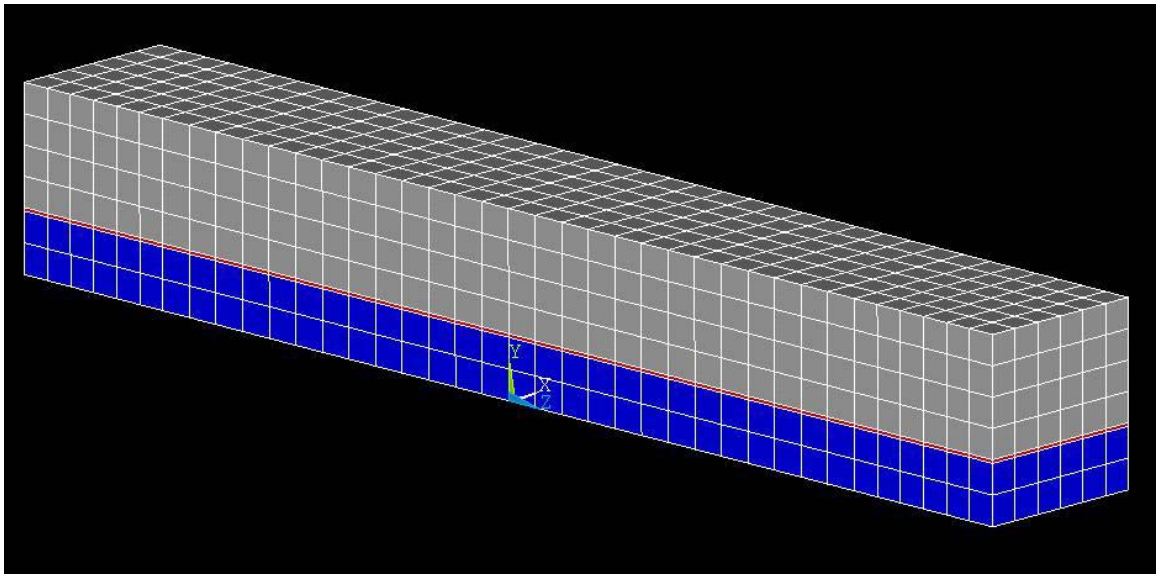

Figure 3.6: Meshed "Delaminated" Model

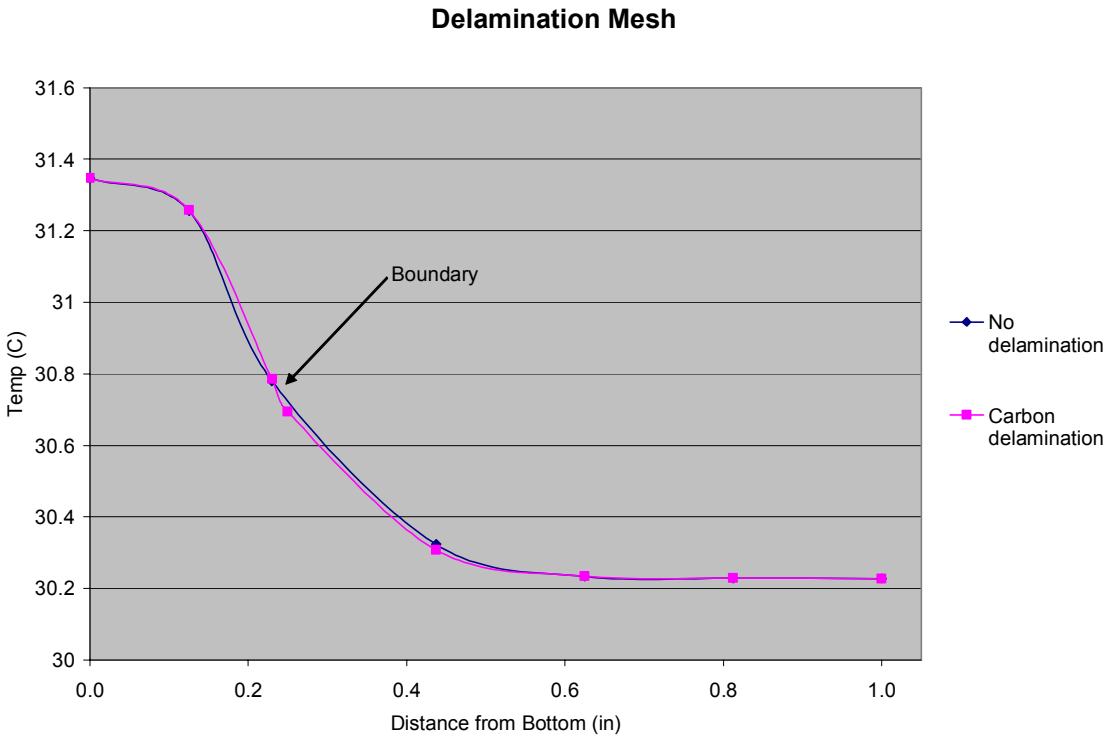

Figure 3.7: Results of the "Delaminated" Mesh with Carbon Region Values

3.5: Creating the Delamination

In order to create a delamination in ANSYS, “something” had to occupy the space between the two material regions. By leaving a gap in which the two materials are not touching, FEA has no way of generating results such that convection and radiation across the gap could take place as in real life. The result would be the free run of the two material regions with no interaction between them with exactly similar results as if they were two different models. So, a thin material had to be inserted in between the carbon and glass regions with the material values selected to represent the effects of the delamination. Figure 3.8 shows the y-z face of the flange with the delamination material in red.

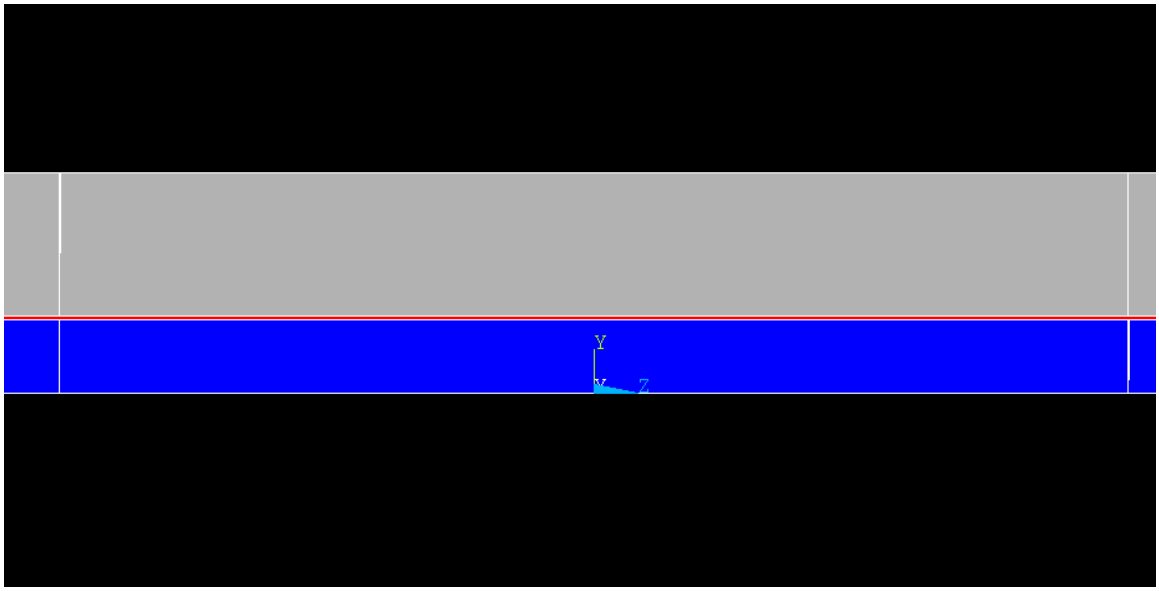

Figure 3.8: “Delamination” Face Close-up

Since the certainty of the relationship between the regions with a delaminated boundary was not exactly known, a material that would simulate characteristics of a delamination needed to be developed. As a base point, a

model with “nothing” or null values was created along with a case where the material properties of air were used in the delamination material. The results showed the differences between the two situations and are displayed in Figure 3.9. The results were similar in that “nothing” did not allow any conduction between the regions while air showed very little. This confirms that air is a thermal insulator and that a “material” would need to be created for a more accurate representation of a delamination. The delamination gap is at .25 inches from the bottom in all the FEA results.

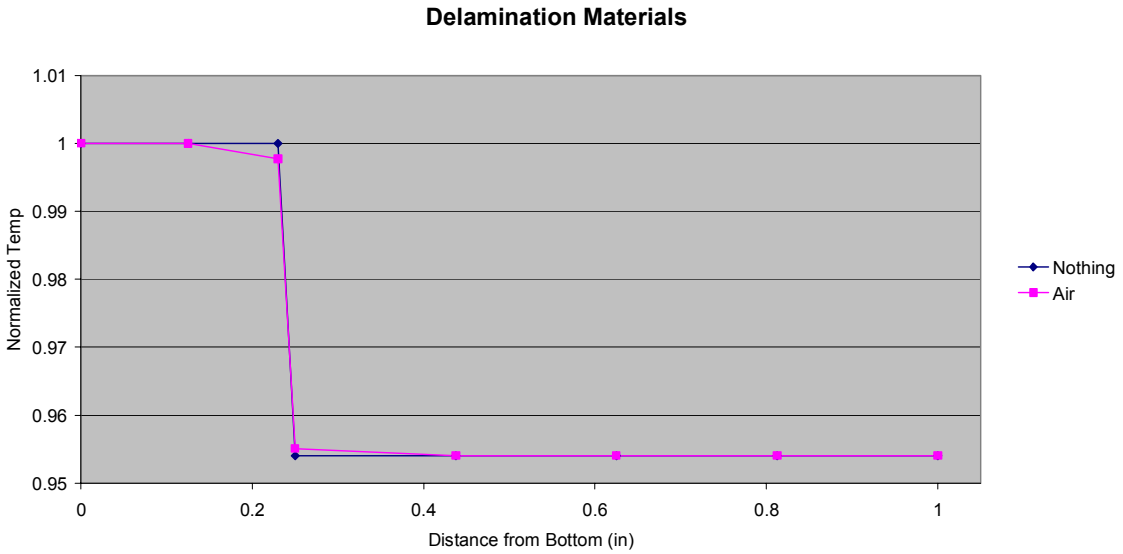

Figure 3.9: Comparison of Air and “Nothing”

Developing a delamination material consisted of testing two thicknesses while varying conductivities. The approach was to not create an exact delamination in the physical sense, but a boundary region that would mimic the thermal response of the delamination. Since the delaminated surfaces may still be in contact with each other, there may be no real thickness to the region. However, by assigning a thickness and reducing the conductivity of the material by some order of magnitude, the resulting material would simulate what would

happen if the materials were still in contact with each other, but with a reduced contact area. Reducing the conductivity values was considered to be the simplest way to model a reduced contact area in the delamination material between the carbon and glass material regions. The two thicknesses for the gaps were .25 and .5 mm with the conductivities being reduced by factors of 10, 20 and 30 of the carbon region values. Figures 3.10 and 3.11 illustrate the results and show that the larger delamination thickness as well as lowering the conductivity of the region would yield a higher resistance to conduction across the boundary. Taking the k/30 plots for each thickness, Figure 3.12 was developed. Based on the laboratory results, the larger delamination thickness with the lowest of the three conductivities was selected as the most appropriate.

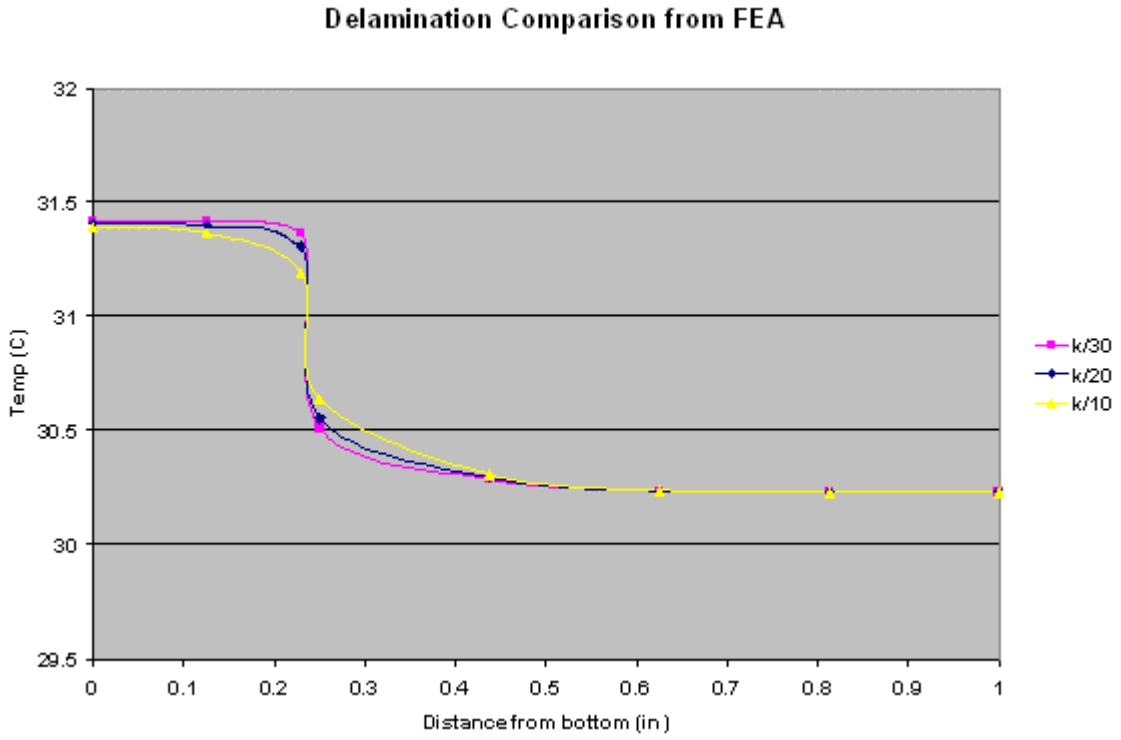

Figure 3.10: Temperature Profiles from a .5 mm Gap

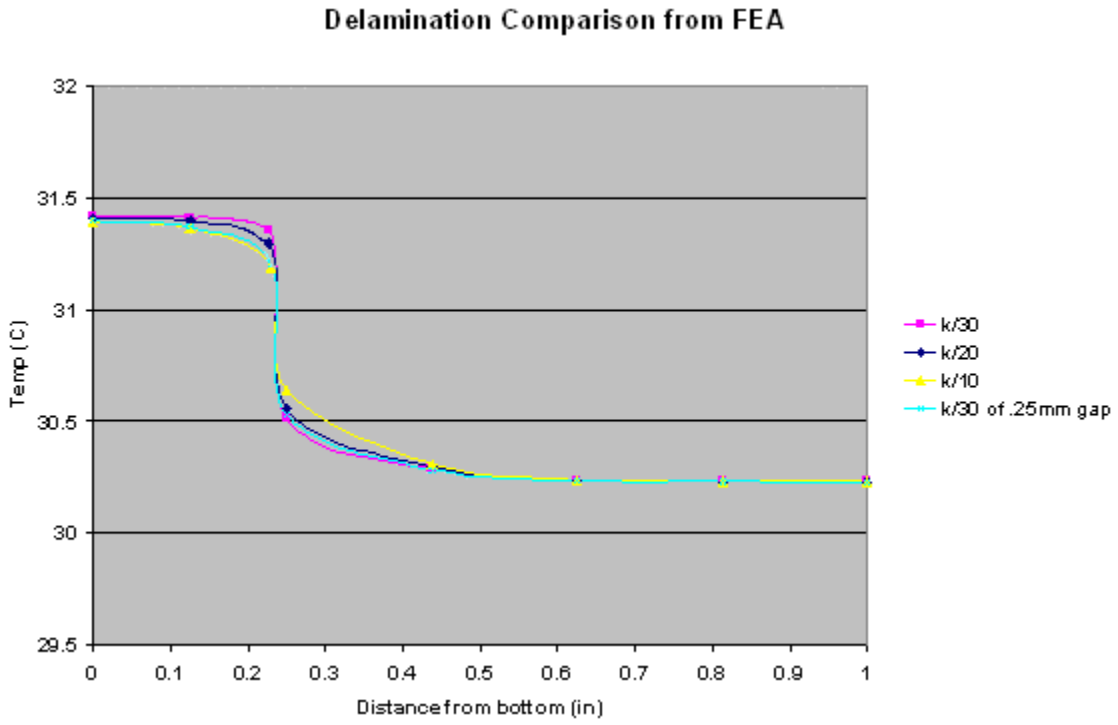

Figure 3.11: Temperature Profile with .25 mm Gap Added

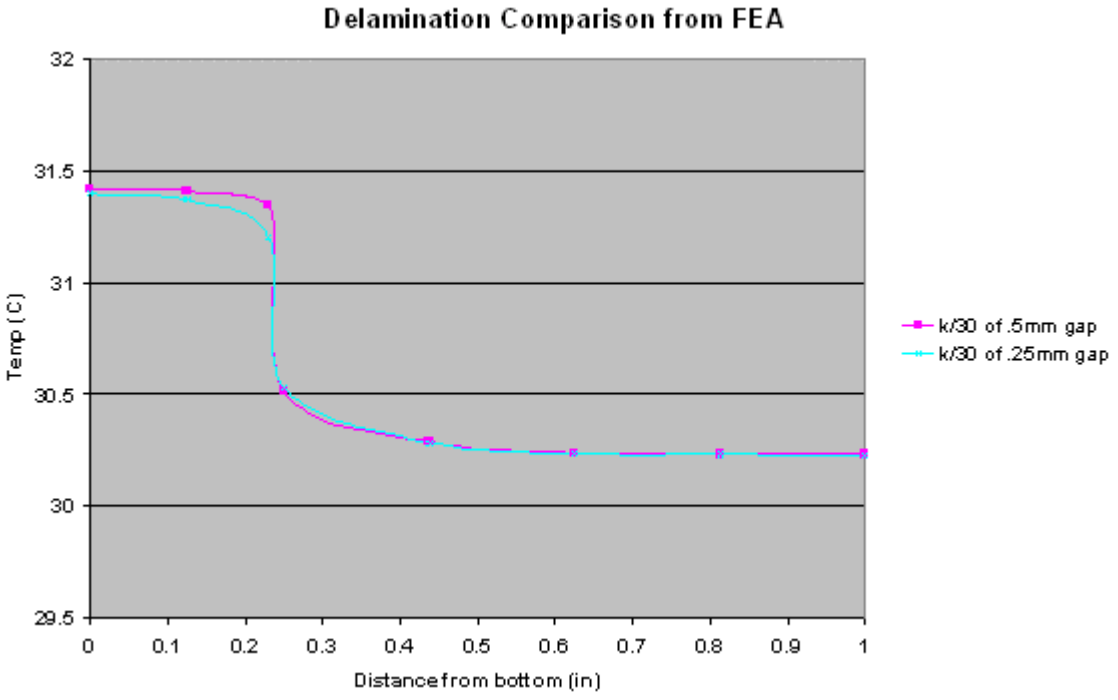

Figure 3.12: Comparison of k/30 of the Two Gap Sizes

3.6: Thermal Loading Characteristics and Running the Model

Thermal loading characteristics for the models consisted of adjusting the initial conditions. The appropriate elevated temperature was determined by measuring the surface temperature of the flange during laboratory heating and interpreting the ANSYS results.

In order to set the initial condition for the models, the initial values of the nodes for the entire model were first set to an ambient temperature. Utilizing the smaller face on the y-z surface of the flange, this face was selected and its associated elements were assigned the higher conditions. Originally, only the surface nodes were selected but this did not produce results that correlated well with the experimental results. Further investigation as to how to better elevate the surface temperature yielded the procedure for loading the surface elements rather than the surface area. This created a thin volume of elevated material and produced the most accurate results.

Running the model consisted of initiating a transient analysis and allowing the heat energy to dissipate over a given time span with data being computed at one second intervals. To be discussed in the following chapter, time periods came from the laboratory procedure and were used to appropriately compare the results from both the laboratory and the FEA.

Collecting the data was a matter of writing the time-temperature data from specified nodes on the heated face to a spreadsheet file.

Chapter Four: Theory in Practice (Experimental Process)

Taking a step away from theory, this chapter goes into the details of the experimental procedure and setup used for collecting laboratory data. Beyond stating the process, the rationale for the approach will be discussed.

4.1: Laboratory Setup

For the entire stint of time in the laboratory, the primary parts of the experimental equipment list stayed the same and included the infrared camera, halogen lamp for heating, three different sections of the beam, and a computer to record, refine, and then analyze the raw data. Following will be a description of each piece of equipment and the part it played in the procedure.

Infrared camera: Raytheon Radiance 1t. This IR camera uses an indium antimonide focal plane array detector most sensitive to radiation between the wavelengths of 3 and 5 microns. The output was in the form of a 256 x 256 pixel 12-bit digital image [Raytheon]. A selection of lens options including 25, 50 and 100 mm lenses were included for use with the camera.

Computer system: Micron PC with 266MHz Pentium II processor, 127Mb RAM, 2Gb hard drive, PCMCI card slot for external image disks, Microsoft Office and the Image Desk II analysis software program that allowed for many different analysis options. The computer and camera were configured to allow camera operation, control, and display to take place via the computer.

Halogen lamp: 500Watt service lamp with the protective screen on its face removed to allow it to be placed close to the beam surface.

Beam sections: The overall size of the beam was 36 inches high and even though it was lighter than a comparable steel beam, it was still quite heavy and the smallest 20 foot sections did not make a full beam portable enough to easily move around a lab. As a result of this, two sections approximately 30 inches long

were cut from one of the full-length beams. Both included the entire flange and about 8 inches of the double web.

The major difference between the two sections of beam was how much they had been delaminated. When the full beam had been loaded to failure, the central area of the beam, more or less, exploded, splintering a majority of the flange (reference Figures 1.4 and 1.5 for images). However, as one would move away from the splintered center section towards the ends, the breakage would diminish. A transition region existed neighboring what would appear to be a perfectly intact remainder of the beam length. The two sections were removed from the transition and intact regions. The one closest to the failure region was fully delaminated, meaning the web had totally separated from the flange at the carbon/glass interface. The second section continued with being fully delaminated and over its length traversed the intermediate region to fully intact at the opposite end. This section would be very important in testing in that it contained fully intact, fully delaminated and partially attached regions depending on where the evaluation was performed on the section. Figure 4.1 shows this section of beam in which the edge of the delamination can be seen along the outside edge of the flange.

Figure 4.1: Beam Section with Crack

4.2: Laboratory Procedure

Once all of the equipment was in place, running the experiments was straightforward. Primarily, it involved a simple routine of preparing the computer for data acquisition, directing the lamp at the beam flange, setting up the camera, starting the computer data acquisition, turning on the lamp for a given time interval, moving the lamp out of the way and then recording the response of the beam over a second time interval. Even though all the times and equipment spacing were adjustable, this general procedure was repeated.

After an initial period of trial and error, the experimental procedure established itself as the following: Heat with the lamp center 1” away from the flange and remove from the camera field of view which was placed 16” away from the flange behind the lamp. It was also necessary to manipulate the raw data from the images into a usable form and analyze the results. Figures 4.2 to 4.4 show the laboratory setup as it was used.

Figure 4.2: Laboratory Setup

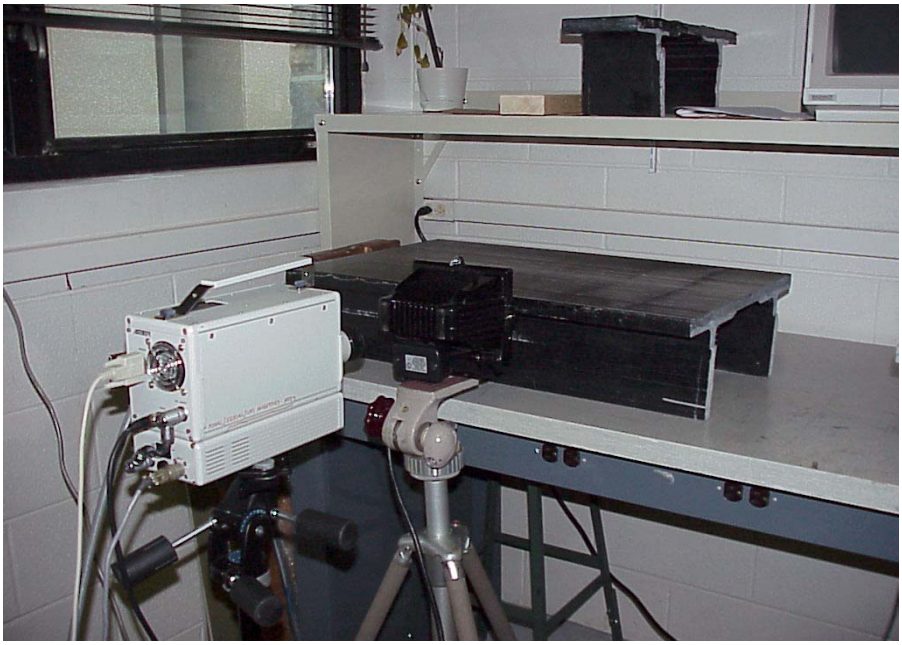

Figure 4.3: Lab Setup-Camera, Lamp, and Beam

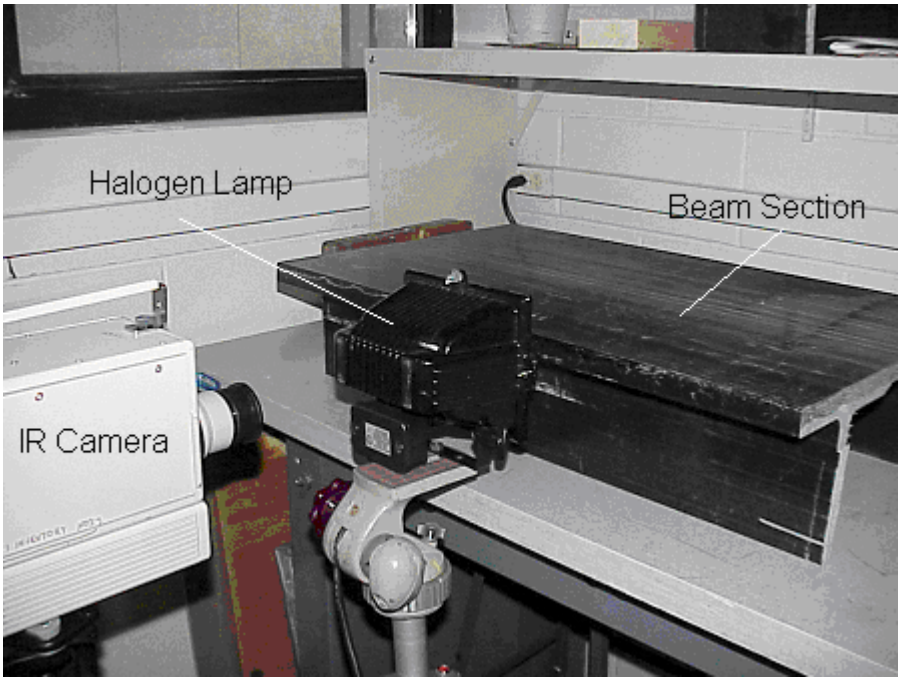

Figure 4.4: Lab Setup- Camera, Lamp, and Beam Close-up

Expanding upon the "trial and error" aspect of developing the test procedure, defining the range of the variables is necessary:

The positioning of the heat lamp and the camera were related in that the lamp had to remain close to the beam in order to produce the most even heating of the surface. Positions closer than one inch had a tendency to damage the surface and those further away yielded irregular surface temperatures. Using the 50mm lens with the IR camera, the 4 to 5" area that the lamp was able to heat would fill most of the acquisition area of the camera when placed 16" away.

The remaining two variables of importance were how long to apply the heat and how long to acquire data. Since field testing would involve many linear feet of flange to examine, one of the original goals was to minimize inspection time. A procedure to gradually increase the heating time and interpret the results

was used. For the most part, heating at either one second or 15 seconds produced similar shaped thermal profiles (with the difference being overall magnitude since a longer heating time resulted in a higher surface temperature) as long as the first few seconds after the heating were able to be captured through the camera. Acquisition time started before the lamp was turned on and continued until the experiment passed out of the highly transient period into something that resembled a steady-state situation where there is heat flow taking place, but the differences between the carbon and glass regions are not distinctive. This time could have been shortened, but having more data to work with was considered better than not acquiring enough.

Chapter Five: The Resulting Data-Validating the Model

Once the halogen lamp was turned on and the initial conditions in ANSYS established, there was the challenge of taking each respective set of results and putting them into a comparable form. Also, in order to be assured that the resulting data were accurate, a set of tests with known materials were developed as verification.

5.1: Collecting the Data

The IR camera collects the surface temperatures of the sample at any one time. From a qualitative standpoint, these surface pictures may be evaluated for irregularities. In order to generate quantitative results, the surface response is collected at one second intervals. If one were to face the beam flange and view the outside surface, the beam flange just after heating would appear as in Figure 5.1.

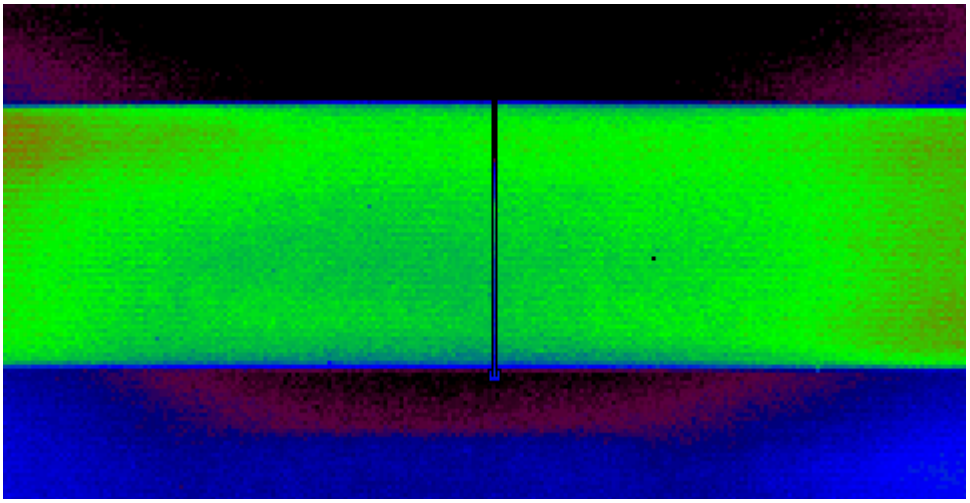

Figure 5.1: IR Picture of Flange Showing AOI Line

To simplify the entire surface image into a more usable form, a specific area of interest (AOI) in the form of a vertical line was selected. Now, instead of comparing an entire surface, the results from a single column of pixel data were compared. This line AOI will generate the thermal response in the following form:

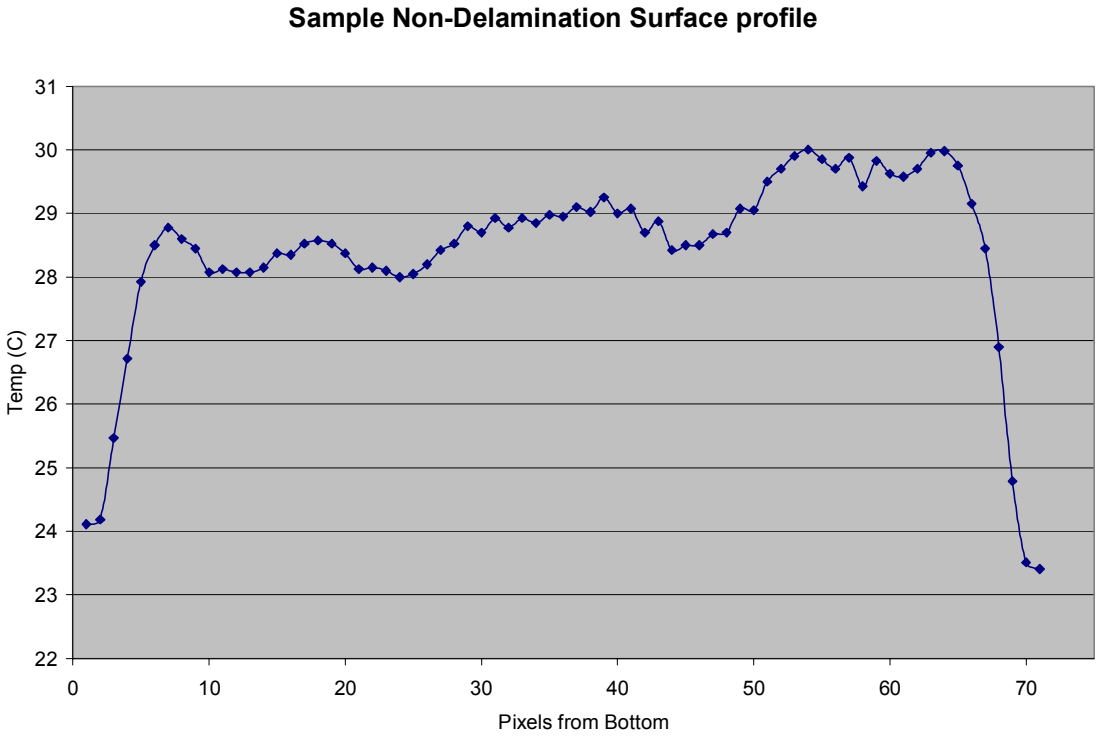

Figure 5.2: AOI Line Profile Displaying Flange Surface Temperature

The far left pixels are the bottom of the flange with the right being the top. The surface of the flange may only range a few degrees and to be sure the entire surface is captured, the AOI line was extended past the edges which explain the lower temperature pixels at either end of the results.

Since a single line profile only shows the results of one second's worth of data, each successive set of data may be plotted to show the surface temperature decay by generating a time-temperature-pixel surface as in Figure

5.3. Figure 5.4 shows the temperature-time decay profile from a single pixel, 57 in this instance. In order to compare the experimental and FEA data in a quantitative manner, it is convenient to use individual points of the surface for correlations rather than the entire surface. Note that the most transient part of the data was observed to occur within the first ten seconds of decay.

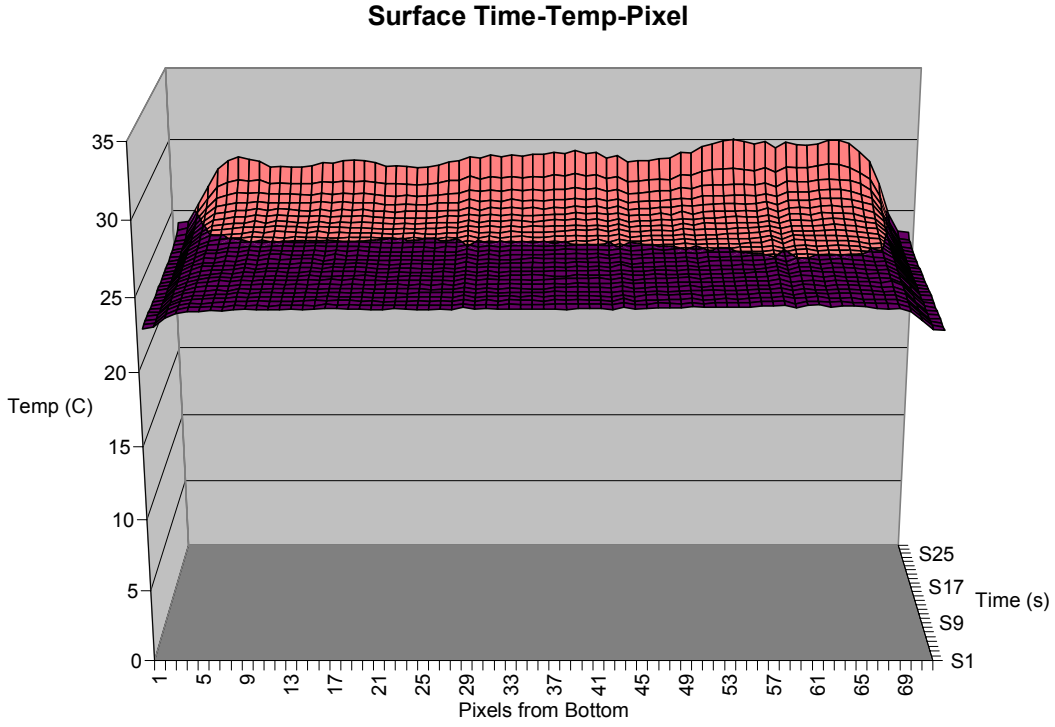

Figure 5.3: Surface Decay Profile

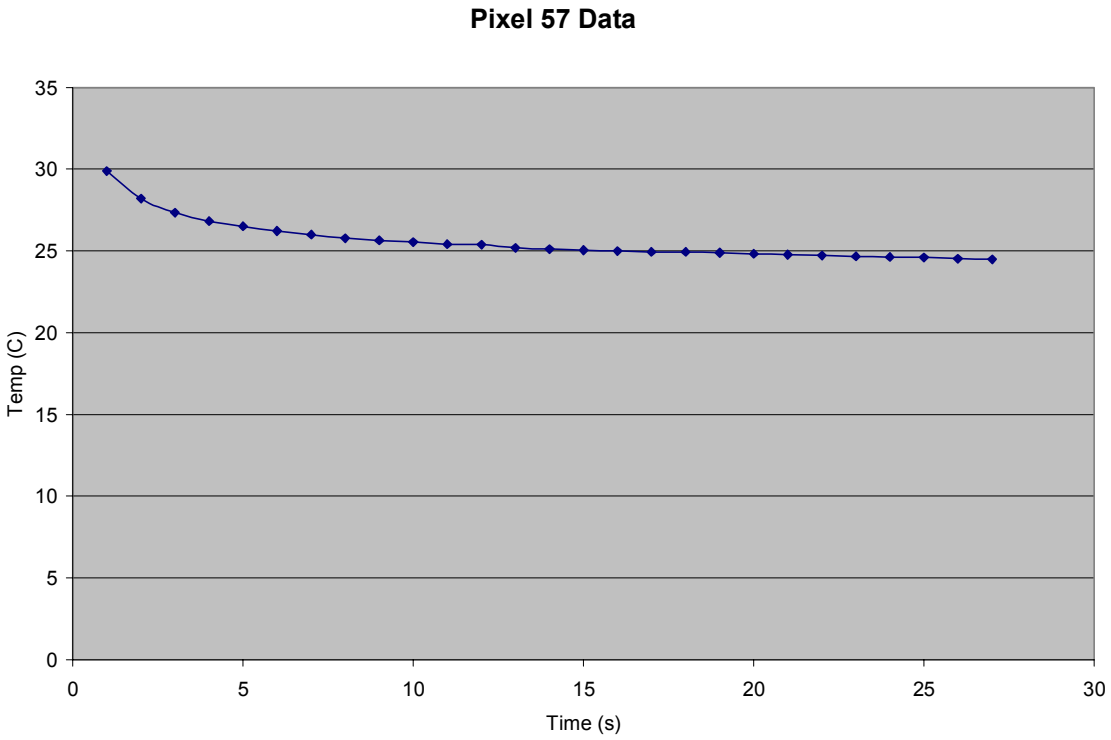

Figure 5.4: Temperature-Time Decay Profile for a Single Pixel

5.2: Fabricated Test Samples

One drawback of testing was the irregularity of the flange layup as first mentioned in section 1.3. A second difficulty was that the values of the material used to create the beam were not available and had to be estimated. In order to show that the ANSYS model was behaving properly and as expected, several test samples were constructed, tested, and analyzed in the same manner as the beam flange. The goal of these validation samples was to take known materials and fabricate test samples for which the material parameters and ratios were either known or could be determined.

The process for making the samples involved the hand layup of thin sheets and then cutting the sheets into strips. The strips were then bonded together with the resulting samples being a set of blocks consisting of

unidirectional carbon fiber and biaxial fiberglass with polyester and epoxy matrices and the general dimensions of the beam flange. This process allowed some minor inconsistencies in the materials to be present. For the most part, these were insignificant, but when applying thermal imaging, they caused slight thermal variations across the surface in the form of undulations as shown in the surface decay profile in Figure 5.5. Since many of these undulations were local with respect to position along the length of the sample, more regular areas were considered. Ultimately, the entire surface was painted flat black which resulted in the most consistent surface profile shown in Figure 5.6.

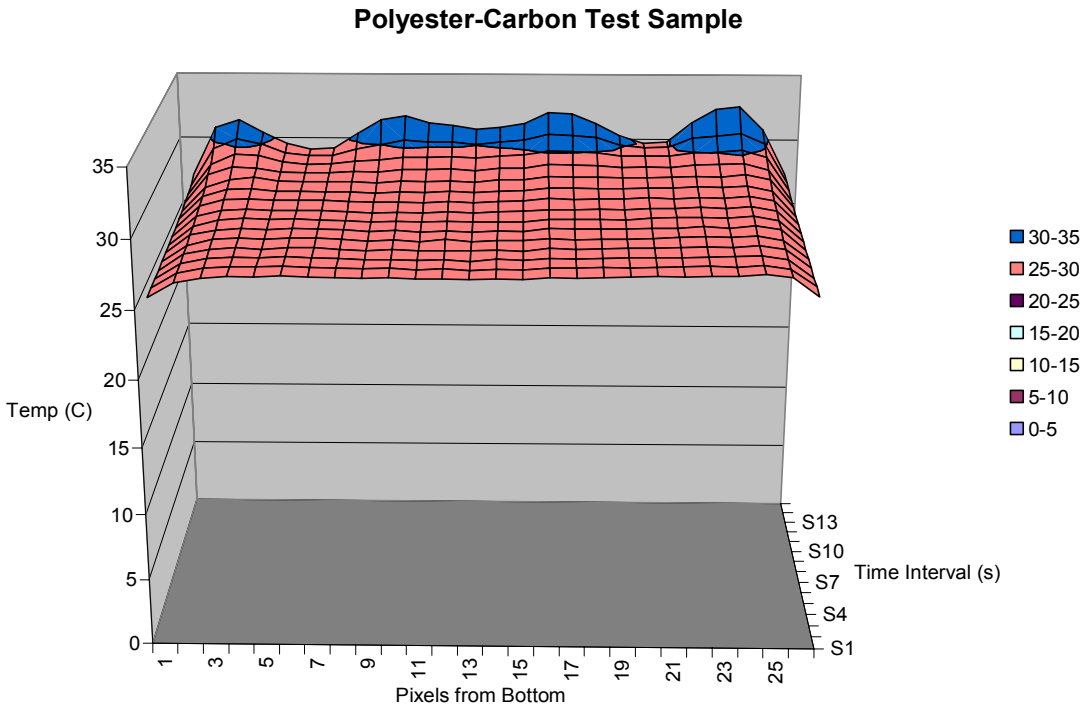

Figure 5.5: Surface Decay Profile of the Polyester-Carbon Test Sample

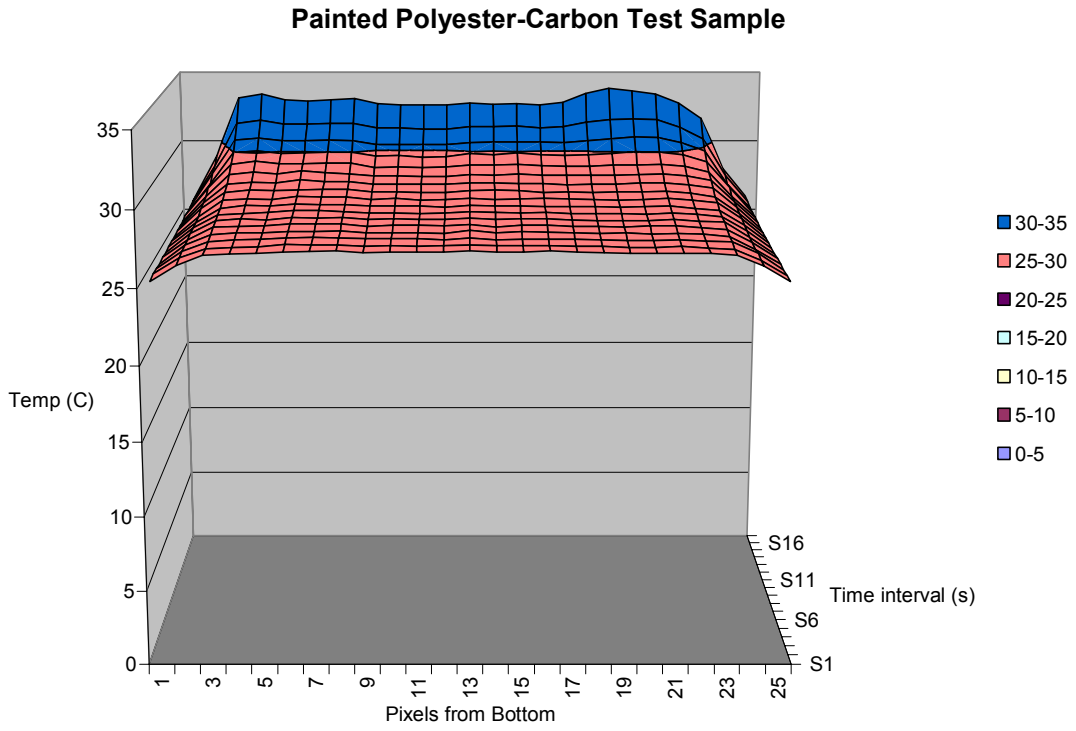

Figure 5.6: Surface Decay Profile of the Painted Polyester-Carbon Test Sample

5.3: Averaging the data

With the ANSYS results, the surface profile is an ideal solution generated from both uniform material values and initial surface conditions. Consequently, there are no variations in the surface results within a single material region except where the boundary between the carbon and glass regions comes into play. In order to effectively compare the ANSYS with the experimental results, the surfaces of the carbon and glass regions were, away from the carbon-glass boundary, averaged to obtain a single temperature-time plot.

For the sake of a continuous line of thought for the following discussion, the results of the polyester-carbon sample will be used and are shown in Figure 5.7.

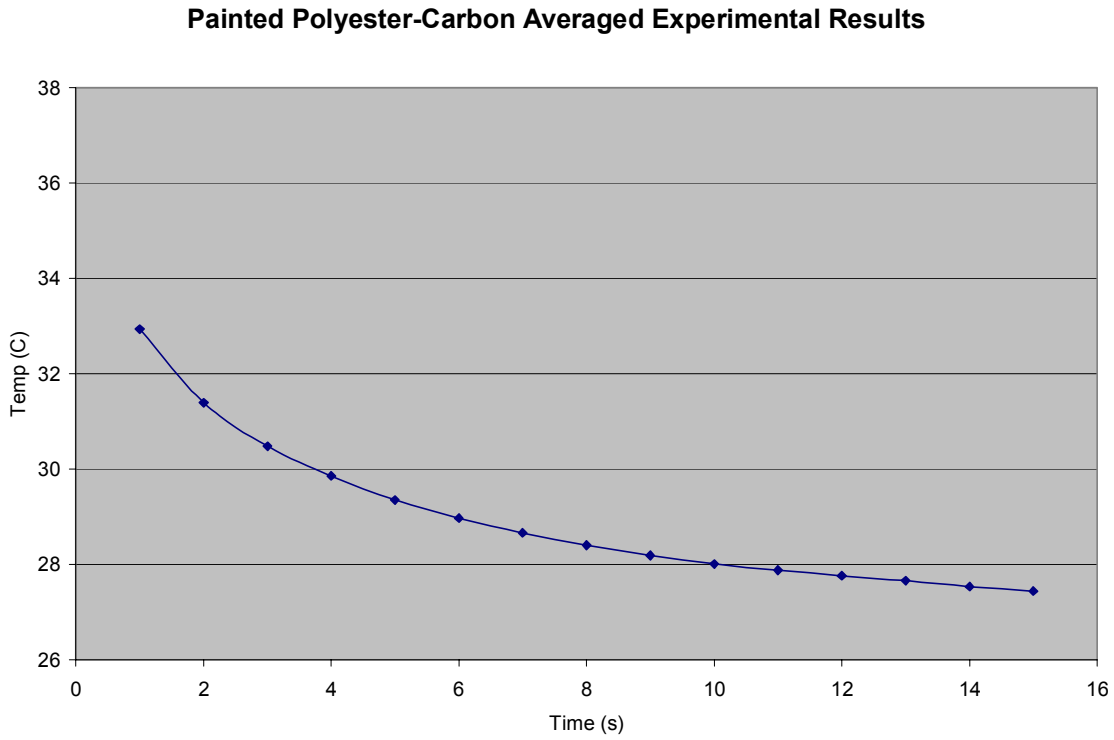

Figure 5.7: Temperature-Time Decay for the Polyester-Carbon Sample

Similarly, the results from the ANSYS FEA can be plotted by using the nodal response of a point within a region and then superimposed over the experimental results. Figure 5.8 shows the decay profile from 5.7 with a set of FEA results. To denote some of the terminology used with the FEA results, the legend calls out two numbers: 45 and 23.2. These are the initial conditions the model was set at with 23.2 degrees C being the ambient and initial temperature and 45 degrees C the temperature of the heated surface.

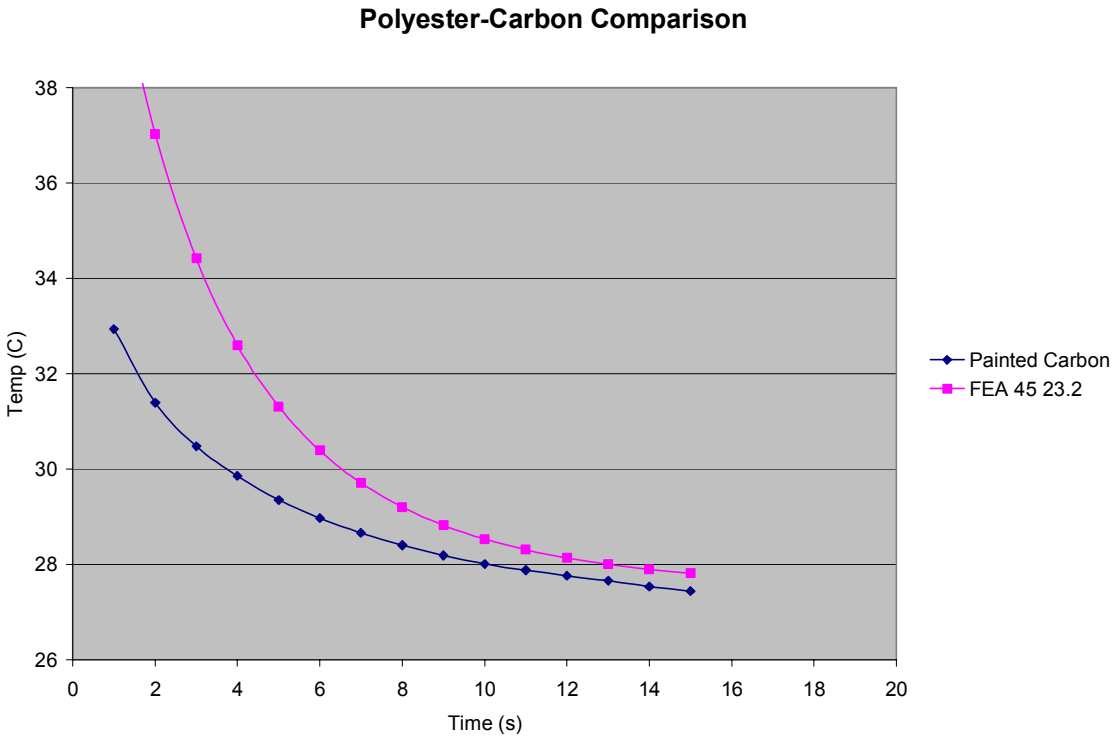

Figure 5.8: Polyester-Carbon Experimental and FEA Comparison

5.4: Shifting the Time Intervals

One might note that the two decay profiles from Figure 5.8 do not match up. This is due to the inability to synchronize the data collection and the cycling of the heating lamp. The result is that the starting point of the time intervals may be slightly different. By this, it is meant that the experimental procedure had two sets of time intervals. If the experiment started at time zero when the camera and computer were initialized and data collection was started, the lamp would be on its own time scale with respect to that starting point. The lamp would be in place and switched on for its pre-selected time interval, switched off and then removed from the camera's view. During this time, the camera is collecting data at its one second intervals so the first several seconds would be disrupted by the back of the lamp.

Also, since the camera and lamp were not synchronized, it may have been at a time interval of approximately 2.5 seconds from the start of the camera timing when the lamp was switched on. If the heated period was to be one second, the actual heating period might have ranged from slightly less than a second to slightly more due to human error in the switch timing. When the lamp is removed, the first second of good data of the sampled surface may actually come several seconds after the lamp is turned off. The result is a lack of an absolute zero time in which the experimental results can be matched up to the FEA. Conversely, synchronization is not an issue with the ANSYS results.

A typical data comparison then resembles the previous figure in which the two temperature-time profiles do not match up. However, if the experimental data were to be shifted ahead in time, the two profiles as seen before actually match up quite well. Figure 5.9 shows the results of a 2.75 second forward shift in the experimental results.

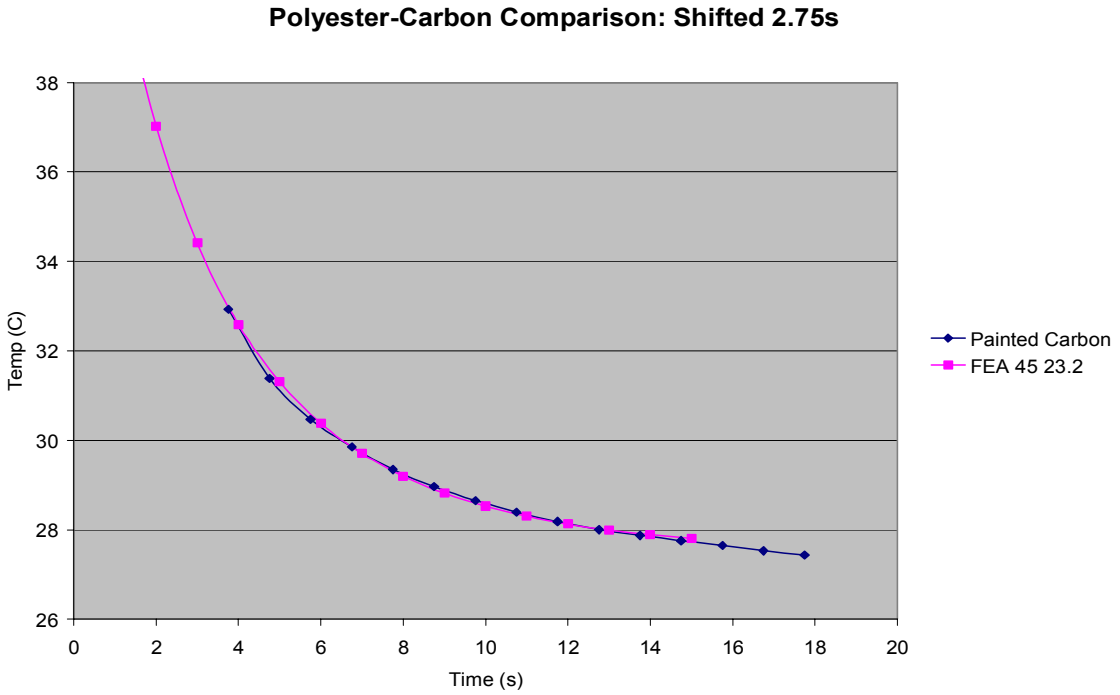

Figure 5.9: Polyester-Carbon Experimental and FEA Comparison with Time Shift

5.5: Determining the Initial Conditions

Another drawback of the unsynchronized lamp and camera was the inability to exactly replicate an experiment. That said, great effort was taken to keep the experiments as uniform as possible but two trials of the same material would be slightly different due to variations in lamp setup and heating time. Also, a few degrees variation in room temperature would affect the ambient conditions that would be needed to have the FEA results match the lab results. Since the ANSYS results could be refined after the experimental data was collected, the initial conditions used in the FEA could be adjusted to achieve a better fit. Figure 5.10 shows the variations in the decay profile of the polyester-carbon FEA results when the initial condition temperatures are varied.

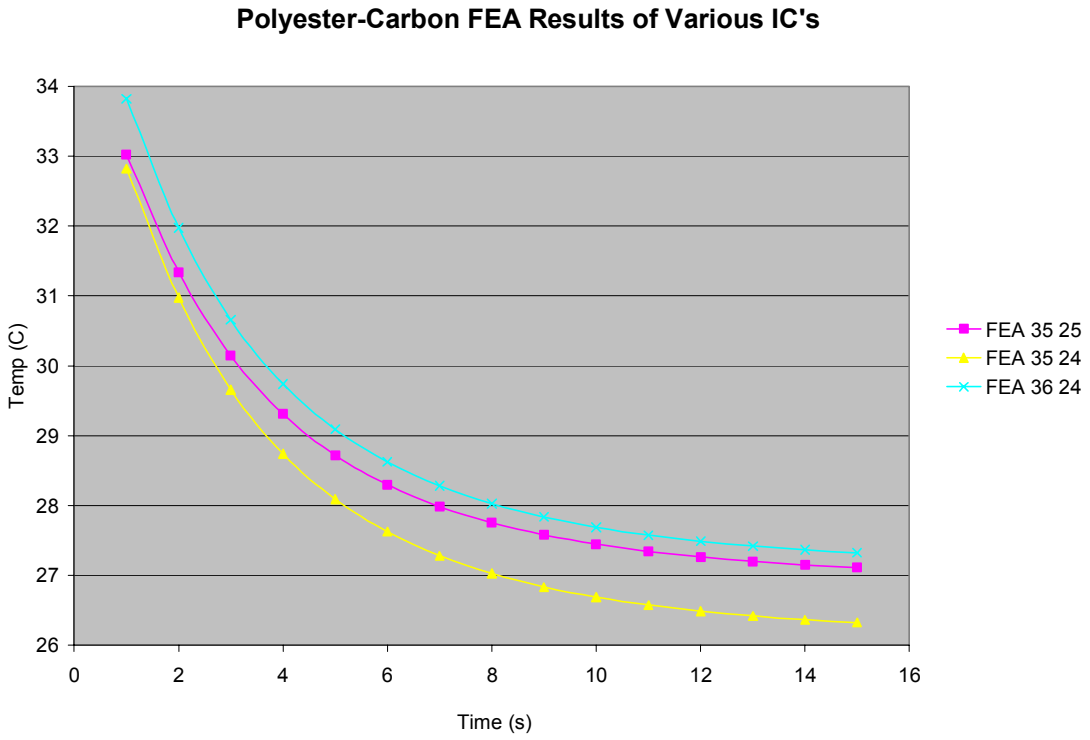

Figure 5.10: FEA Results from Various Initial Conditions

5.6: Results of the Test Samples

The results of the polyester-carbon comparison were shown in Figure 5.9. Following, in Figures 5.11 through 5.13 are the results of the other combinations of materials.

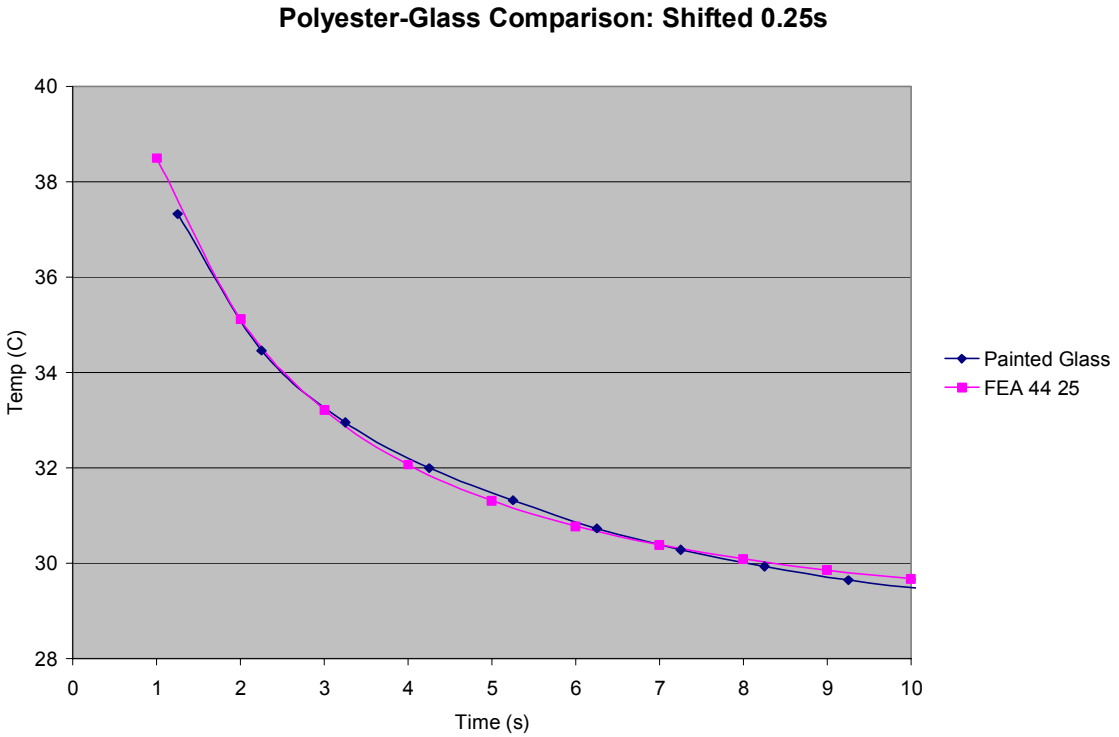

Figure 5.11: Polyester-Glass Comparison

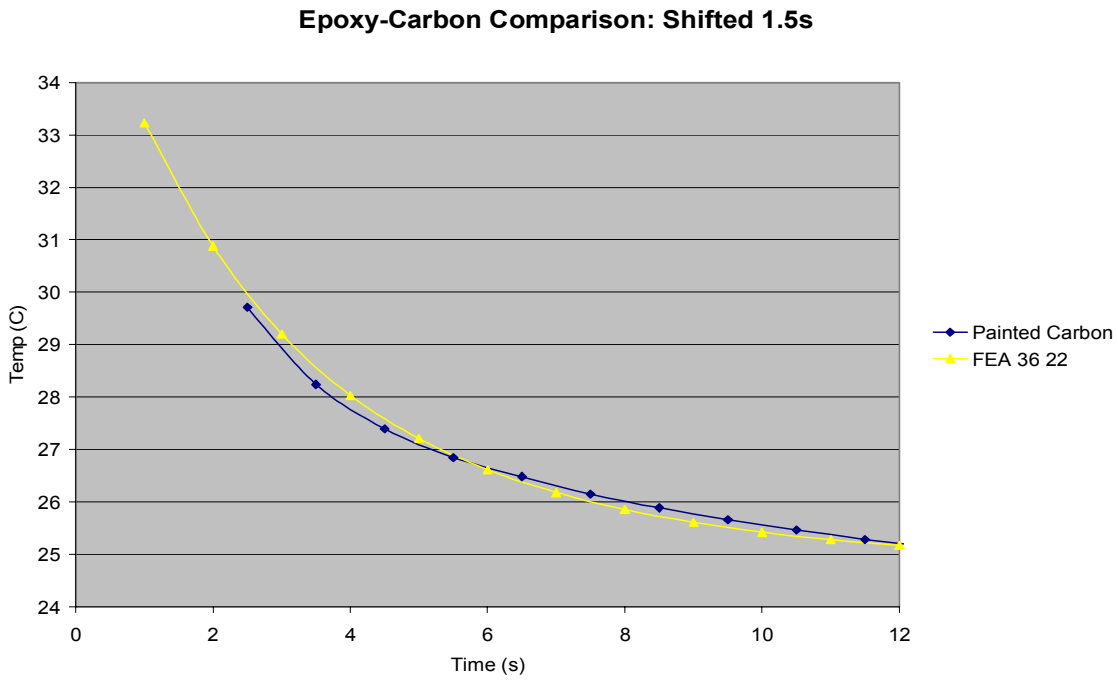

Figure 5.12: Epoxy-Carbon Comparison

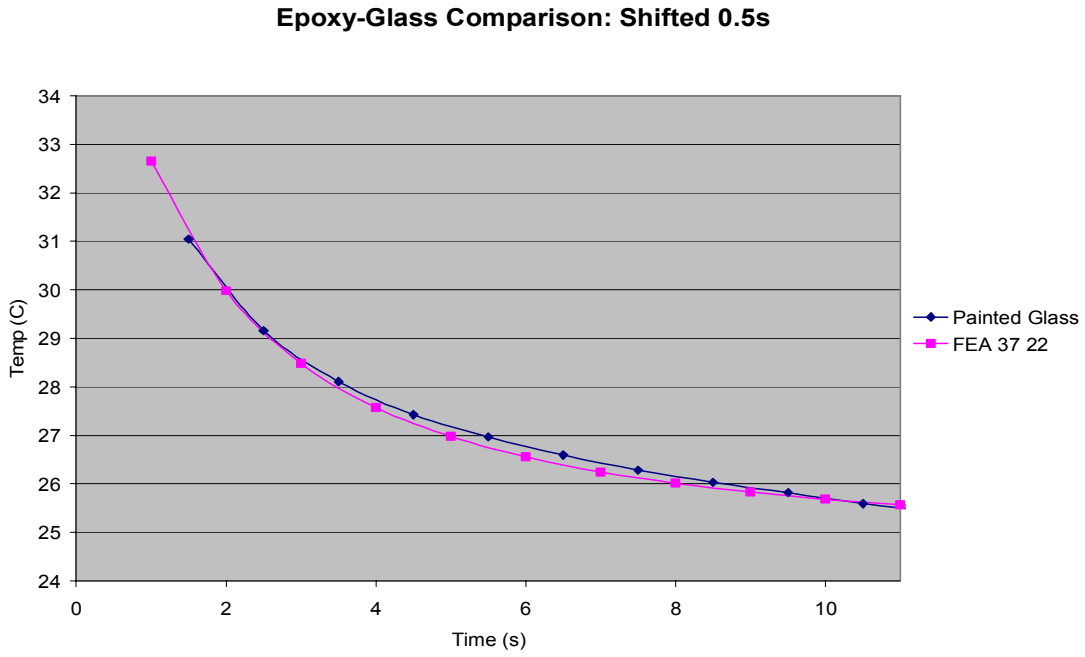

Figure 5.13: Epoxy-Glass Comparison

5.7: Comments on the Test Samples

After reviewing the data from the four different test samples, it became apparent that with some minor fine tuning of the FEA parameters, the experimental and the ANSYS data showed similar responses. Of the validation samples, the worst correlation occurred in the epoxy-glass sample in Figure 5.13 with the maximum difference of approximately .25 degrees C between the two decay profiles.

Chapter Six: The Resulting Data-Applying the Model

This chapter will use the validated ANSYS model to interpret the experimental results of the beam flange. Also, in an effort to develop an inspection schedule for the beam, a parametric study was conducted as well as a second delamination model was developed to guide the interpretation of the results.

6.1: The Flange Results

In a similar manner derived from the validation sample of the previous chapter, the following are the results of the testing of the beam flange:

6.1.1: The Intact Flange

Matching the time decay for the averaged material values of an intact beam flange sample and FEA results by only adjusting the IC's without any time shifts produces the following results:

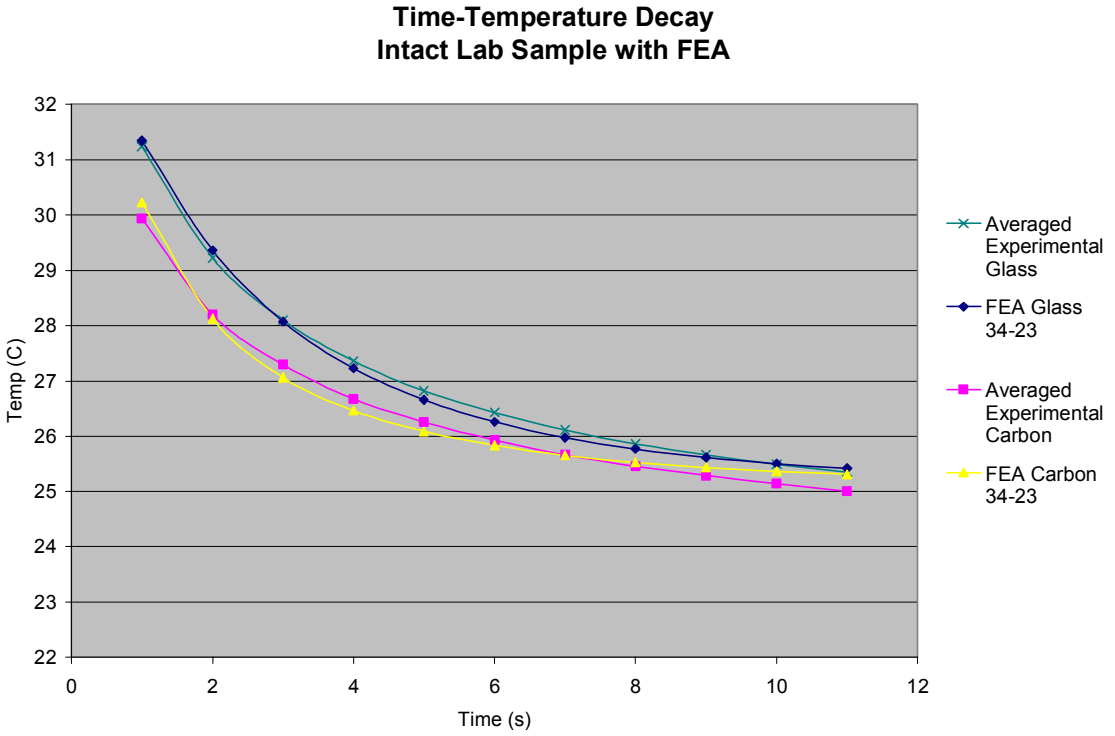

Figure 6.1: Averaged Material Decay Comparison of an Intact Sample

Unlike the validation samples which were primarily separate blocks of carbon and fiberglass used to compare material response, the beam flange was a single piece. Under the original assumptions that the surface emissivities were constant and differences in absorptivity would not be a factor in flash heating, correlations between the glass and carbon regions under the same IC's became difficult. With the results for the intact samples, the glass regions would match up fairly well while the correlations for the carbon regions were not as close. This raises the concern of the accuracy of the material values used in the ANSYS model of the beam flange.

The data at the second time interval matches the closest between the FEA and experimental results for both material regions. At the second time interval, the vertical surface profile of the experimental results is shown in Figure 6.2.

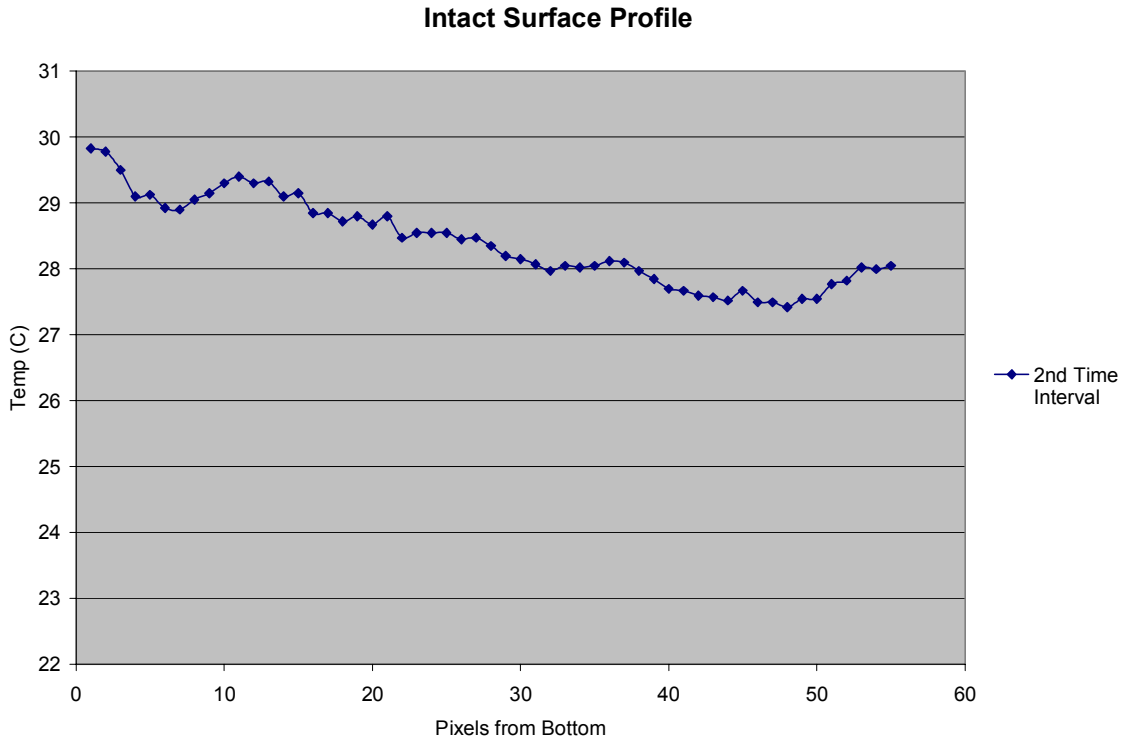

Figure 6.2: Experimental Surface Profile of an Intact Sample

While the results show some jagged areas, there are no drastic changes between the material regions of the glass on the left and carbon on the right such as the shoulder produced in the preliminary delamination FEA results from Figures 3.10-12. Since the actual boundary between the regions in the flange does not hold to one location over the length of the beam and is not apparent from a visible inspection if not fully cracked, one can only assume the transition area by interpreting the results as the glass region as pixels 1-15 and the carbon region to be 40-55. The boundary between the two would occur somewhere in between where the temperature gradient is present in the gradually sloping cooler material trend. The lack of some type of shoulder in the results would suggest that this is a non-delaminated sample which was easily verified by a visual inspection of the nearby end of the beam sample. Data from the previous

plot was taken from a region near the right of this flange section. The visible crack ends near the 12 inch mark on the ruler and does not extend to the end of the beam. Figure 6.3 shows the flange surface from which the results were taken. The intact region was towards the right, far away from where the visible crack ends near the 12 inch mark. The crack does not extend to the end of the beam.

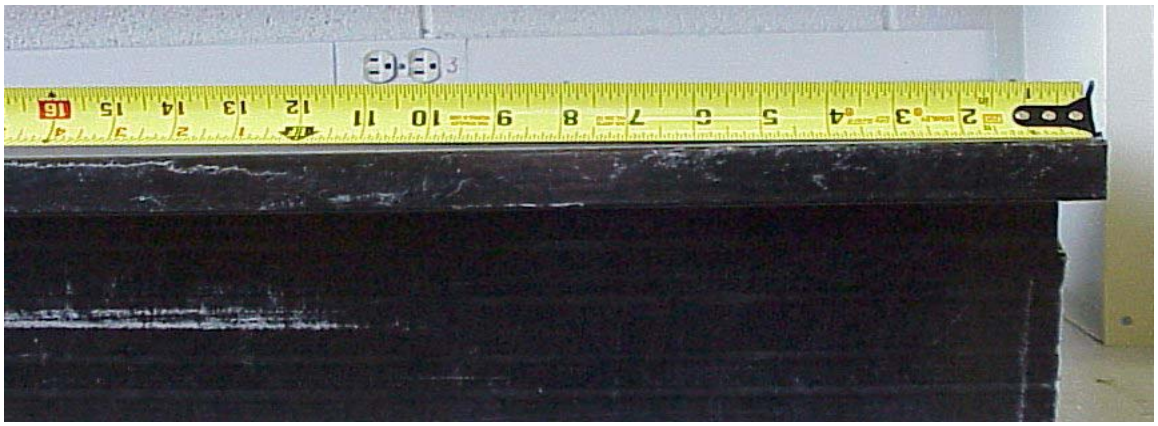

Figure 6.3: Picture of Tested Flange with Ruler

The corresponding FEA results for the second time interval would appear as in Figure 6.4. In order to plot the two surface profiles together, the pixel axis (x-axis) of the experimental lab data was normalized and then displayed in Figure 6.5.

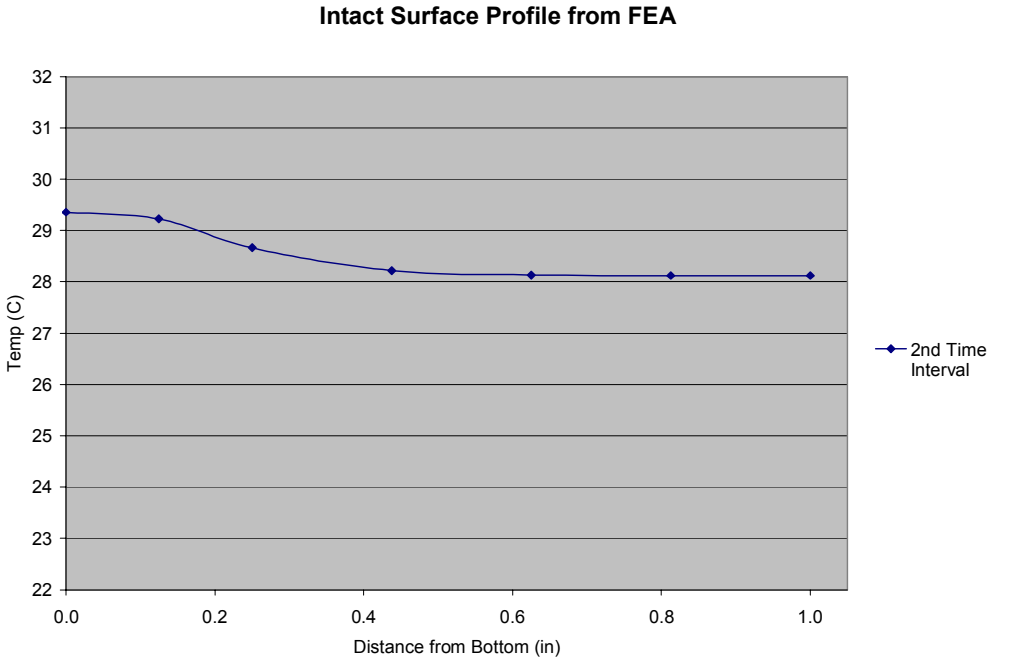

Figure 6.4: FEA Surface Profile of an Intact Sample

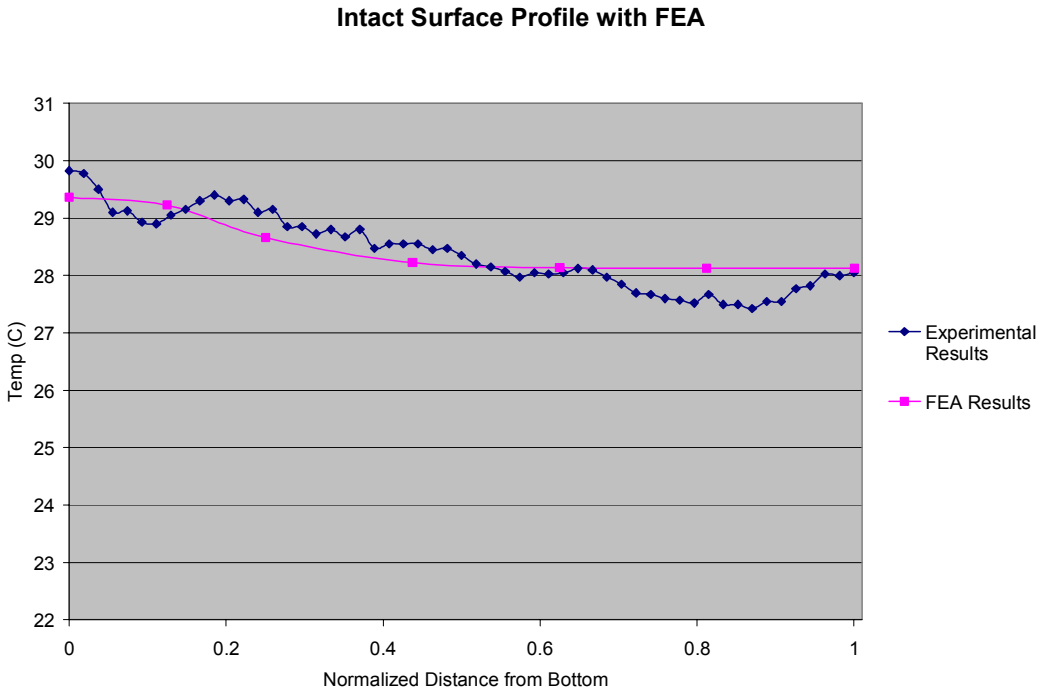

Figure 6.5: Surface Profile Comparison of an Intact Sample

Since the FEA results were derived from averaged lab data, the profiles will not entirely match up. However, a qualitative correlation appears to exist.

6.1.2: The “Intermediate” Flange

From the same flange section pictured in Figure 6.3, another test was conducted near where the visible crack ends with a close-up of the region as follows in Figure 6.6. This region was deemed “intermediate” in that the visible surface crack ended at the 12 inch mark on the ruler. However, it was believed that the crack extended into the flange at an angle in a way that the crack would be present behind the surface for some unknown distance past where a visual surface indication would be present. For that matter, the experimental IR results would show some manner of delamination or difference from the intact experimental results. Tests in this region were conducted near the 9 inch mark. The material decay profiles for this test area are found in Figure 6.7.

Figure 6.6: Close-up Picture of the “Intermediate” Flange Area

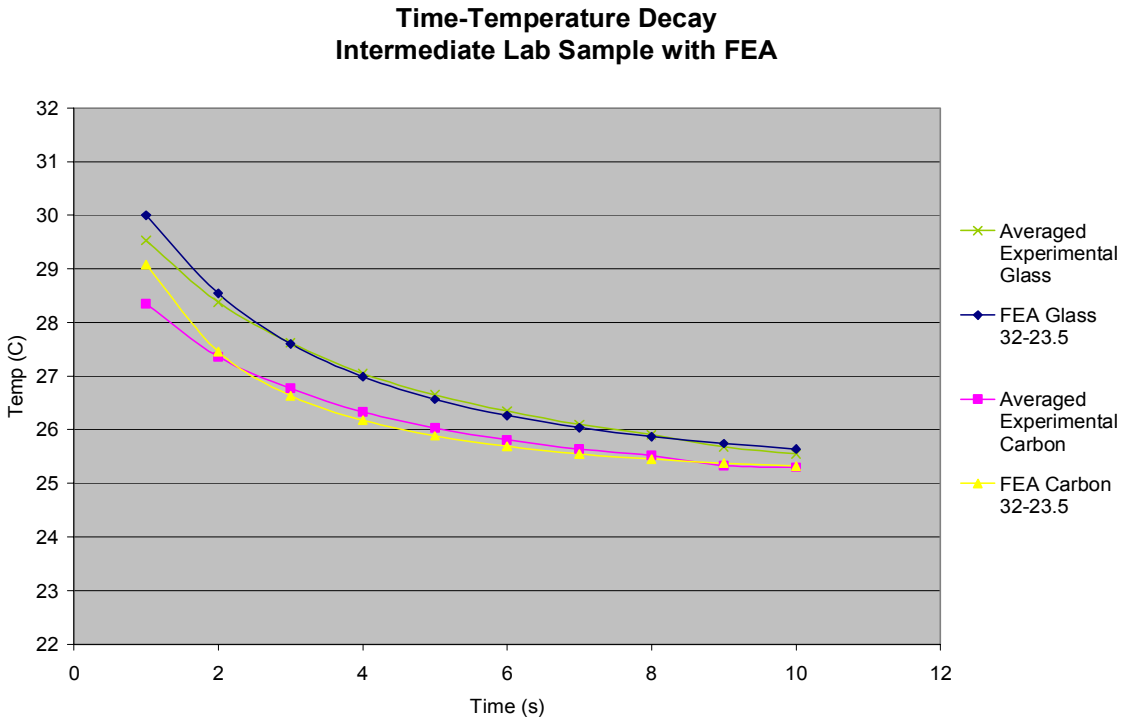

Figure 6.7: Averaged Material Decay Comparison of an Intermediate Sample

Even though this is the same flange as tested in the intact region, averaged surface profiles were generated for this local area. As mentioned before and will be discussed in detail later, the material region boundary placement varied along the length of the beam. For that reason, a localized set of averaged material profiles were used for each area tested.

One difficulty with this set of data was the alignment of the first time interval between the experimental and FEA data. Otherwise, the decay profiles matched quite well except for the first time interval. If we then compared the surface profiles at the second time interval, the results would appear as in Figure 6.8.

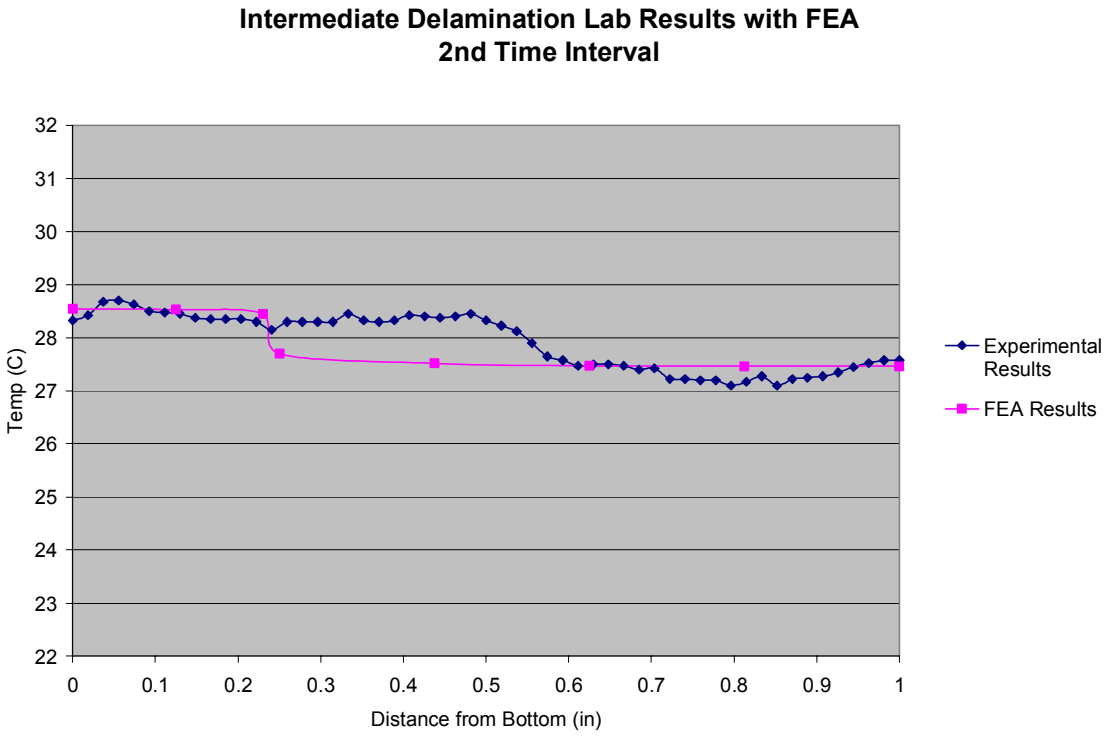

Figure 6.8: Surface Profile Comparison for an Intermediate Sample

Unlike the intact results, the intermediate surface profile shows a slight shoulder around the half inch mark with two distinct plateaus for the material regions on either side. This is even more pronounced in the first time interval profile of the experimental results:

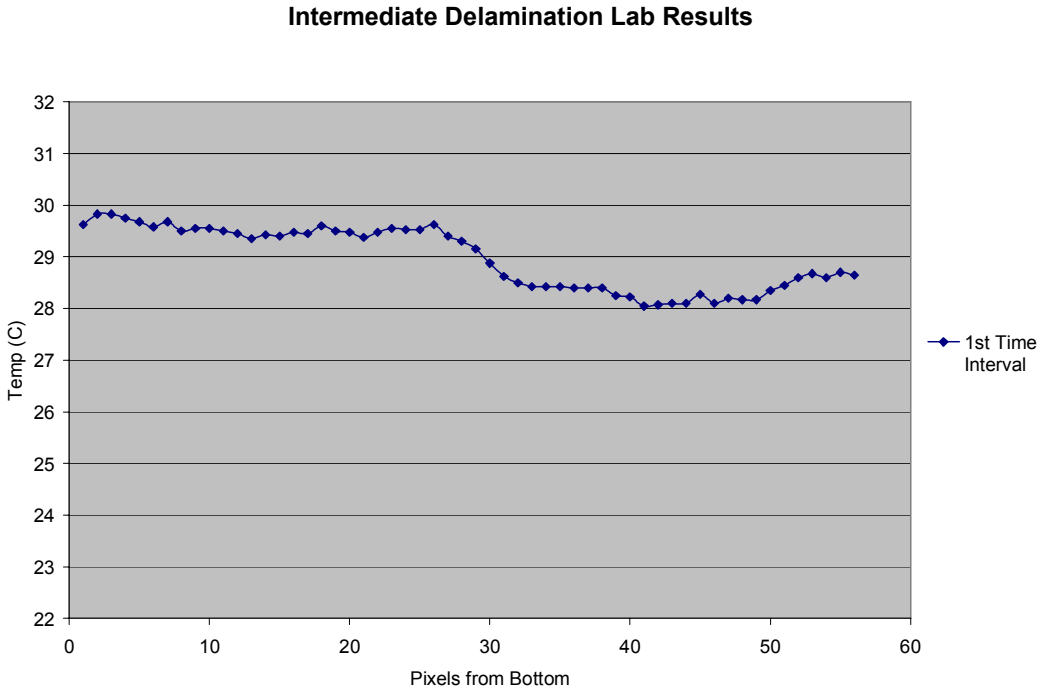

Figure 6.9: Experimental Surface Profile of the Intermediate Sample

The major discrepancies between the lab and FEA would be the location and severity of the shoulder. As for the location, the boundary's location varies along the length of the beam and does not consistently lie in one area. Following in Figure 6.10 is a picture showing how the crack meanders along the length of the flange.

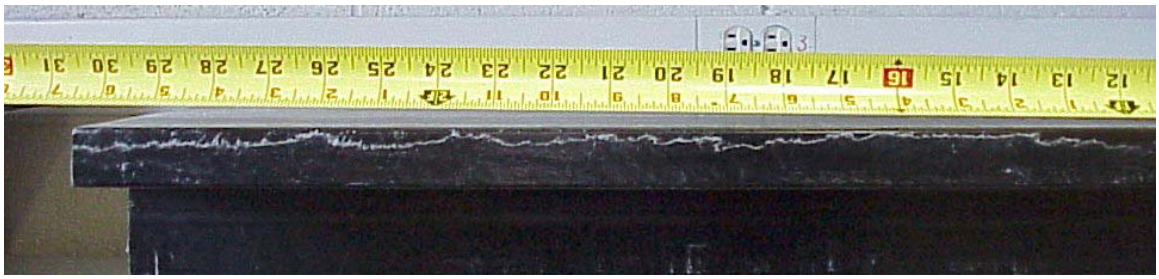

Figure 6.10: Crack Location along the Length of the Flange

Since the crack's location cannot be explicitly determined, the only other issue would be the severity in which the FEA depicts the shoulder. For a base comparison, the FEA results from the intact and delaminated models are plotted together using the same set of IC's and the first time interval at one second. This is shown in Figure 6.11.

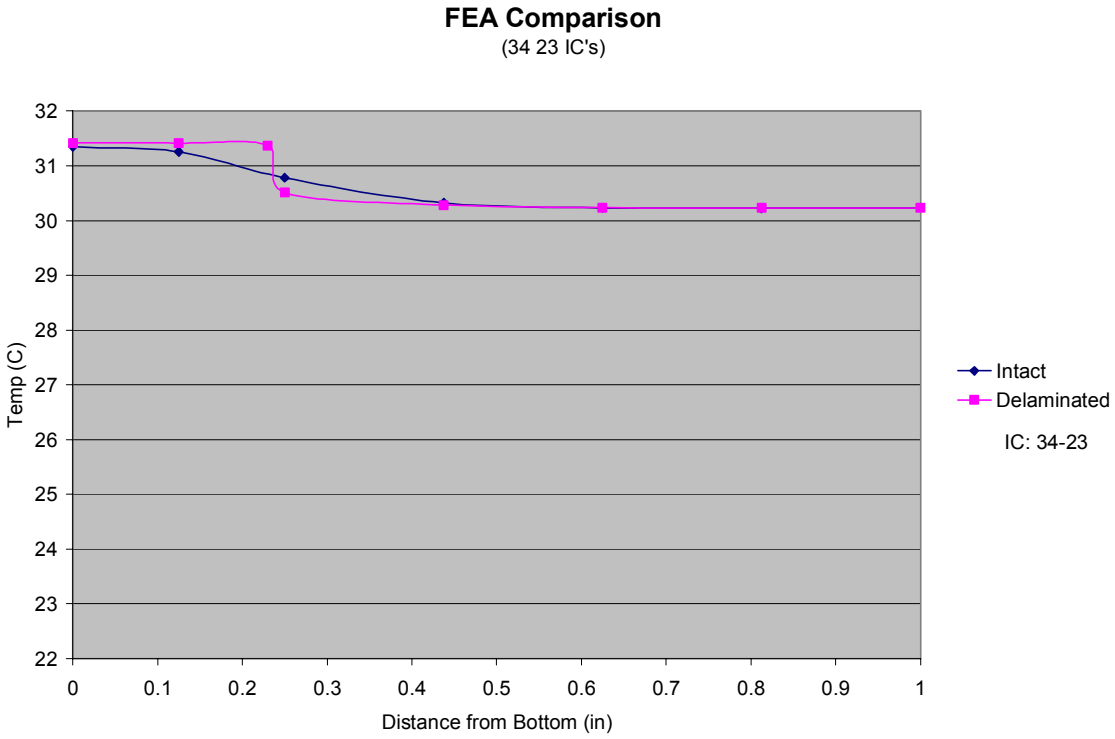

Figure 6.11: FEA Comparison between Intact and Delaminated Models

If the material values for the delaminated material region are adjusted, the shoulder can be reduced by lessening the restriction of heat flow across the boundary due to the reduction in conductivity values. Holding to the same IC's and time interval, the results of k/30, k/20 and k/10 are as displayed in Figure 6.12 on the same scale as Figure 6.11. Figure 6.13 readjusts the y-axis scale in order to better display the results. Figure 6.14 then adds the FEA results from the intact model.

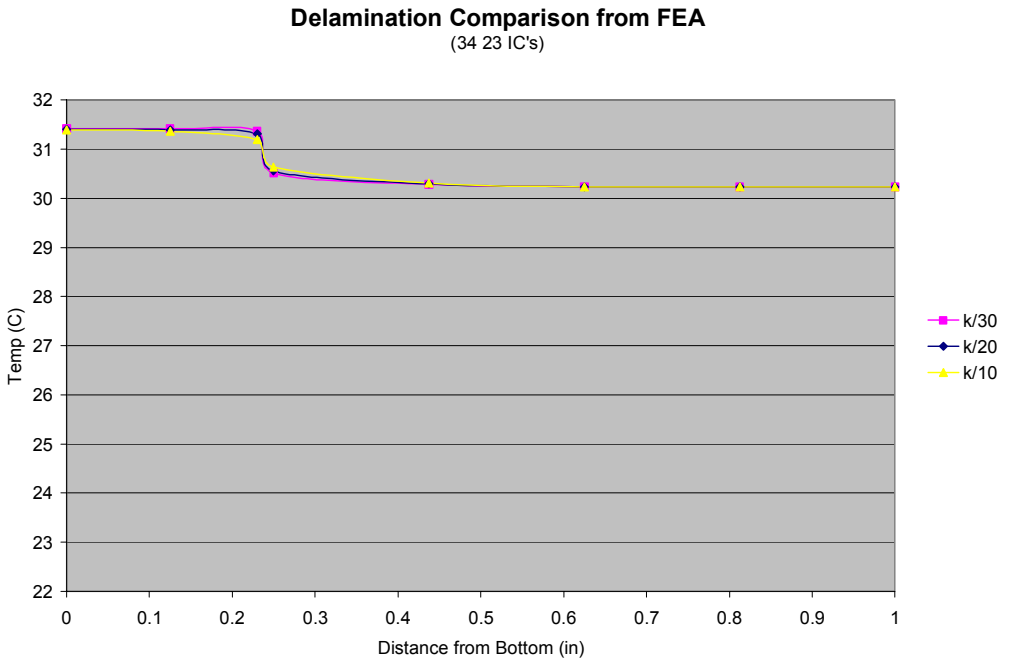

Figure 6.12: FEA Delamination Comparison

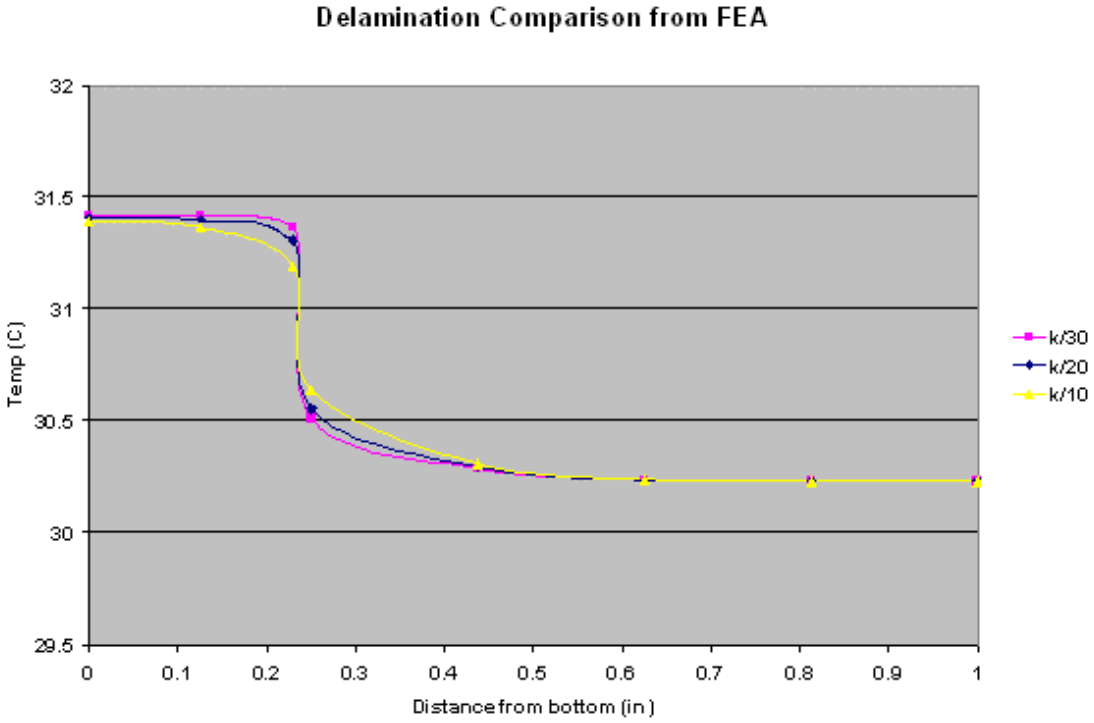

Figure 6.13: FEA Delamination Comparison with Revised Scaling

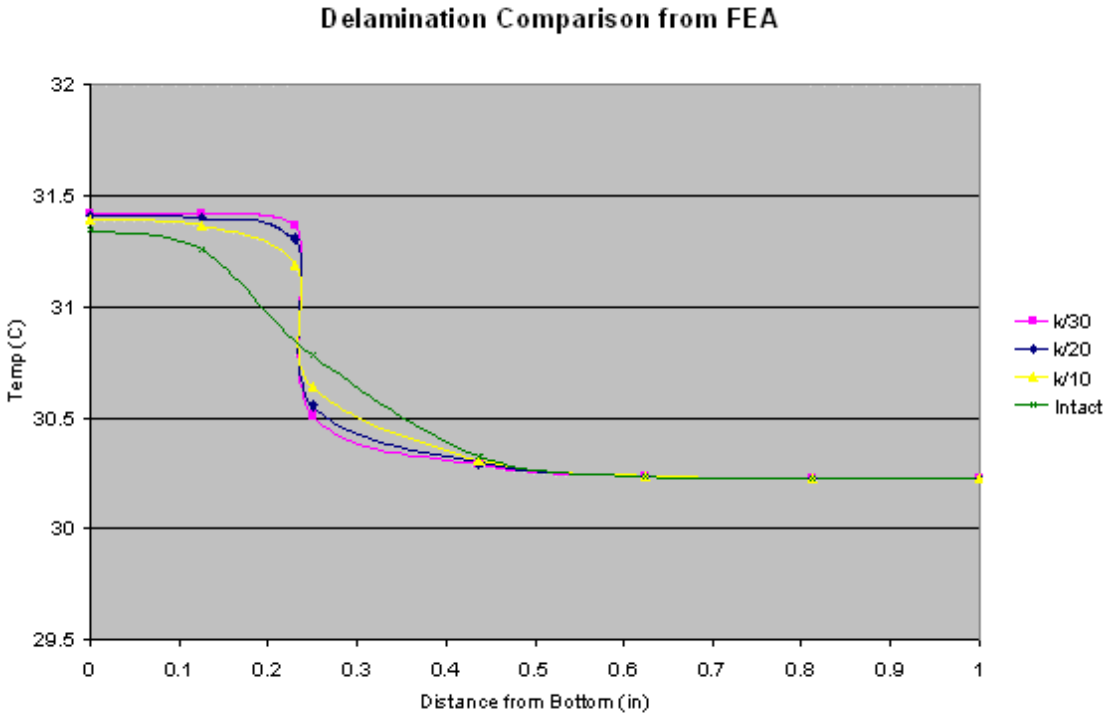

Figure 6.14: FEA Delamination Comparison with Intact Results

As displayed in the previous three profiles, the FEA model shows the severity of the shoulder between the material regions to be dependent upon the level of delamination present. Qualitatively, two of the validation samples were tested where the carbon and glass blocks were compressed together with clamps. Since this was an extreme form of a delamination, the resulting thermal profile showed two distinct material regions with a temperature dip between them where a small gap was located. See Figure 6.15 for the surface profile.

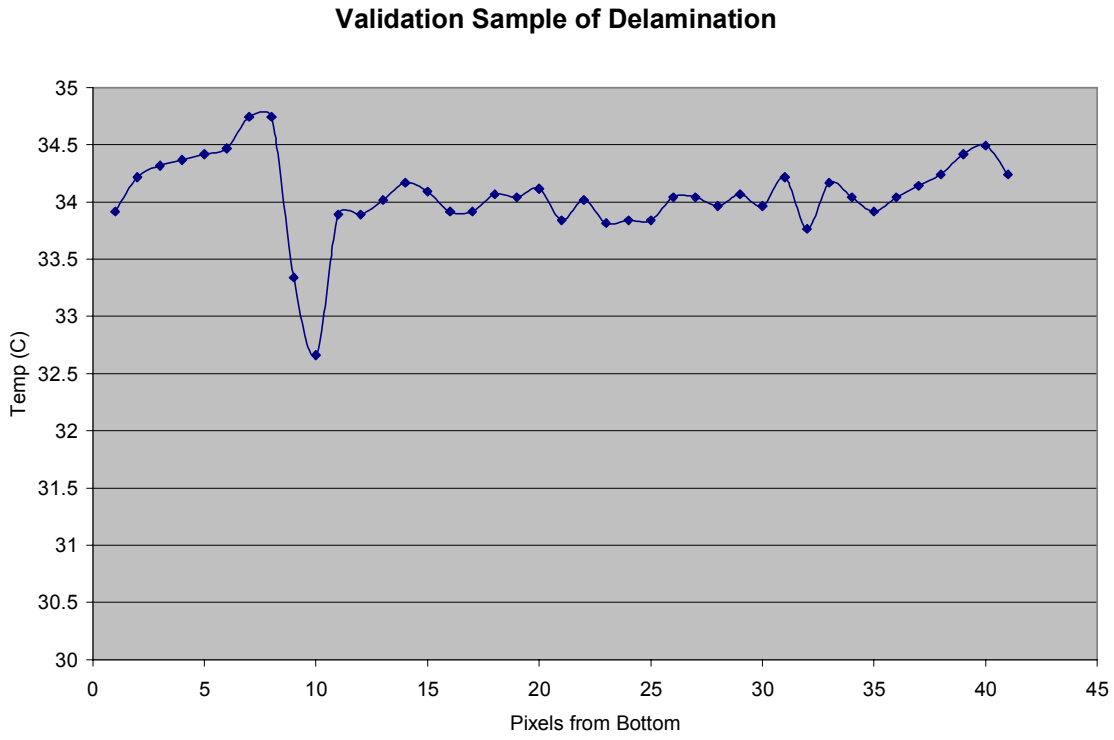

Figure 6.15: Surface Profile of a Fabricated Delamination Validation Sample

6.1.3: The Fully Delaminated Flange

Further pursuing the full delamination discussion, a third area on the flange was tested. Opposite the intact end of the flange sample, the flange had become fully separated. After the thermal imaging, the averaged temperature decay results did not match as closely as with the intact or intermediate results and are shown in Figure 6.16. However, if the lab results are time shifted, an alignment starts to form. Figure 6.17 shows the shifted results. Note that while the experimental results start to correlate to the FEA glass results, the separation between the averaged glass and carbon regions is negligible. Also, contrary to previous results and material trends, the averaged carbon region shows to be hotter that the glass region which is peculiar due to the thermal differences in materials. Figure 6.18 shows the surface profile from the experimental results at

the first time increment.

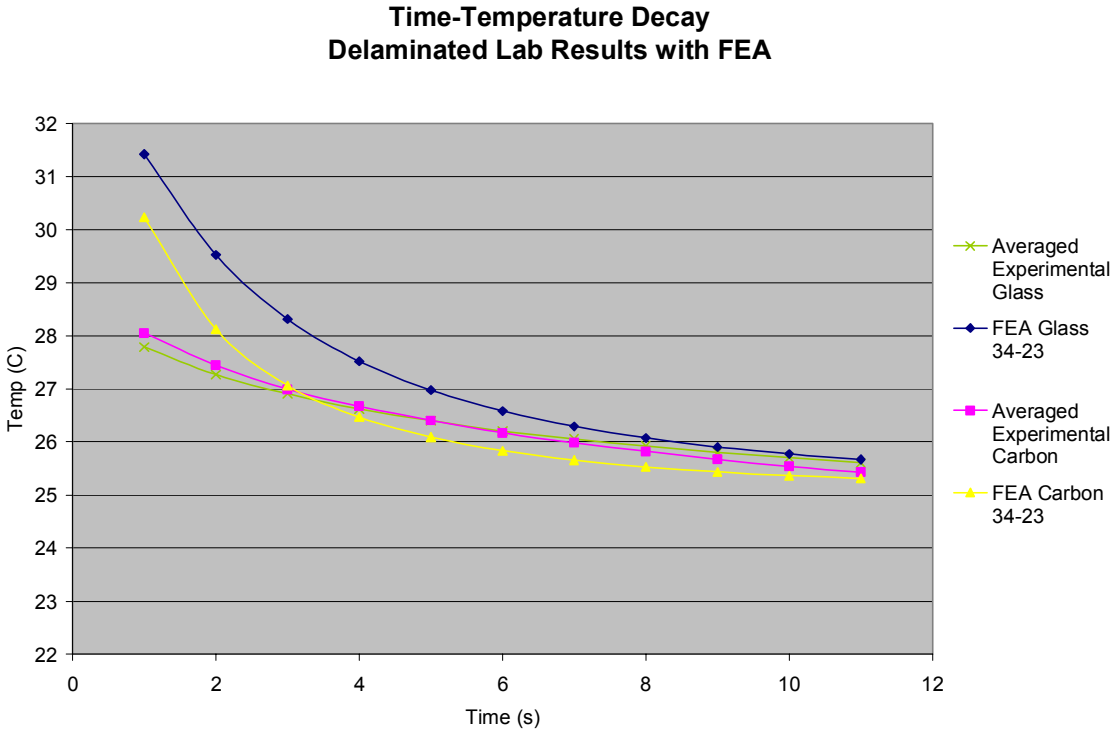

Figure 6.16: Averaged Material Decay Comparison of a Delaminated Sample

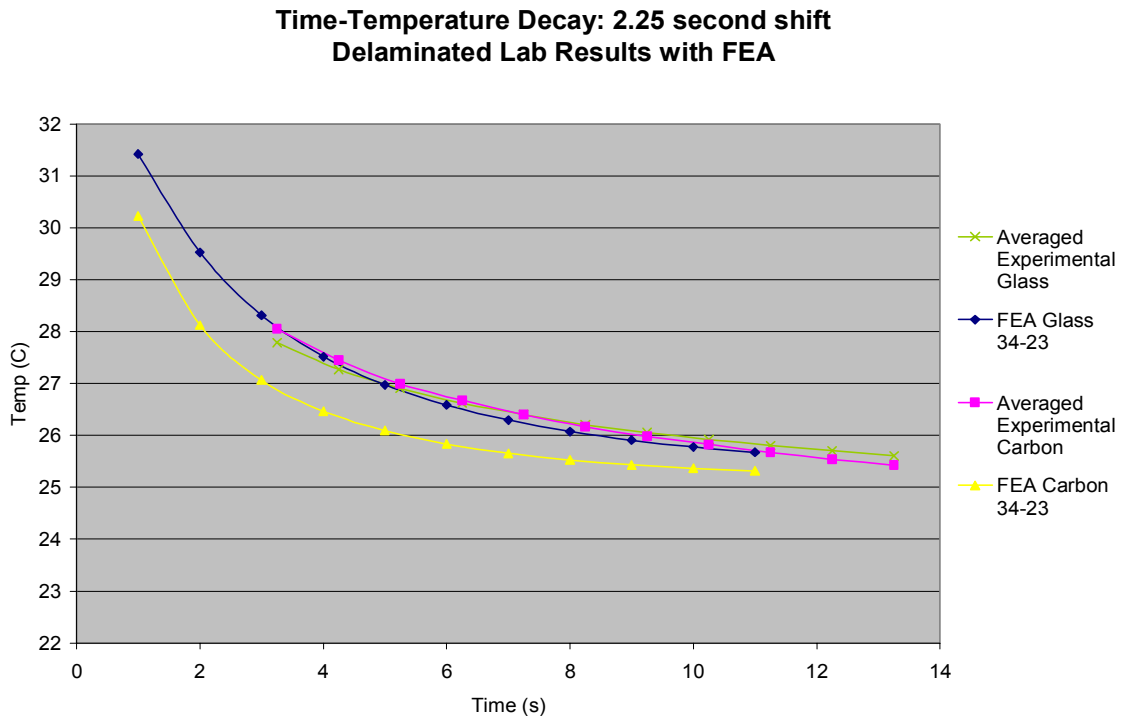

Figure 6.17: Averaged Material Decay of an Delaminated Sample with Time Shift

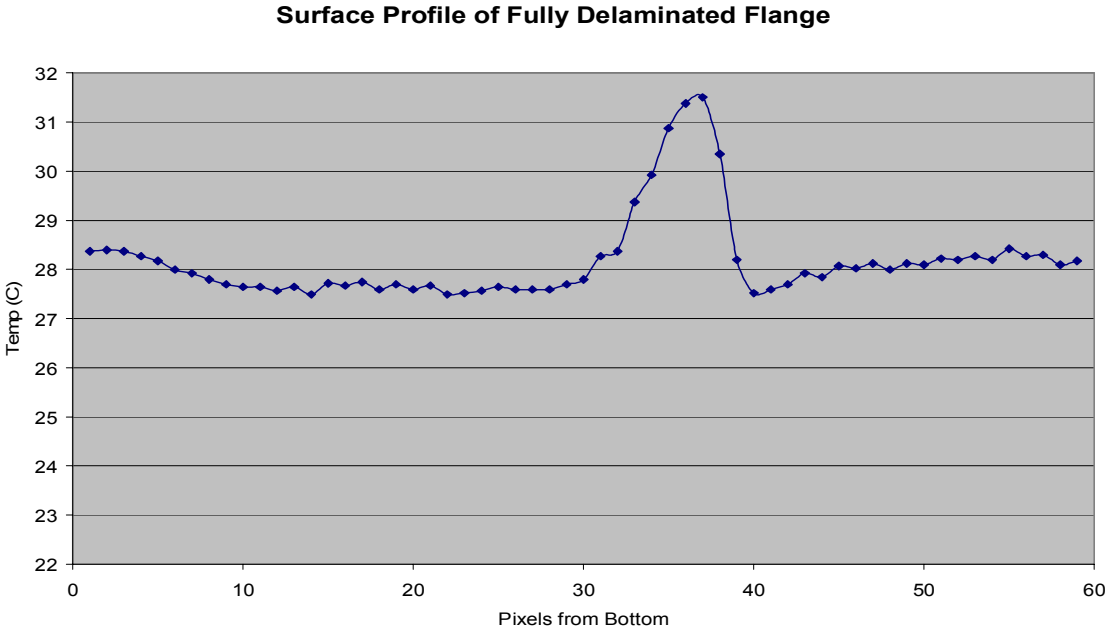

Figure 6.18: Surface Profile of Fully Delaminated Experimental Results

Upon further visual inspection of the cut end of the beam near the inspection region, the cross section shows a typical glass region but the carbon region appears to be nearly void of carbon fibers leaving a large resin pocket. If comparing material values, those of the two regions are not that dissimilar to each other and if the volume fraction of the carbon region was reduced, the glass region could easily become the region of greater conductivity. A picture of the cross section is in Figure 6.19.

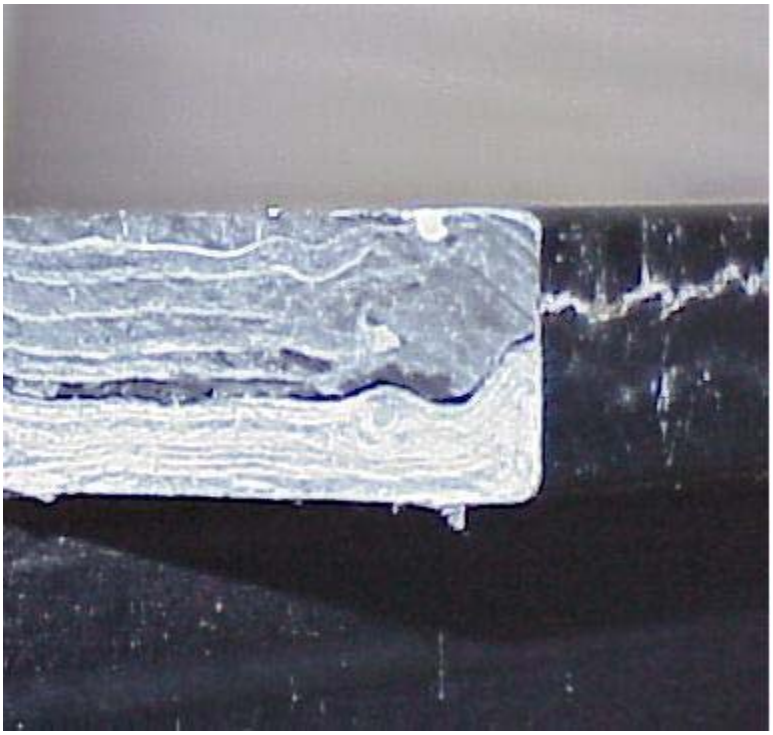

Figure 6.19: Cross Section of Fully Delaminated Flange

One thing that was noticed is that the FEA results never generated a hot spot between the regions quite like the delaminated experimental results did. However, the heat transfer in the FEA was only restricted in the vertical direction across a horizontal delamination and, as the picture in Figure 6.19 shows, the

experimental sample had a crack cutting off the heat flow directly into the flange as well. If the heat energy cannot cross the boundaries due to restricted conductivity and there is no thermal difference along the length or vertically within the regions due to uniform heating, there would be next to no heat transfer in this small area near the crack. This would explain why the peak surface temperature would change very little from a heated temperature of 34 degrees C from the IC's. Furthermore, once the heat energy has time to propagate into the thickness in the glass region, the surface temperature of the glass region will decrease and a gradient will develop from the small delamination area down into the glass region. The peak will then decrease in a similar manner as the glass region at a delayed time interval.

6.2: The Parametric Study

In order to illuminate the aspects of the experimental response that were not fully understood, the FEA model was used to help guide the further development of an inspection method.

6.2.1: Heating Schedule

Without a thermal difference between the material regions the surface profile of the experimental results would only show what appears to be a single material. Developing this statement would lead one to the notion that the greater the thermal difference between regions, the more likely an anomaly at the boundary would be detectable. Using the FEA model with the full-length delamination, the heated surface temperature of the initial conditions was compared by plotting the surface profiles at the first time interval of each set of initial conditions. The ambient temperature (23 deg C) was held constant while the heated temperature was raised in one degree intervals.

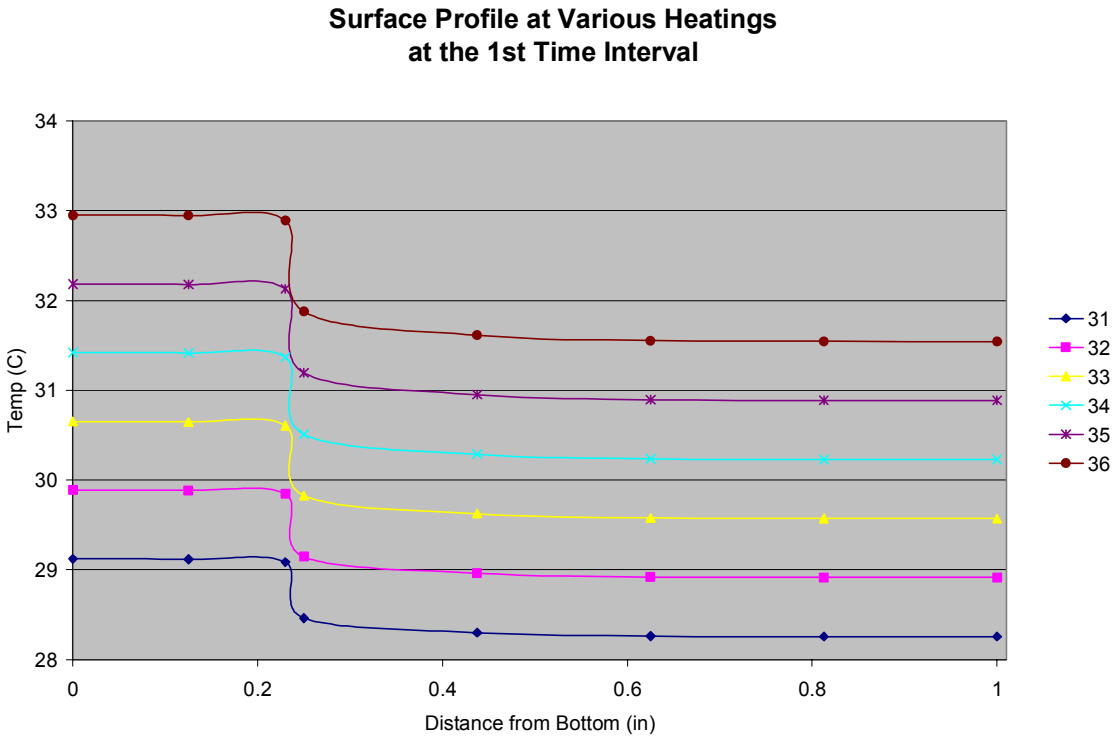

Figure 6.20: Surface Profiles at Various Heatings

Visually, as the heated temperature rises, the difference between the glass and carbon regions, left and right, respectively, can be seen as a greater difference with the elevated temperature. When plotted, this difference would appear as in Figure 6.21.

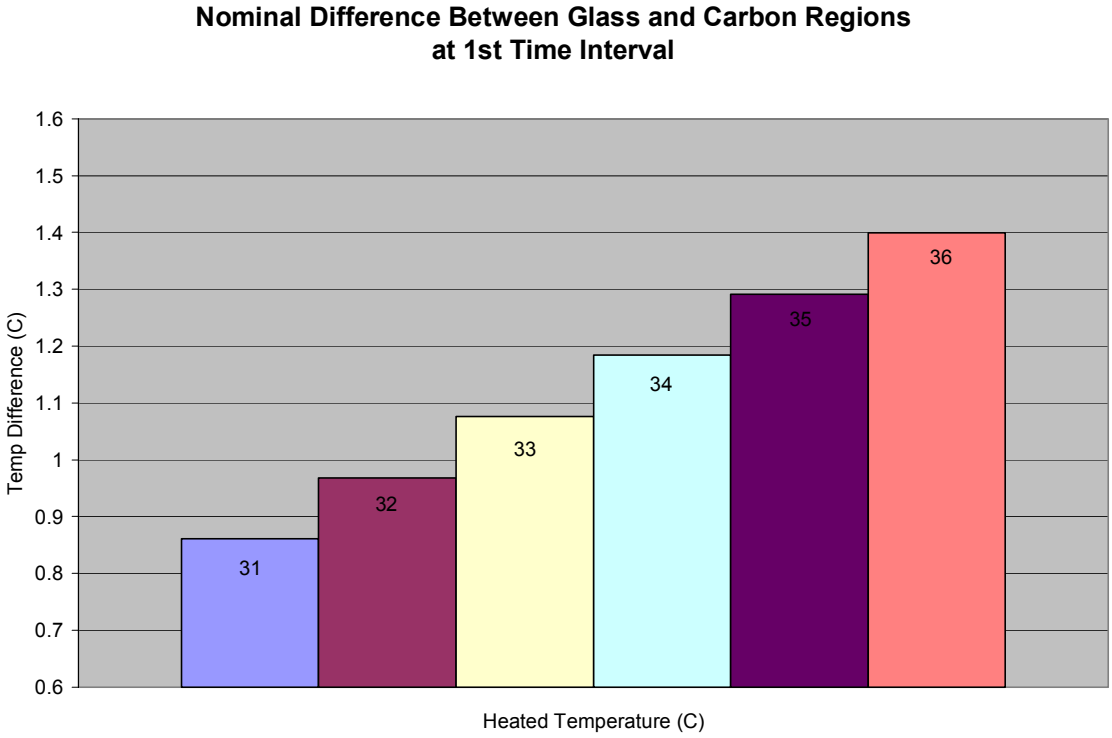

Figure 6.21: Temperature Difference between Material Regions at Various Heatings

By taking the difference between consecutive temperature intervals of the difference between regions, the results are in the following table:

Table 6.1: Difference between Differences

Between 31 and 32	.1076 deg C
Between 32 and 33	.1076 deg C
Between 33 and 34	.1075 deg C
Between 34 and 35	.1078 deg C
Between 35 and 36	.1076 deg C

Accordingly, even though the difference between the successive heating temperatures does not vary significantly, for each degree the heated temperature is raised, a little more than a tenth of a degree will be added to the difference between the regions. If one were to want to see a greater temperature difference, more heat would need to be added. Experimental results of a 10 second heating with the IC's of 90 and 23 degrees C follow in Figure 6.22.

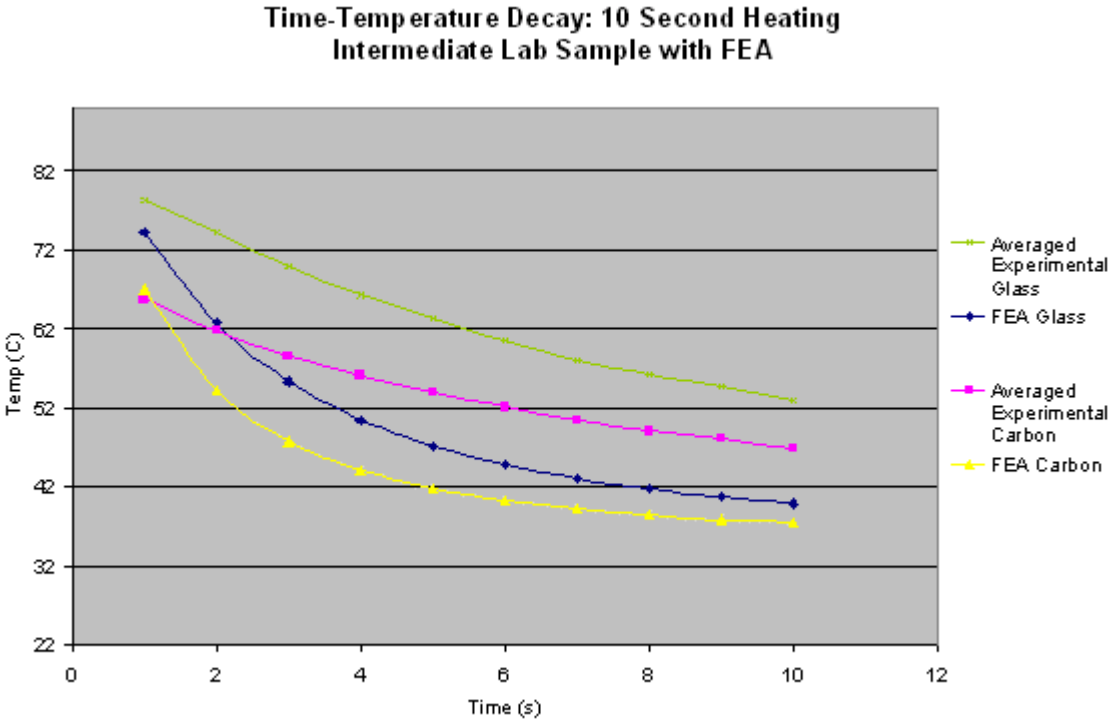

Figure 6.22: Averaged Material Region Decay of a 10 Second Heating

For the sake of this experimental process, more heat would be acquired through a longer heating time. At one second of heating, the beam flange is raised nearly 10-15 degrees. Similarly, at ten seconds of heating, the elevated temperature would be between 60 and 80 degrees higher, as shown in the results.

The lack of correlation between the experimental and FEA results of

Figure 6.22 exposes one limitation of the model. The manner in which heat energy is applied would need to be changed in order to simulate extended heating. With the short, 1 second, heating schedule, the surface elements are raised to a specified temperature as an initial condition and the analysis starts at these set points. The overall length of the analysis has been between ten and twenty seconds. The longer heating time would require a certain amount of energy to be applied to the surface for a given amount of time during the analysis since heat energy would be propagating into the material during the heating; the absorptivities of the material regions would come into play in this scenario. Therefore, the current model, developed for flash heating, does not accurately simulate extended periods of heating.

Returning to the discussion of a test procedure, the experimental results of the one and ten second heatings are similar in form and differ only in magnitude. The following two plots in Figures 6.23 and 6.24 show the surface profiles at the 1st time interval of the two tests; both profiles were taken from the same general region of the flange.

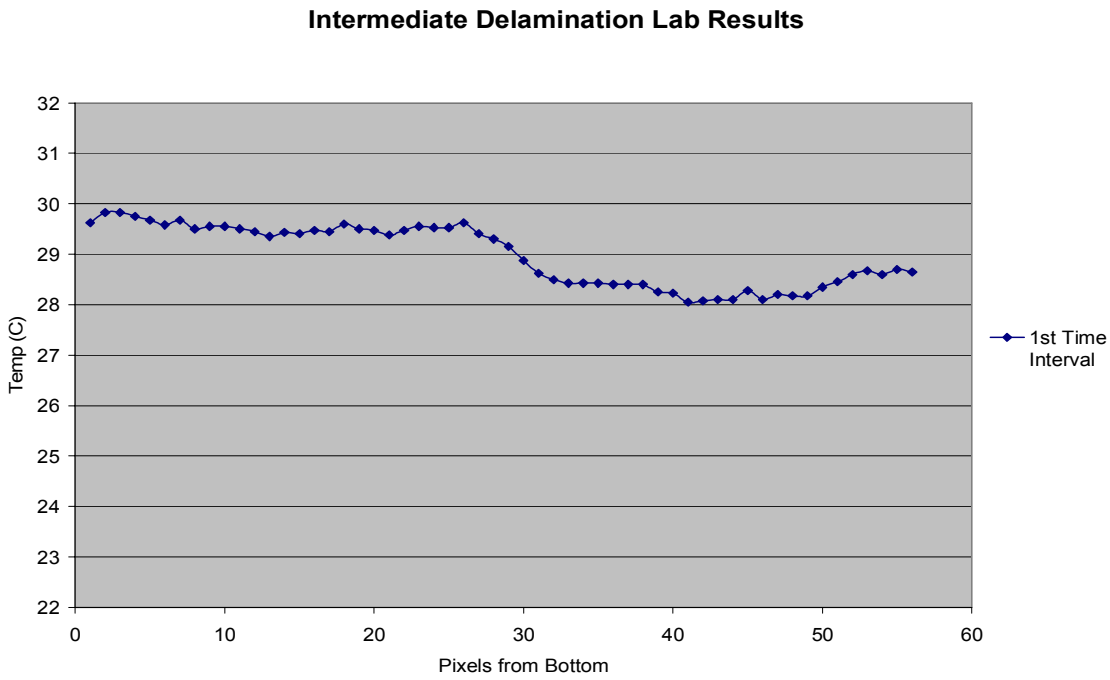

Figure 6.23: Experimental Surface Profile of 1 Second Heating

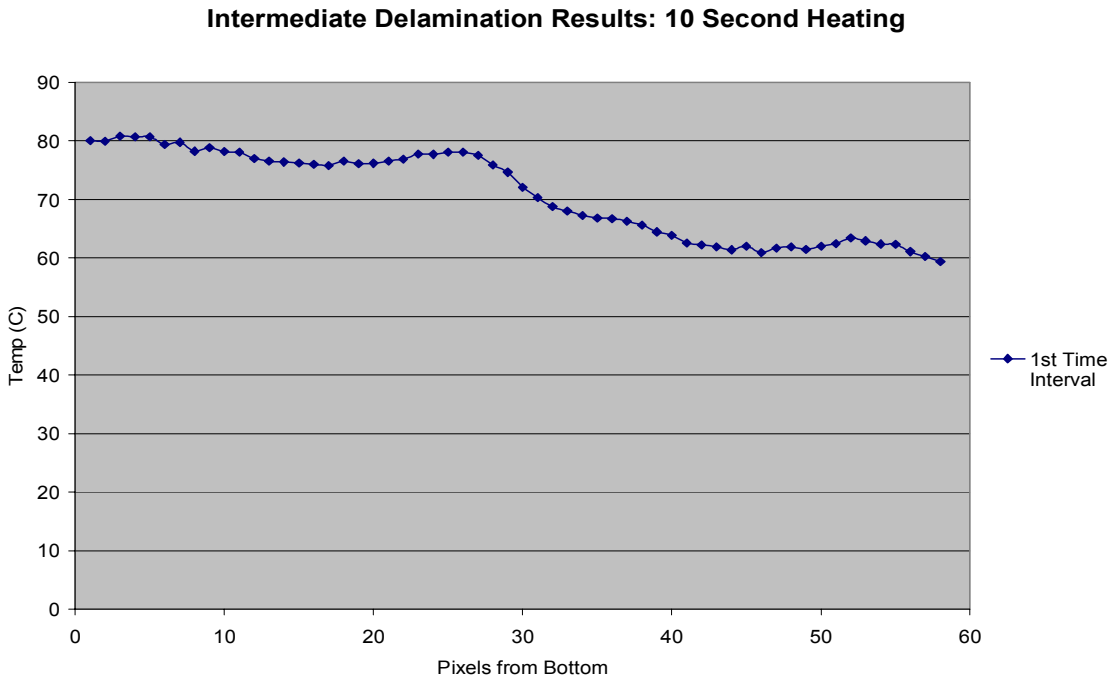

Figure 6.24: Experimental Surface Profile of 10 Second Heating

For the sake of simplicity of testing and modeling, the longer heating time would only complicate matters more than necessary. However, the results do show that a warmer surface does produce a greater thermal difference between the two regions. Consequently, a higher output lamp or some other method that could put more energy into the flange in a short time interval may be an option.

6.2.2: Testing Time Interval

Holding to the one second heating achieved with the current experimental setup, the 36-23 degrees C set of initial conditions showed the greatest thermal difference in the FEA results. With respect to temperature decay versus time, plotting the surface profiles of each successive time interval will yield the following data:

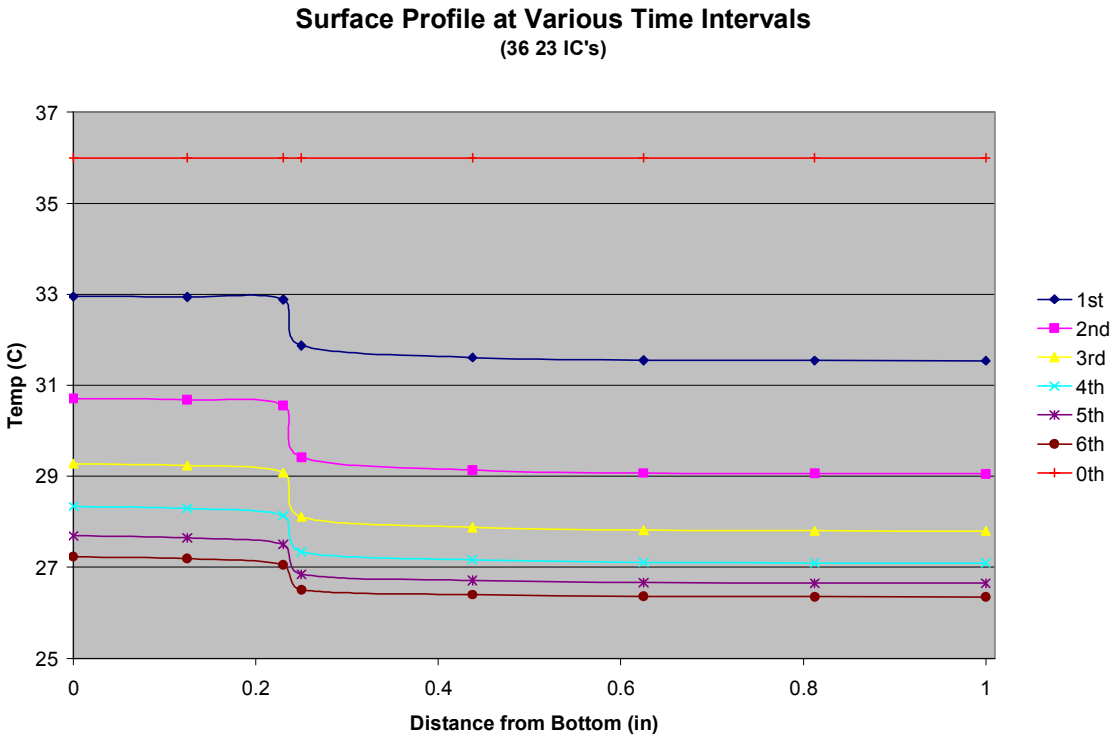

Figure 6.25: Surface Profiles at Successive Time Intervals

To show where the FEA experiment began, the zeroth time interval was plotted at the initial temperature for reference with respect to the successive profiles. Visually, the greatest temperature difference within a region appears between the zeroth and 1st intervals. However, if the time interval in ANSYS is manually forced to initially start the analysis at .1 second intervals and allowed to automatically adjust itself once the short increment is no longer necessary, the greatest difference occurs at the time of 1.25 seconds after heating as shown in the following plot in Figure 6.26.

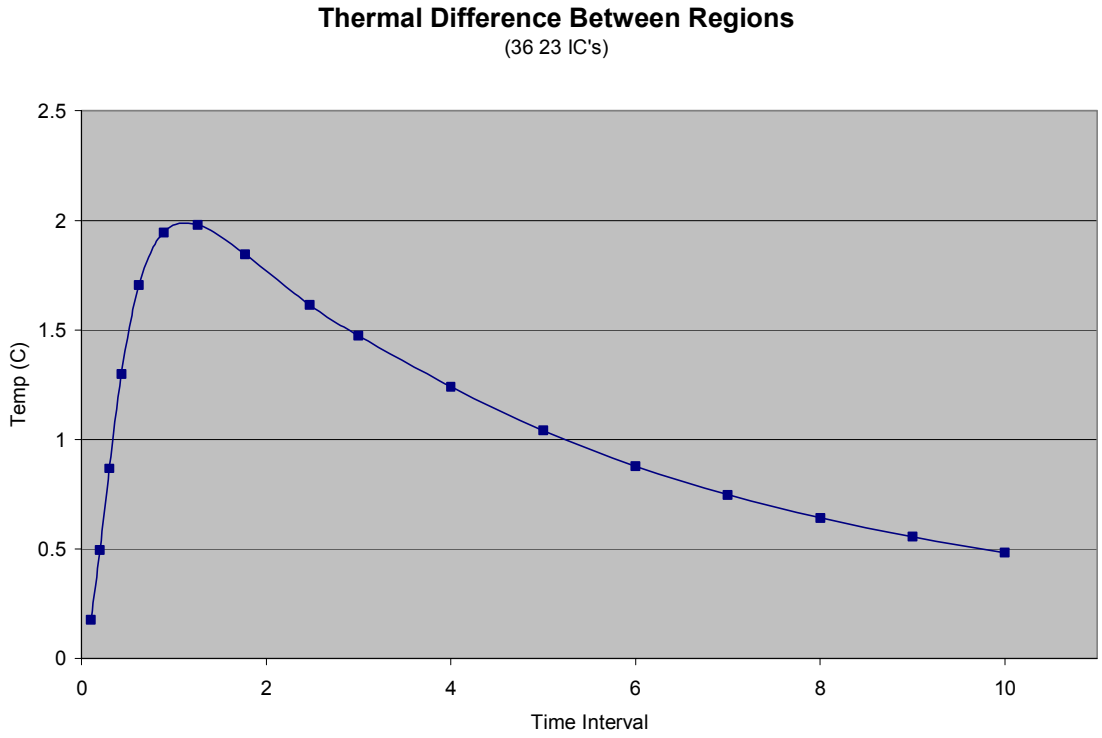

Figure 6.26: Thermal Difference between Regions with Respect to Time

According to the FEA results, a one second heating with an instantaneous inspection 1.25 seconds later would show the greatest thermal difference between the regions.

Comparing the thermal difference of the FEA to experimental results, the initial conditions would need to be set back at 34-23 degrees C as correlated in the intermediate results. These results generate a similar difference decay profile as in Figure 6.26 with the peak at 1.1 seconds and a max difference of 1.8 degrees Celsius.

6.3: The 1” Delamination Model

Understanding the effect of a delamination on the experimental response can be guided by the results of the FEA. A 1” delamination model was created to study the thermal response near the edge of delaminated regions for the purposes of determining the sizing capabilities.

Using the 36-23 degrees C set of IC’s, heating the same front face as the full-length delamination model, and k/30 for the delamination material, the surface profiles for the fully delaminated model, the intact model, as well as the center and right edge of the model in Figure 6.27 are plotted in Figure 6.28 and 6.29.

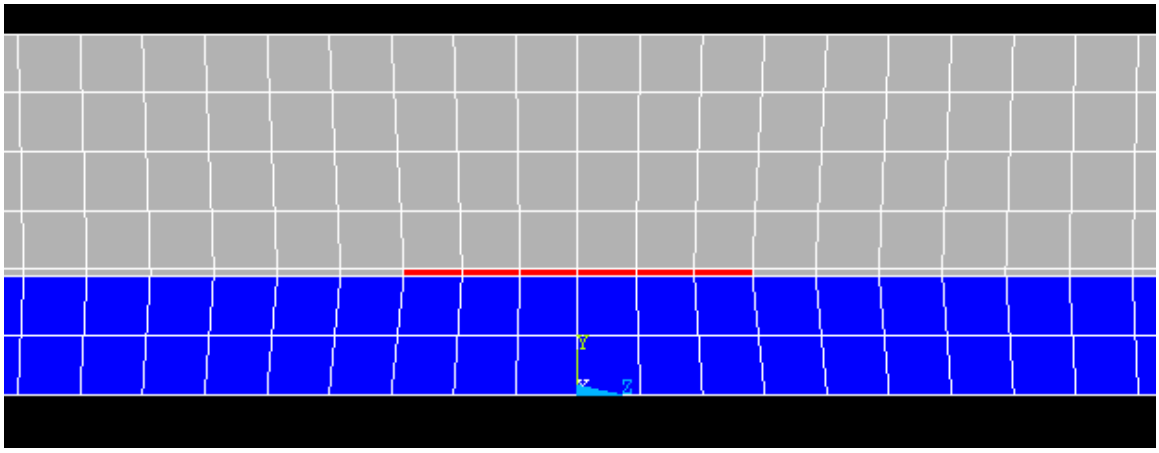

Figure 6.27: 1” Delamination Model with Mesh

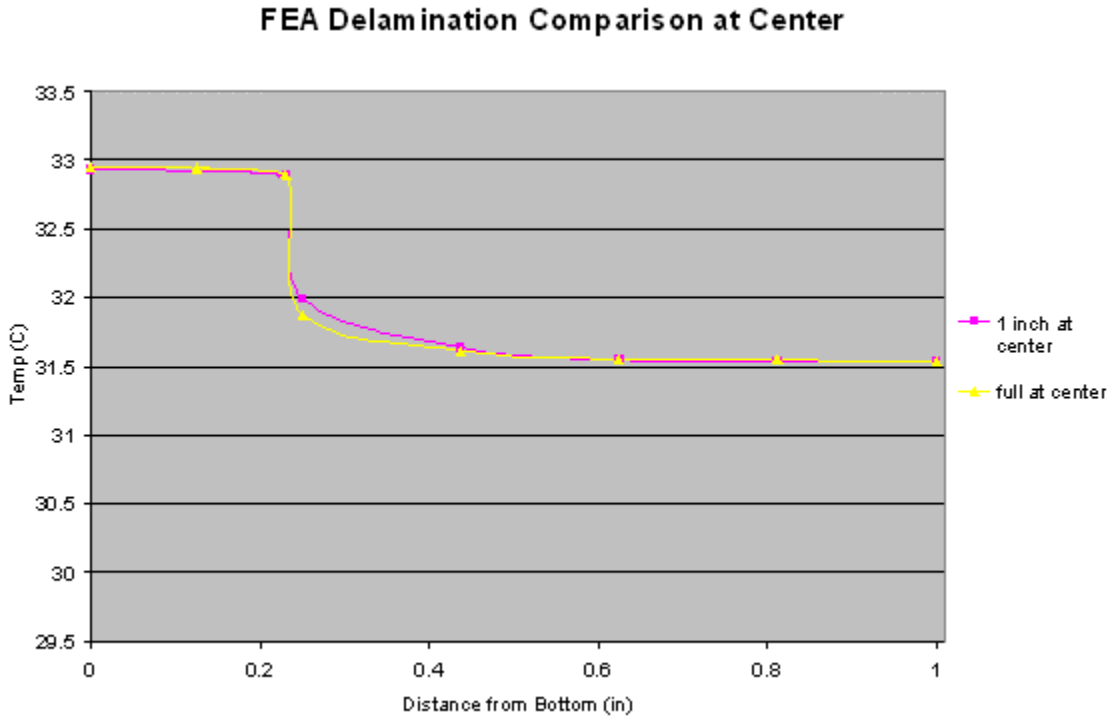

Figure 6.28: Surface Profile Comparison at the Center of the 1" and Fully Delaminated Models

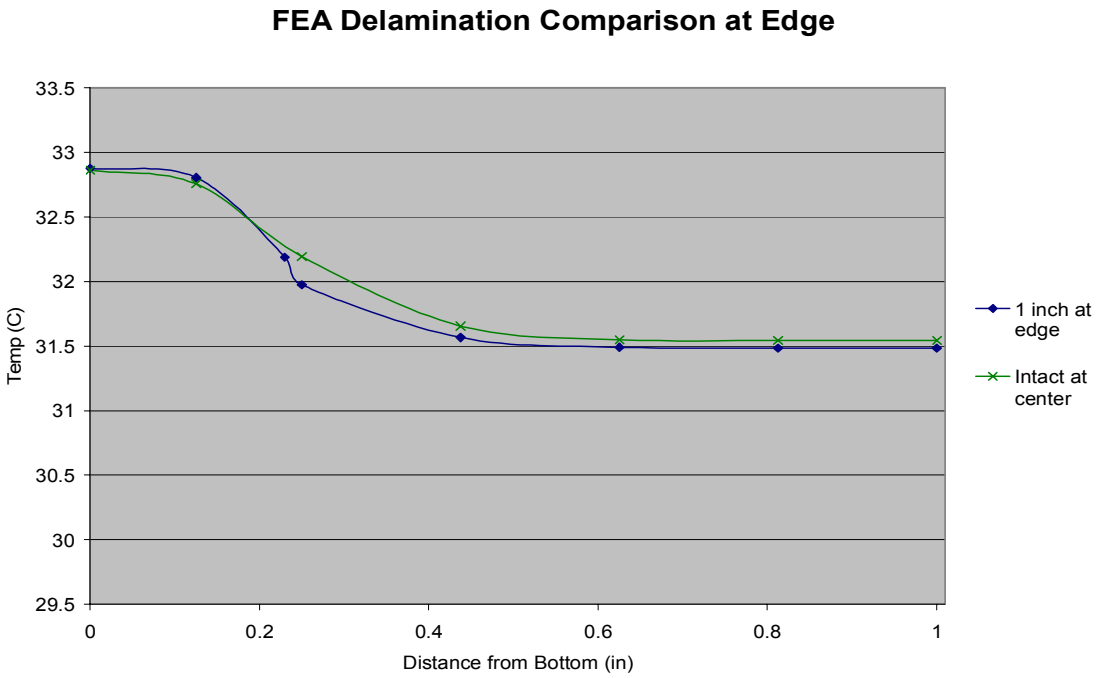

Figure 6.29: Surface Profile Comparison at the Edge of the Intact and 1" Delamination Models

Interestingly, the center of the full and 1" delaminations don't show much difference as well as the edge of the 1" and the intact models. If we were to use this model as a gage for severity of delamination, it may be able to show the length of a delamination by the profile changes as one scanned the length of the beam. Comparing the changes in the surface profile of only the 1" delamination results, the response of each vertical line of nodes from the center to just right of the delamination in Figure 6.27 are plotted in Figure 6.30.

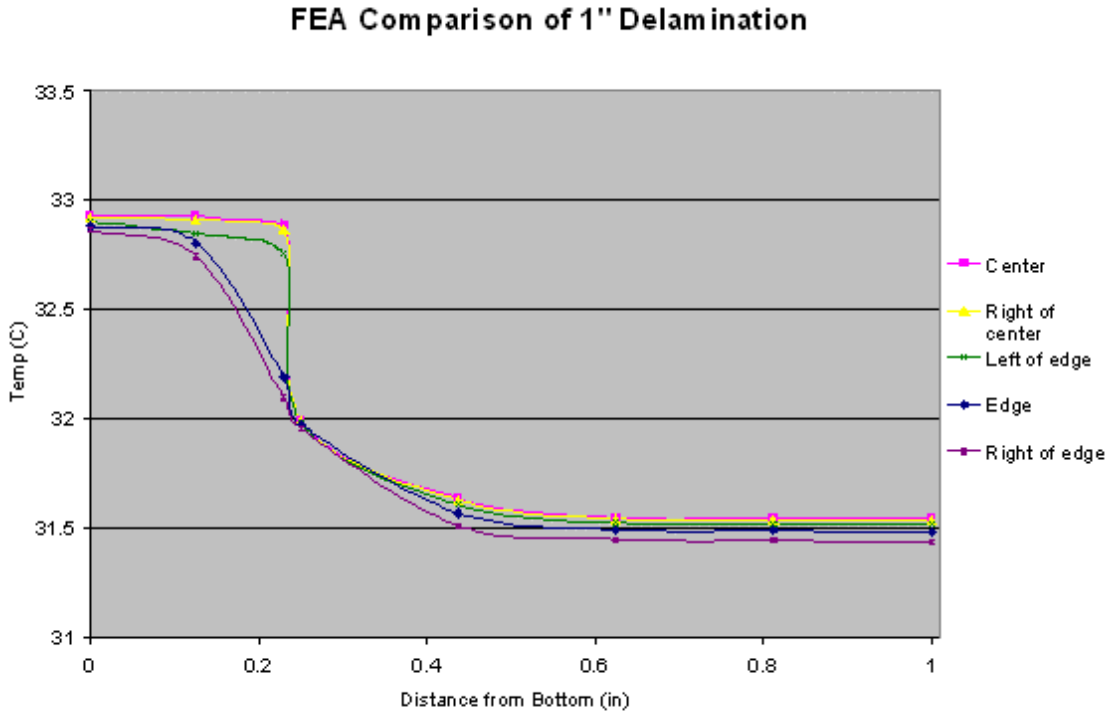

Figure 6.30: Surface Profile Comparison from the 1" Delamination Model

One might deduce from the FEA results that a delamination of approximately a half inch would be detectable as having a shoulder such as the green profile in Figure 6.30. However, the shoulder would only show at the center of the delamination and if a shoulder is the thermal signature of a delamination, one small instance of a shoulder could easily be disguised in the typical thermal variations along the length of the beam. Also, if the approximately half inch delamination is the smallest that would generate a shoulder, the critical size would have to be larger than the smallest delamination that would produce a shoulder since the distinctive thermal indications of delaminations are likely to under estimate the size. Furthermore, the FEA results show that the full 1 inch delamination should be able to be detected with the current test method.

Chapter Seven: Conclusions and Recommendations

Once all the data has been collected and the analysis complete, there comes a time when everything needs to be drawn together. This is the point when one has to determine how well the results match up and what can be done to improve the procedure.

7.1: Conclusions

Simply stated, the correlation between the experimental and theoretical results is quite good for the well characterized validation samples. While further refinement may occur with more exact input data from the material values, both general trends of the intact and simulated delamination models match. Furthermore, the differences between the delaminated and intact models and laboratory work are distinct and allow for the differentiation of “good” and “bad” sections of the beams. However, for this research to be practically useful, narrowing down the assessment of the beams with a specification of a critical delamination “size” is important.

This study demonstrates that a one inch delamination can be detected but the length would be underestimated. If the bridge designers plan to use damage tolerance in design they need to design so as to accommodate damage that is the size of the largest imperfection not reliably detected or larger. Due to the significant material property variability in these particular bridge beams there is some doubt that a smaller delamination might be detected even though the FEA model might indicate a distinctive thermal feature.

7.2: Architecture Changes to the Beam

One issue previously mentioned was the internal waviness and inconsistencies of the fiber architecture of the beam cross-section. While this was

an issue in itself and hindered the application of UT and the determination of where the carbon-glass boundary was located, something that was not previously addressed was that there were two different generations of beams. The initial proof testing and construction of the bridge were done with what was later dubbed the first generation beam and, for the most part, was the version of the beam that the analysis in this report was focused on due to the interest in an application for the bridge inspection. The second generation beam, externally, did not appear different but as an added aid in trying to keep the layers more planar and thus avoiding some of the waviness that caused the analysis problems, it had a fine fabric woven into the individual layers to hold them in place. This helped, but did not fully eliminate the issue of the waviness (see Figure 7.1 for a comparison with Figure 1.7). Since the bridge was not built of this version of the beam and structural differences had not yet been determined, the aspect of evaluating the second generation beam for the analysis was not pursued further.

Figure 7.1: Reduced Waviness of the Second Generation Beams

Continuing the thought of internal waviness, one aspect of the experimental testing should be brought up. This has to do with the waviness and how it changes along the length of the beam. A sample of a non-delaminated surface profile was first shown in Figure 6.2. Two more follow here in Figures 7.2 and 7.3. While these next two surface profiles were generated with different experimental setups which do not allow them to be quantitatively compared, they have general qualitative trends that allow comparison. More importantly, along with Figure 6.2, these all came from the same general region of the flange which shows that even though they may all be good, they are still different and show that the internal material conditions are variable which lead to variations along the length of the beam.

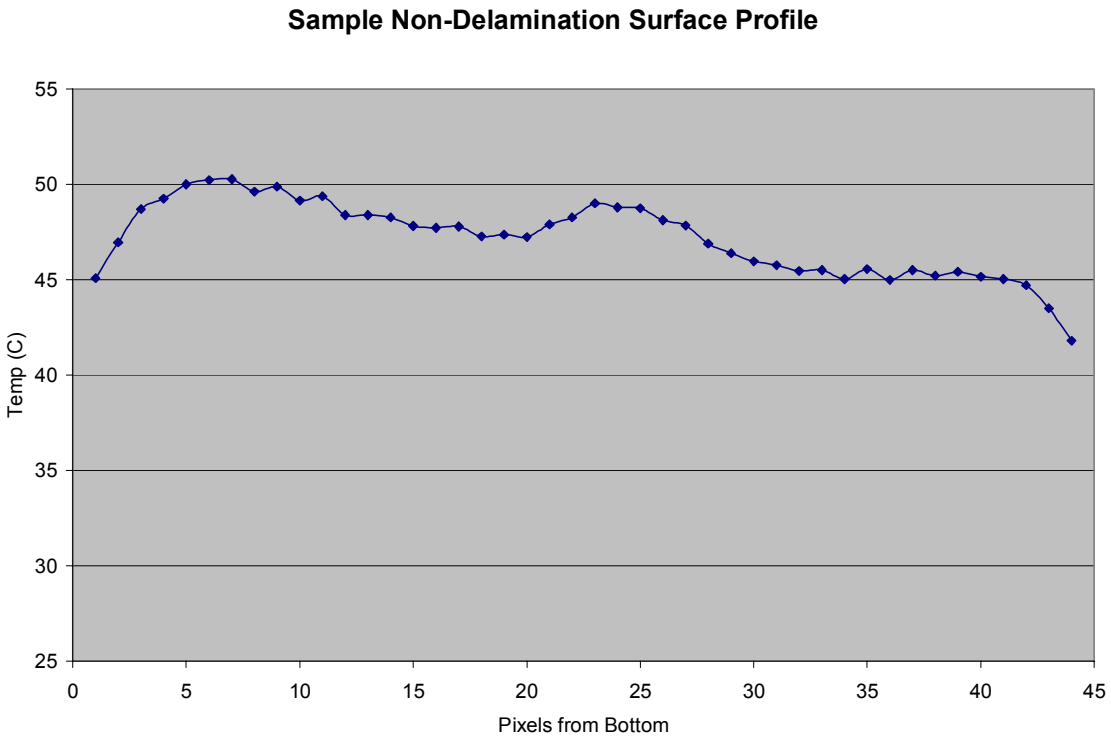

Figure 7.2: Example of a Non-delaminated Surface Profile

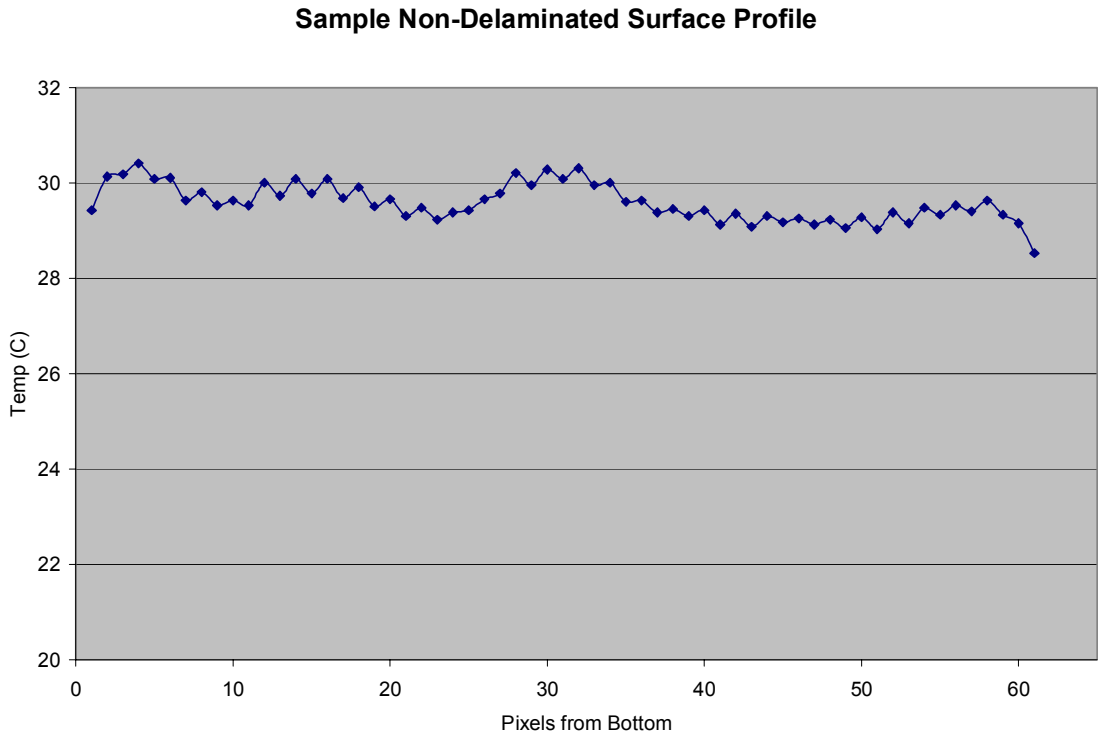

Figure 7.3: Example of a Non-delaminated Surface Profile

Another issue of consideration for change on the beam was some of the surface irregularities. While not an issue when selecting flange areas of the laboratory samples for testing, it would be an issue for other areas of the beam surface. Beyond what was needed in this study, a brief amount of time was spent scanning the larger surfaces of the beam. Since the web of the beam was not noted as being an area of interest for the life expectancy of the beam, the large surface of the top of the flange was scanned for irregularities. In several areas, some of the internal waviness resulted in bunching of strands on the surface of the beam. This either showed up as longitudinal streaks as in the lower edge of Figure 7.4 or, for lack of a technical term, globs of random fiber as in the upper part of the figure. Also seen in this figure as well as Figure 7.5 are how some of the rovings in the material cover the edge of the flange. While these areas could

be avoided in the experimental process, they would need to be considered for a complete bridge inspection.

Figure 7.4: External Irregularities

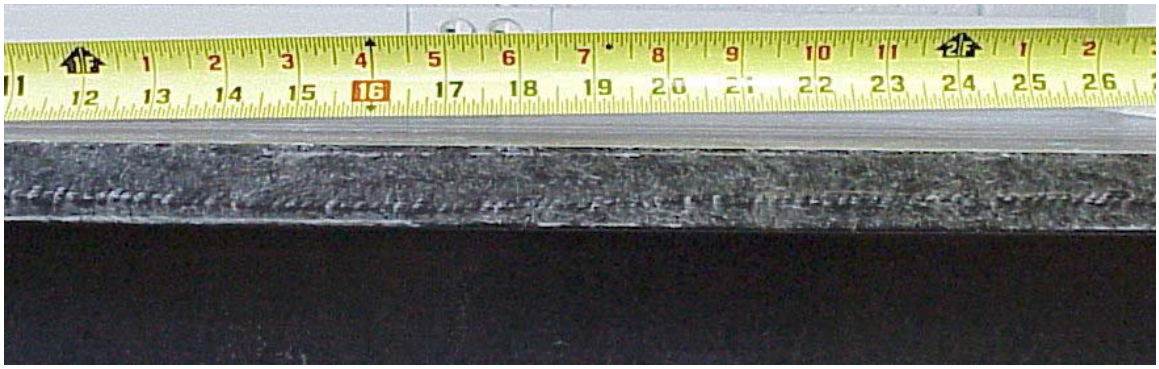

Figure 7.5: Flange Surface Irregularities

Some of these longitudinal streaks are also seen in Figure 7.6 and turn up in the IR images of the same region. Also present are chalked markings (upside-down “14”) that designated the beam for testing purposes and are also seen on the bridge beams. Cleanliness of the inspection surfaces will affect the thermal imaging as the emissivities will be changed.

Figure 7.6: Surface Irregularities

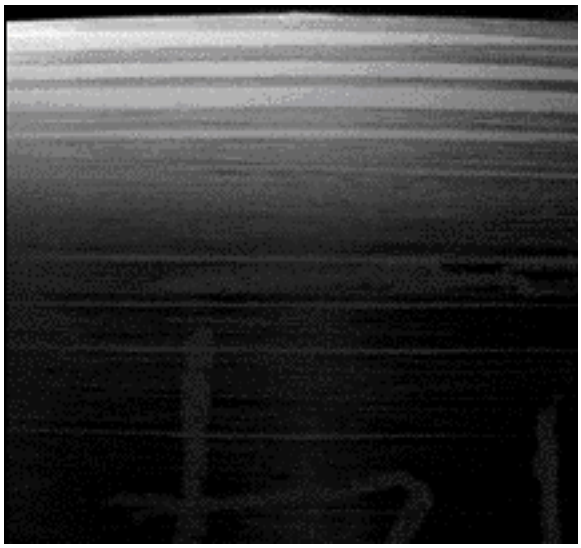

Figure 7.7: Surface Irregularities Shown with IR

7.3: Balancing the Theoretical and Experimental Worlds

Beyond blaming the internal structure of the beam for a lack of experimental correlation, one must also consider the versatility of the computer model. If the beam were perfect, there would be no need to inspect for non-conformity since they would not exist. Conversely, the perfect FEA model would incorporate all of the irregularities and material inconsistencies that the real life beam included. Since the likelihood of either of these happening is extremely low, a compromise must be explored.

I once found a fortune cookie that included this message: “it is better to idealize the real than realize the ideal.” Based on finding a compromise between the experimental and analytical methods the available resources need to be brought up. The information that was used to create the FEA model was based on the intended final result of the manufacturing process. Instead of holding to these characteristics throughout the building of the model, it may have been more beneficial to determine an average set up geometries taken from several

cross sections of the flange. While this would not have been the ideal layout, it might have well been more realistic when building and comparing the FEA and experimental data.

Furthermore, the materials used are typically designed around mechanical properties, not thermal. As a result, even if one knew exactly what materials were used, the thermal properties beyond combustibility are not likely to be known, even by the fiber manufacturer. By having the geometry of the model set, using general ranges of available material values and matching them to the experimental results was the best method available.

With the validation samples, the relationship between actual and the ideal computer model was much closer. While neither was perfect, the levels of control in fabrication of the samples was much higher and by having the knowledge of the materials and their properties resulted in having better data to input into the FEA model.

With respect to modeling capabilities, newer versions of ANSYS do allow for thermal properties to be implemented into the layered elements specifically created for usage with composite materials. While still limited by the discrepancies between the physical flange and the ideal one created in ANSYS, by using this new feature, the CompositePro program used to generate material values could be removed from the process and ANSYS could do everything. This will yield layer by layer results instead of general material regions. However, they would still rely on the experimental samples for correlation.

7.4: Delamination Characterization

The intent of the 1” delamination model was to explore the effects of delaminations smaller than the length of the modeled section. While much more realistic since a full length delamination would, more or less, represent a failed beam, there were no successful attempts at fabricating a delamination of this

type in either the validation samples or delaminated flange samples that were fixed back together with resin.

If it had been possible to control the shape and size of a fabricated delamination, the resulting experimental data could have been used to compare and contrast the FEA data with what could be related to interpreting the location and size of an unknown imperfection. An added benefit of this type of analysis would be to create several imperfections of varying sizes in different samples and determine the smallest detectable delamination. This, along with the resolution characteristics of the data acquisition system could be used to compare with the non-conformity limit to assess the need for better equipment or, conversely, less detail that would allow for an increased inspection speed.

7.5: Testing the Bridge

One difficult matter of selecting an evaluation technique and developing a process for evaluating the beam was how the beams would be situated in the bridge. Unlike testing in the laboratory where the beam could be sectioned and orientated such that it would favor the advancement of an inspection technique, testing at the bridge site would not allow for these adjustments. Since the Dickey Creek Bridge was not built with considerations for the application of an NDE technique, considerations would have aided the optimization and reliability of inspection methods.

As shown in Figure 7.8, the ends of the beam are almost butted up to the face of the concrete abutments. Although the area of interest for the research was at the outside of the flange edge, having access to the inside of the beam would have increased the options for evaluating the web, heating, or viewing the beam from the inside, such as location “B” from Figure 1.8. To accomplish this, the bridge design would need access points to the interior boxes of the beam. The nature of access would depend entirely on what would be placed inside the

beam. If it were the camera, the gap between the end of the beam and the concrete embankment would have to be at least six inches. If it were the heat lamp, then the gap could be just slightly less. Also, depending on how an alternative inspection technique might be developed and applied, a device might be needed to guide the camera or lamp along the beam and would also need to fit through the gap. Since the structural analysis of the Dickey Creek Bridge was not something that this study considered, the small gap at the end of the beam may have been something that was changeable.

Figure 7.8: End Constraints

7.6: Field-testing in General

When considering field-testing, external elements of weather conditions and accessibility need to be considered. In the lab, the environment is controlled and issues concerning differences in ambient temperature, whether or not the beam is wet, the water level in the creek, or the time available for inspection did

not impact the experimental data collection. In other words, the temperature was constant and regulated, the beam remained dry and the issues of night and day did not affect the data. In the field, however, these factors will make a significant difference. For the most part, the beams would be sheltered from the elements due to the fact that they are underneath the deck but a cross-wind, different time of day, or the changing seasons of the year will also change the way the bridge might be inspected. An appropriate inspection schedule would need to incorporate environmental considerations.

During the early stages of this project, before the small sections of the beam were removed and relocated to the laboratory environment, preliminary analysis took place in a gravel lot outside the laboratory. At this point, since everything was out in the open and not sheltered by a bridge, a rainy day would hamper any work done since the equipment would not handle getting wet and running a long extension cord, power strip, several pieces of electronics in the rain also posed as safety issue. One thing that was accomplished in these early tests was that when the beam was a relatively cold 6 degrees C, compared to the constant lab temperature of 20 degrees C, it would take a different set of initial conditions to generate a comparable thermal profile in FEA. Also, at the cooler temperature, more energy was needed to be added to develop a thermal gradient. This also meant a lot more time involved in the heating process and it was already mentioned that the FEA model was not set up for this situation. In one instance, what should have taken no more than a few seconds ended up being over twenty minutes and the gradient that was developed was weak and difficult to image. In order to apply an IR NDE technique in this type of situation, the time and energy issue plays a large part in how well a technique will work [Silk, 1987].

Conversely, on a clear, hot day of around 95 degrees F (35 C), adding energy to the beam was difficult in that the sun had heated the beam to the point

where it was extremely hot to the touch, making it difficult to increase the surface temperature with the heating lamp used. In this instance, the heat energy may be beneficial in that the beam is already heated and when it cools as the ambient air temperature drops below the beam temperature as the day goes on and use the natural thermal gradients in the inspection process. However, this is not a controlled technique and relies extensively on the elements and weather conditions throughout the day. Also, since no two days are alike, the ability to duplicate similar testing conditions and results would be difficult.

Finally, with respect to equipment portability, the IR camera in itself could be moved to the bridge site and run on battery power. In order to evaluate the entire bridge, a mechanism of some type to guide the camera and lamp along the surface would also need to be developed.

7.7: Procedural Changes

The general process for collecting data involved the heating of the beam with a lamp and then a collection of time-dependent data from the IR camera into the computer. For a small-scale laboratory example, this procedure worked well but for implementation on a larger scale or in the field, several revisions would need to take place. Primarily, a specific time in which to collect the IR image would need to be determined to eliminate the need to acquire a progression of images and would greatly aid the application of the process outside the lab.

Another consideration would be directed towards the limits of data computation. Since patience will cover any time constraints involved with laboratory work and computing speed, the bottom line on computation would end up with the resolution of the data. In this characteristic and with how the camera-computer system processes data in the picture form, the ultimate smallest size of an imperfection to be detected will be governed by the resolution of the system. For the most part with this project, this was not an issue since much of the data

was processed with a resolution of about 25 pixels per inch. If the level of imperfection were greater than the critical non-conformity, the inspection would not be acceptable since there would be imperfections larger than the non-conformity limit missed by the inspection. In this situation, a new inspection process would need to be developed to encompass all the criteria or the design modified to tolerant of detectable imperfections [Balageas, 1991].

7.8: Closing Comments

It is expected that as the use of reinforced polymeric materials increases in infrastructure applications that the quality of the materials will improve, taking full advantage of the properties of these types of materials. The present low quality with regard to fiber and matrix distribution, reinforcement orientation and alignment, and uniformity along the length despite the inherent nature of the pultrusion process in the latter regard hindered quantitative comparison of modeling and experimental results. To achieve quantitative agreement, the FEA model would have needed to represent the extensive material property irregularities which were neither practical nor possible in the context of nondestructive assessment. Nevertheless the successful validation of the model and the associated experimental results suggests that the infrared thermal imaging approach offers significant potential for challenging field applications.

References:

AGA Thermovision 780 Handbook, pp 11.1-11.11.

Almond, D.P., Lau, S.K., "Defect Sizing by Transient Thermography. I: An Analytical Treatment," **Journal of Applied Physics, Vol. 27**, Bath, United Kingdom, 1994.

Alqennah, Hasan, "Detection of Subsurface Anomalities in Composite Bridge Decks Using Infrared Thermography," West Virginia University, WV, 2000.

Armstrong, Keith B., Barrett, Richard T., **Care and Repair of Advanced Composites**, SAE, Warrendale, Pa., 1998.

Balageas, Daniel L., Delpech, Phillippe M., Boscher, Daniel M, Deom, Alain A., "New Developments in Stimulated Infrared Thermography Applied to Nondestructive Evaluation of Laminates," **Review of Progress in Quantitative Nondestructive Evaluation, Vol. 10a**, Plenum Press, New York, 1991.

Beiser, Arthur, **Concepts in Modern Physics**, McGraw-Hill Companies, Inc., New York, 2003.

Bray, Don E., Stanley, Roderic K., Nondestructive Evaluation: A Tool in Design, Manufacturing, and Service, CRC Press, New York, 1997.

Callister, William D., Jr., **Material Science and Engineering: An Introduction**, John Wiley & Sons, Inc., New York, 1997.

Chapman, Alan J., **Heat Transfer**, Macmillan Publishing Co., Inc., New York, 1984.

Coakley, Scott. "Beyond Skin Deep: Using Thermal Imaging," Composites Fabrication, May 2004.

Duke, John C., Jr., "NDE Method Selection for Advanced Materials," Proceedings of the 25th SAMPE Technical Conference, Philadelphia, Oct. 1993.

Gibson, R.F., **Principles of Composite Material Mechanics**, McGraw-Hill, New York, 1994.

Halliday, David, Resnick, Robert, Walker, Jearl, **Fundamentals of Physics: Extended**, John Wiley & Sons, Inc., New York, 1997.

Hyer, Michael W., Stress Analysis of Fiber-Reinforced Composite Materials, MC/McGraw-Hill, 1998.

Lesko, Jack, Cousins, Tom, Duke, Jack, Gomez, Jose, "Construction of a Virginia Short Span Bridge with the Strongwell 36" Double-Web I-Beam."

Maldague, Xavier, P.V., Theory and Practice of Infrared Technology for Non-Destructive Testing, John Wiley & Sons, Inc., New York, 2001.

Matweb Website: www.matweb.com.

Miceli, Marybeth, "Assessment of Infrared Thermography as NDE Method for Investigation of FRP Bridge Decks," Virginia Polytechnic and State University, VA, 2000.

Puttick, K.E., "Thermal NDT Methods," Non-Destructive Testing of Fiber-Reinforced Plastic Composites, V1, 1987.

Shepard, S.M., Lhota, J.R., Ahmed, T., Rubadeux, B.A., Wang, D., "Quantification and Automation of Pulsed Thermographic NDE," **Nondestructive Evaluation of Materials and Composites V, Proceedings of SPIE, Vol. 4336**, Newport Beach, 2001.

Schniepp, Timothy, "Design Manual Development for a Hybrid, FRP Double-Web Beam and Characterization of Shear Stiffness in FRP Composite Beams," Virginia Polytechnic and State University, VA, 2002.

Silk, M.G., Stoneham, A.M., Temple, J.A.G., **The Reliability of Non-Destructive Inspection**, Adam Hilger, Bristol, 1987.

Suryanarayana, N.V., **Engineering Heat Transfer**, West Publishing Company, New York, 1995.

Radiance PM User Manual, Raytheon Amber, Goleta, CA, pp 2.

Winfree, William P., Zalameda, Joseph N., "Thermographic Depth Profiling of Delaminations in Composites," **Review of Progress in Quantitative Nondestructive Evaluation, Vol. 22**, Plenum Press, New York, 2003.

Zalameda, Joseph N., Winfree, William P., "Thermal Imaging of Graphite/Epoxy Composite Samples with Fabricated Defects," **Review of Progress in Quantitative Nondestructive Evaluation, Vol. 10a**, Plenum Press, New York, 1991.